

DEVELOPMENT OF A NEW CLASS OF
MICRORNA CONTROLLED OHSV VECTORS
FOR TREATMENT OF GLIOBLASTOMA

by

Lucia Mazzacurati

Laurea in Biotechnology, University of Bologna, Italy, 2001

Submitted to the Graduate Faculty of
Department of Human Genetics
Graduate School of Public Health in partial fulfillment
of the requirements for the degree of
Doctor of Philosophy

University of Pittsburgh

2012

UNIVERSITY OF PITTSBURGH
GRADUATE SCHOOL OF PUBLIC HEALTH

This dissertation was presented

by

Lucia Mazzacurati

It was defended on

June 28, 2012

and approved by

Michael Barmada, PhD, Associate Professor, Department of Human Genetics, Graduate School of Public Health, University of Pittsburgh

Joseph C Glorioso III, PhD, Professor, Department of Microbiology and Molecular Genetics, School of Medicine, University of Pittsburgh

Paola Grandi, PhD, Assistant Professor, Department of Neurological Surgery/Microbiology and Molecular Genetics, School of Medicine, University of Pittsburgh

Laura J Niedernhofer, M.D, PhD, Associate Professor, Department of Microbiology and Molecular Genetics, School of Medicine, University of Pittsburgh

Dissertation Director: Robert Ferrell, PhD, Professor, Department of Human Genetics, Graduate School of Public Health, University of Pittsburgh

DEVELOPMENT OF A NEW CLASS OF
MICRORNA CONTROLLED OHSV VECTORS
FOR TREATMENT OF GLIOBLASTOMA

Lucia Mazzacurati, PhD

University of Pittsburgh, 2012

Glioblastoma Multiforme (GBM) is a highly aggressive brain tumor for which there is no treatment. Oncolytic Viruses (OVs) are attenuated tumor-selective viruses designed to replicate in and kill tumor cells without affecting normal tissue. Herpes Simplex Virus type-1 derived oncolytic vectors (oHSV-1) are a promising and safe alternative to current GBM therapies, but the deletions that render these oHSV-1 incapable of replicating in normal tissue also compromise their lytic activity in tumor cells. Consequently, these viruses fail to eradicate the tumor.

In this study, I developed a new oHSV-1, named ICP4-miR124t, whose selective replication in GBM cells does not rely on defective genes, but rather is mediated by micro (mi)RNAs differentially expressed between normal tissue and GBM. MiRNAs recognize complementary target sequences in mRNAs resulting in repression of the mRNA. MiR124 is one of the most abundant miRNAs in developing and mature neurons, but is absent in GBM since its presence is incompatible with the tumor phenotype and viability. After introducing four tandem copies of the miR124 target sequence in the 3'UTR of the HSV-1 essential ICP4 gene, I observed robust replication of the resulting ICP4-miR124t oHSV-1 in primary glioblastoma cells, while viral growth was highly impaired in the same cells upon induction of mir124. Toxicity tests involving intracranial injection of immunocompetent and immunodeficient mice showed a dramatic reduction in vector toxicity compared to unregulated control virus. Moreover, ICP4-miR124t-injected animals showed a loss of viral DNA in the brain over time, whereas an increase was observed in control virus injected animals.

In conclusion the ICP4-miR124t oHSV-1 developed in this study is promising for GBM treatment because it is capable of killing miR124-negative tumor cells as efficiently as wild-type HSV-1, while lacking toxicity for normal brain. These results are of major Public Health importance not only as a potentially more effective alternative to current inefficient GBM treatments, but also as a new paradigm to treat other kinds of tumors by taking advantage of the differential miRNA expression between tumor and normal tissue.

TABLE OF CONTENTS

AKNOWLEDGEMENTS	X
ABBREVIATIONS	XI
1 INTRODUCTION	1
1.1 Glioblastoma Multiforme (GBM) is the most malignant form of brain tumor without available effective treatment	1
1.2 Herpes Simplex Virus Type-1 (HSV-1) based Oncolytic Viruses (OVs) are a promising but still ineffective therapy against GBM	4
1.3 MiR124 absence is specific for GBM cells.....	8
2 METHODS	13
2.1 Cell lines	13
2.2 HSV-1 infection on U2OS and VERO cells	14
2.2.1 Infection to test viral growth	14
2.2.2 High scale viral production	14
2.2.3 Viral titration in plaques forming units (p.f.u /ml)	15
2.2.4 Viral titration in Viral Genome Copy Number (gc /ml) calculated by qPCR	15
2.3 Polymerase Chain Reaction	16
2.4 Cloning techniques	17
2.4.1 DNA restriction digest and purification from agarose gel.....	19
2.4.2 Ligation of DNA fragments and transformation of competent bacteria	19
2.4.3 Transformation of competent bacteria cells	19
2.4.4 DNA extraction for screening of transformed bacteria colonies	20
2.5 Engineering of a firefly-Luciferase expression plasmid carrying the miR124 responsive element, 4xTmiR124	20
2.6 Analysis of MiR124 activity on the 4xT124 response element	21
2.7 Engineering of the HSV-1 Genome	22
2.7.1 Insertion of T2A-eGFP in gC 3'end	25
2.7.2 Insertion of 4xT124 responsive element in ICP4-3'UTR	31
2.7.3 BAC minipreps	42

2.7.4 Transfection of BAC-DNA into U2OS to produce KBG and ICP4-miR124t-BAC oHSV-1 viruses	42
2.7.5 Transfection of BAC-DNA into U2OS-Cre cells to produce BAC-free KG and ICP4-miR124t oHSV-1 viruses	42
2.8 Creation of Tet-on-miR124 stable cell line.....	44
2.8.1 Extraction of total DNA from U87 cells.....	44
2.8.2 Engineering of a Tet-On-miR124 construct.....	45
2.8.3 U2OS transfection and selection of stable clones.....	48
2.8.4 RT-qPCR for miR124 quantification.....	48
2.8.5 oHSV-1 infection of U2OS TetO stable lines, SHSY5Y, 50B11, PC12 following miR-124 inducing drug treatment with either doxycycline (Dox), Forskolin or Nerve Growth Factor (NGF).....	49
2.9 Creation of a transiently expressing Lenti-miR124 and Lenti-miR137A Primary Glioma Cells	49
2.9.1 Engineering of pCDH-miR124 expression construct.....	49
2.9.2 Engineering of pCDH-miR137A control expression construct	51
2.9.3 Production of Lenti-miR124 and Lenti-miR137 viruses.....	51
2.9.4 Lentivirus titration calculated in colony forming units (c.f.u. /ml).....	52
2.9.5 Lenti-miR124 infection of primary glioma cells	52
2.9.6 KG and ICP4-miR124t oHSV infection of primary glioma cells.....	53
2.10 In Vivo Toxicity Testing.....	53
2.10.1 Viral injections in immunocompetent mice	53
2.10.2 Viral injections in immunocompromised mice.....	54
3 RESULTS.....	55
3.1 Validation of the use of a joint deleted HSV-1 as backbone to create a GBM oncolytic vector.....	55
3.2 Testing of a firefly-Luciferase expression plasmid (pLuc) carrying the miR124 responsive element 4xT124.....	56
3.3 Engineering and Production of a ICP4-miR124T oHSV-1 Oncolytic Vector	57
3.3.1 Engineering of the HSV-1 genome.....	57
3.3.2 Production of KG and ICP4-MIR124t viruses	60
3.4 In Vitro Testing of ICP4-miR124T Vector for Growth Selectivity	61
3.4.1 ICP4-miR124t replication efficiency in transiently miR124-transfected cells ...	61

3.4.2 ICP4-miR124t replication efficiency in miR124-inducible stable cell lines	62
3.4.3 ICP4-miR124t replication efficiency in cells expressing endogenous miR124.....	66
3.4.4 ICP4-miR124t replication efficiency in patient-derived primary glioma spheroid lines (GICs) in the presence or absence of induced miR124 expression.....	68
3.5 In Vivo Testing of ICP4-miR124T Virus for Growth Selectivity.....	72
3.5.1 Toxicity testing for virus safety in immunocompetent mice.....	72
3.5.2 Toxicity testing for virus safety in immunodeficient mice	74
4 DISCUSSION	77
BIBLIOGRAPHY	85

LIST OF TABLES

Table 1: Conventional GBM classification.....	2
Table 2: Novel molecular-based GBM classification.	3
Table 3: oHSV-1 in clinical trials.	6
Table 4: PCR primers used.....	16
Table 5: DNA constructs generated in this study.	18

LIST OF FIGURES

Figure 1: Organization of the HSV-1 genome.....	5
Figure 2: MicroRNAs biosynthesis.....	9
Figure 3: MiRNAs involved in the development of the Central Nervous System (CNS).	10
Figure 4: Design of a miR124-controlled Luciferase construct.....	21
Figure 5: Organization of the KBBJ genome.	22
Figure 6: Two steps Gene-Bridges Red/ET temperature-shift-mediated recombination in gC locus.....	23
Figure 7: pBad-I-SceI two steps modification of the Gene-Bridges Red/ET temperature-shift-mediated recombination in the ICP4 locus.....	24
Figure 8: PCR to amplify the counter-selection cassette (CS) with homology arms for gC 3' end	26
Figure 9: 1st step: counter-selection (CS) cassette insertion in gC 3'UTR.....	28
Figure 10: 2nd step: counter-selection (CS) replacement with T2A-eGFP in gC 3'UTR.....	30
Figure 11: Schematic of pEntr-ICP4-T124-kan generation, Steps 1-3.	32
Figure 12: Schematic of pEntr-ICP4-T124-kan generation, Steps 4-6.	33
Figure 13: Schematic of pEntr-ICP4-T124-kan generation Step 7-8.	35
Figure 14: PCR amplification of 4xT124-ICP4-ISceI-Kan selection-cassette to be inserted in ICP4 3'UTR.....	36
Figure 15: 1st step: I-SceI-kan selection cassette insertion in ICP4 3'UTR.....	38
Figure 16: pBad-induced ISceI-kan selection cassette removal in ICP4 3'UTR.	40
Figure 17: pBad plasmid removal.	41
Figure 18: PCR to verify correct removal of the BAC after infection of U2OS-Cre cells.	44
Figure 19: Generation of the TetO-inducible miR124-expressing construct: Step 1.....	46
Figure 20: Generation of the TetO-inducible miR124-expressing construct Step 2.....	47
Figure 21: Generation of pCDH expression constructs.....	50
Figure 22: Replication efficiency of Joint deleted KOS-BAC (KBJ) in vitro.....	56

Figure 23: MiR124-controlled Luciferase Activity.....	57
Figure 24: KBG BAC-DNA transfection into U2OS to verify BAC-DNA ability to generate virus.....	58
Figure 25: ICP4-miR124t BAC-DNA transfection into U2OS to verify BAC-DNA ability to generate virus.....	60
Figure 26: ICP4-mir124t oHSV-1 replication efficiency after mir124 transient transfection.	61
Figure 27: Tet-inducible construct for Hu-mir124-3 expression.....	63
Figure 28: RT-qPCR for mir124 expression in U2OS TetO clones and in cells expressing endogenous miR124.	64
Figure 29: ICP4-mir124t replication efficiency in TetO-mir124 stable cell lines.....	65
Figure 30: ICP4-mir124t oHSV-1 replication efficiency in TetO inducible clones.	66
Figure 31: ICP4-mir124t oHSV-1 replication efficiency in cells expressing endogenous miR124.	67
Figure 32: ICP4-miR124t oHSV replication efficiency in patient-derived mir124-negative (GICs).	69
Figure 33: ICP4-miR124t oHSV replication efficiency in (GICs) following plenti-induced miR124 expression.....	70
Figure 34: RT-qPCR of miR124 expression in Lenti-miR124 infected Gli68.	71
Figure 35: In vivo toxicity testing of the ICP4-miR124t oHSV-1 for vector safety in immunocompetent mice.	73
Figure 36: in vivo toxicity testing of the ICP4-miR124t oHSV-1 for vector safety in immunodeficient mice.....	75

ACKNOWLEDGEMENTS

I would like to thank my Committee members, my advisor Dr. Paola Grandi, Dr. Joseph Glorioso, Dr. Michael Barmada, Dr. Laura J. Niedernhofer, and Dr. Robert Ferrell for all their guidance and their help in completing this work.

I also want to thank all the people who worked with me in the Glorioso lab, Justus Cohen and William Goins, Marco Marzulli, Bonnie Reinhart, Lilly Laemmle, Yoshitaka Miyagawa, Mark Doyal, Gianluca Verlengia, Daniela Leronni, Mingdi Zhang, George Huang, Shinichi Kawahara, and Chang-Sook Hong, for all their advice and assistance. I couldn't have achieved any of this without them.

A special thank you to my family, my husband Tony for his endless support, my sixteen month old child Alexander, my pride and my joy; my parents, my brother and my grandma for being their listening and comforting me even from across the Atlantic.

Finally, I would like to dedicate this work to my first and most important mentor, Dr. Maria Alessandra Santucci, the first person who believed in me and decided that I was smart and strong enough to leave Italy and find my way in the U.S.

ABBREVIATIONS

GBM	Glioblastoma Multiforme
AA	Anaplastic Astrocytoma
OV	Oncolytic Vector
HSV-1	Herpes Simplex Virus Type-1
oHSV-1	HSV-1 derived Oncolytic Vector
ICP4	HSV-1 Infected-cell Polypeptide 4
miR	MicroRNA
miR124	MicroRNA-124
3' UTR	3'-end Untranslated Region
LOH	Loss of Heterozygosity
LAT	HSV-1 Latent-specific RNA
U _L	Unique Long HSV-1 Region
U _S	Unique Short HSV-1 Region
mRNA	Messanger-RNA
miRISC	miRNA-ribonucleoprotein Complex
RNAi	RNA-interference
ESCs	Pluripotent Embryonic Stem Cells
NSCs	Multipotent Neural Stem Cells
NPCs	Lineage-specific Neuronal Progenitors
MOI	Multiplicity of Infection
rpm	Revolutions per Minute
p.f.u.	Plaque Forming Units
RT	Room-Temperature
g.c.	Genome Copy
qPCR	Real-time Polymerase Chain Reaction
RTqPCR	Real-time Reverse Transcription Polymerase Chain Reaction
gD	HSV-1 Glycoprotein D
Amp	Ampicillin
fLuc	Firefly-Luciferase
rLuc	Renilla-Luciferase
4xT124	Tandem array of four miR124 target sequences
BAC	Bacterial Artificial Chromosome
KB	HSV-1 genome strain KOS containing BAC
KBJ	Joint-deleted KB

gB	HSV-1 Glycoprotein B
gB:NT	D285N/A549T double mutation in gB
KBBJ	KBJ containing gB:NT mutation
gC	HSV-1 Glycoprotein C
eGFP	Enhanced Green Fluorescent Protein
KBG	KBBJ containing eGFP in frame with gC
T2A	2A translation-pause Sequence
Kan ^R	Kanamycin-Resistance gene cassette
Strep ^S	Streptomycin-Sensitivity gene-cassette
Tet ^R	Tetracyclin-Resistance gene cassette
CS	Kan ^R -Strep ^S containing counter-selection cassette
FIGE	Field Inversion Gel Electrophoresis

1 INTRODUCTION

1.1 Glioblastoma Multiforme (GBM) is the most malignant form of brain tumor without available effective treatment

Glioblastoma Multiforme corresponds to the worst grade in Glioma classification according to the World Health Organization (WHO grade IV). The classification includes all tumors arising from the glial lineage in the brain and divides them into four grades (I-IV) depending on tumor phenotype, clinical behavior and prognosis. GBM is defined as an infiltrating glioma, biologically aggressive and resistant to therapy, characterized by the presence of tumor cell necrosis and/or angiogenesis, cytological atypia and mitotic activity^{1,2,3}.

GBM is the most common form of astrocytoma in the adult population, accounting for 50-60% of all gliomas and 2% of all human tumors, with an incidence in the US of 4-5 cases per 100,000 persons per year. GBM incidence is higher in males and increases both with exposure to ionizing radiation and with age (from 0.2 cases per 100,000 persons per year in people below 14 years of age to 4-8 cases per 100,000 persons per year in people above 45 years of age), making these three variables the main GBM risk factors. GBM is a sporadic tumor, but its incidence is increased in familial cancer syndromes, especially in Li-Fraumeni syndrome characterized by loss of functional p53, a tumor suppressor protein^{1,2,4}.

GBMs have traditionally been sub-classified into two distinct types based on genotypic and phenotypic differences (Table 1). The first and most common type (>90% of GBM patients) includes primary tumors arisen de novo with no evidence of pre-existing lower grade glioma, typically diagnosed in older patients. 70% of primary GBM are characterized by loss of heterozygosity (LOH) of the long arm of chromosome 10, 36% show amplification of *EGFR* or its *EGFRvIII* tumor variant and 25% show mutation of *PTEN*. The second type includes secondary tumors derived from a lower grade astrocytoma, more often found in younger patients. Most secondary GBM present mutations of *TP53* (65%) and overexpression of both *PDGF* and its receptor¹. Despite their genotypic differences, both GBM classes show a common miRNA expression pattern that is completely different from the one found in normal

brain, characterized among others by miR21, miR17 and miR10 overexpression and of miR124, miR137, and miR128 downregulation⁵

Table 1: Conventional GBM classification.

	Phenotype	Mean age of onset	Genotype	miRNA profile compared to normal brain
Class I >90% of all GBM	Primary tumors arisen de-novo	62 years	70% LOH 10q 36% amplification of EGFR and EGFRvIII 25% PTEN mutations	↑miR21, miR17, miR10
Class II <10% of all GBM	Secondary tumors derived from a pre-existing lower grade astrocytoma	35 years	68% TP53 mutations 54% LOH 10q, 19q 82% LOH 22q high rate of PDGF overexpression	↓miR124, miR137, miR128

A different, more accurate and more recent (2008) GBM classification is based on the molecular heterogeneity associated with human gliomas and divides GBM in four molecular sub-types, Mesenchymal, Proneural, Classical and Neural, based on the genomic abnormalities identified by the Cancer Genome Atlas Research Network (TGCA) on 206 GBM patient samples (Table 2)⁶. The Mesenchymal subtype is characterized by either hemizygous deletions of the 17q11.2 region containing *NF1*, or mutations in the *NF1* gene and by chromosome 7p amplification associated with over-expression of *EGFR* and *EGFRvIII* tumor variant. The Proneural subtype molecular signature includes *TP53* mutation (or LOH) together with amplification of *PDGFRA* on 4q12, point mutations of *IDH1* and alterations of *PDGF*. Most of secondary GBM belong to this subtype. The Classical subtype presents chromosome 10q loss including the *PTEN* gene, chromosome 7p amplification associated with over-expression of *EGFR* and *EGFRvIII*, and 9p21 deletions containing *CDKN2A* and *CDKN2B* genes. The Neural subtype is associated with the expression of neuronal markers like *NEFL*, *GABRA1*, *SYT1* and *SLC12A5* and chromosome 7p amplification associated with over-expression of *EGFR* and *EGFRvIII*. Interestingly, by comparing the expression profiles of these four molecular GBM subtypes with normal brain transcriptome data, it appears that each subtype is derived from a different neural cell type, with the Classical group being similar to astrocytes, the Proneural

group to oligodendrocytes, the Mesenchymal group to astroglia and the Neural group to neurons. Moreover, there seems to be a correlation between a specific molecular subtype and its response to standard GBM treatment, with the Classical group having the best outcome and the Proneural group the worst⁶.

Table 2: Novel molecular-based GBM classification.

	Genotype and Expression Pattern	Transcriptome	miRNA expression pattern
Mesenchymal 35% of all GBM	17q11.2 hemizygous deletions (NF1) 7p amplification inducing EGFR and EGFRvIII over-expression	similar to normal astroglia	↑ miR21, miR17, miR10, miR9
Proneural 34% of all GBM (most of secondary GBM belong to this class)	TP53 LOH or mutations (54%) PDGFRA amplification on 4q12 IDH1 mutations PDGF alterations younger age of onset	similar to normal oligodendrocytes	↓ miR124, miR137, miR128, miR7
Classical 23% of all GBM	10q loss (expressing PTEN) 7p amplification inducing EGFR and EGFRvIII over-expression 9p21.3 deletions (CDKN2A/2B)	similar to normal astrocytes	
Neural 15% of all GBM	expression of neuronal markers (NEFL, GABRA1, SYT1, SLC12A5) 7p amplification inducing EGFR and EGFRvIII over-expression	similar to neurons	

The four sub-types of GBM show different genotypic alterations, but the same miRNA expression signature, including miR124 down-regulation.

Currently there are no effective therapies for GBM. The prognosis for patients diagnosed with the disease is usually very poor with an average survival of only 14 months after standard therapy. The standard therapy for GBM includes three steps that typically increase the lifespan of the patient by only of few months and have multiple side effects. First is surgery to remove as much as possible of the tumor mass and to provide diagnostic certainty. Second is radiotherapy to kill tumor cells through induction of DNA damage and apoptosis. Localized radiotherapy on the tumor bed has proven useful in increasing the lifespan of GBM patients without major

cognitive complications. Third is chemotherapy but the blood brain barrier (BBB) limits the number of compounds that can reach the brain. BCNU (1,3,bis(chloroethyl)-1 nitrosurea), Temozolomide (alkylating agent) and bevacizumab (an artificial antibody against VEGF) are currently used to treat GBM patients after surgery, in association with radiotherapy².

The limitations of the current GBM therapies clearly illustrate the need for a novel strategy to combat this very aggressive tumor. Oncolytic viruses represent a promising new approach to cancer therapy to be used alone or in combination with existing procedures.

1.2 Herpes Simplex Virus Type-1 (HSV-1) based Oncolytic Viruses (OVs) are a promising but still ineffective therapy against GBM

Oncolytic vectors (OVs) are attenuated lytic viruses designed to specifically replicate in tumor cells without affecting the surrounding normal tissue⁷. Herpes Simplex Virus Type-1 (HSV-1) is an attractive platform for the development of a GBM-specific OV because of its neurotropism, high efficiency of infection, and its ability to rapidly replicate in infected cells. HSV-1 infectivity is much higher than that of other viruses used to generate OVs in that a 1:1 ratio of the number of HSV-1 viral particles and the number of target cells is sufficient to infect 100% of the cells. Infectivity is much lower in the case of Vesicular Stomatitis Virus (VSV), which requires a ratio of 1:5000 between the number of host cells and viral particles to achieve efficient infection, or in the case of Adenovirus (AdV) where the effective ratio of cells to virus is 1:3000. Moreover, at least half of the very large, 152-kb genome of HSV-1 codes for functions that are not essential for viral propagation *in vitro* and can be deleted or modified without affecting the ability of the virus to quickly infect and spread. Lastly, several anti-herpetic drugs are readily available to keep oncolytic HSV (oHSV) replication under control in therapeutic applications⁸.

HSV-1 is a double-stranded DNA virus with a very wide host cell range. In many cells, once the virus enters, its lytic replication process begins, causing cell death and release of viral progeny as quickly as 10h after initial infection. The HSV-1 lytic cycle starts with the interaction between the viral essential glycoprotein gD and one of its receptors on the cell surface, followed by a signaling cascade that activates the two other essential glycoproteins gB and gH, both necessary to complete the fusion/entry process; the HSV-1 envelope and cell membrane fuse to allow entry of the viral DNA-containing capsid into the cytoplasm. To infect its target cell HSV-1 can use several different common receptors, including HVEM (HveA), Nectin-1 (HveC) and 3-O-sulfated heparan-sulfate^{9,10}. Virtually all cells express at least one of these receptors,

accounting for the broad host range of the virus. Upon entry into the cell, capsids inject the viral DNA into the nucleus where the replication process takes place. Newly synthesized viral DNA is assembled into new viral capsids in the nucleus, and then the DNA-containing capsids acquire new envelopes by nuclear membrane budding and further processing through the Golgi apparatus. The mature virus finally exits into the extracellular space by lysis of the infected cell¹¹⁻¹³. Only in sensory neurons HSV-1 can establish a latent state, characterized by silencing of lytic genes, expression of latency-specific RNAs (LATs) and persistence of the viral genome as an episome with no risk of insertional mutagenesis of the host genome. The HSV-1 genome is organized into a Unique Long (U_L) and a Unique Short (U_S) region, each flanked by inverted repeats (Figure 1)^{11,14,15}. The junction between the internal repeats is called the joint and contains one copy of the ICP0, ICP4 and γ 34.5 genes.

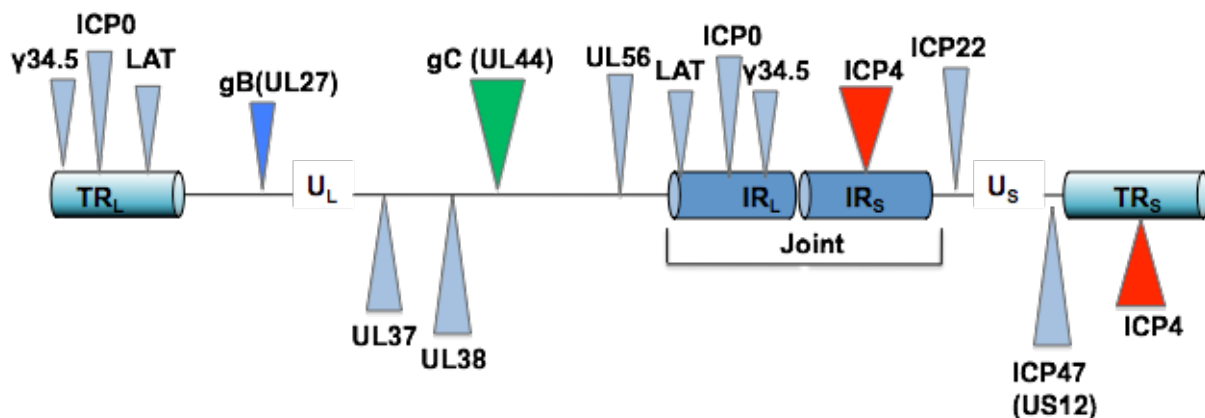


Figure 1: Organization of the HSV-1 genome.

The 152-kb HSV-1 genome is organized into a Unique Long (UL) and a Unique Short (US) regions, each flanked by inverted repeats, terminal (TR) and internal (IR). The region between UL and US, called the joint, consists of the two internal repeats and contains one copy each of the LAT, ICP0, ICP4 and γ 34.5 genes. The unique regions can flip back and forth, creating four possible HSV isomers. Here is depicted the isomer conventionally used to represent the HSV-1 genome. All most relevant genes for this study are depicted.

The unique regions can flip back and forth, creating four possible HSV isomers and making the HSV genome unstable and prone to internal recombination¹⁶. The viral genome codes for at least 84 proteins plus several untranslated transcripts. Its genes are expressed in a temporal cascade in which the five immediate early (α) genes that code for regulatory proteins (ICP0, ICP4, ICP27, ICP22, ICP47) are expressed first and drive the expression of early (β) genes, necessary for DNA replication, and late (γ) genes that code for structural proteins assembled

into viral particles. HSV-1 genes are also classified into essential and non-essential based on their requirement for viral growth *in vitro*. Only half of HSV-1 genes are absolutely necessary for viral reproduction both *in vitro* and *in vivo*. The remaining genes are mainly involved in virus-host interactions that allow the virus to overcome the natural defenses of the cell against infection *in vivo*^{11,15}.

One of the most common designs to create a tumor-specific oHSV takes advantage of the deletion of one or more of the non-essential genes that HSV-1 uses to block the cell's natural antiviral defenses. The result of the deletion is a replication-impaired vector that grows very poorly in normal cells but can replicate efficiently in cancer cells where these antiviral pathways are impaired or non-functional. Two different conditionally replication-defective oHSVs named HSV1716 and G207 have been tested in clinical trials on GBM patients while a third, named OncoVEX, is undergoing clinical trials on melanoma patients and a fourth, named NV1020, has been tested in clinical trials on metastatic colorectal cancer (CRC) patients (Table 3). Each of these has been shown to be safe for patients but evidence of anti-tumor efficacy has been sporadic^{2-4,17}.

Table 3: oHSV-1 in clinical trials.

<i>oHSV1716 (Δy34.5)</i>	<i>GBM patients</i>	Completed I-III phase	Well tolerated up to 1×10^5 p.f.u. per patient
<i>G207(Δy34.5, ΔICP6)</i>	<i>GBM patients</i>	Phase I completed -> OV too weak to effectively kill xenografts tumor models	Well tolerated up to 1×10^9 p.f.u. per patient
<i>OncoVEX (Δy34.5, ΔICP47, + GMCSF)</i>	<i>Melanoma patients</i>	Phase III started	Well tolerated. Shown some promising immuno-mediated antitumor effect
<i>NV1020 (Δjoint, ΔUL56, ΔUL24, restricted TK expression under ICP4 promoter)</i>	<i>CRC patients</i>	Phase II completed	Well tolerated. Slight increase in median survival of treated patients

Four replication-compromised oHSV-1 have been tested in clinical trials, the first two on GBM patients. All demonstrated to be safe for patients, but too attenuated to effectively overcome the tumor.

HSV1716 carries deletions of the *RL-1* gene encoding the γ 34.5 protein. This protein is normally expressed by the virus to overcome the activity of PKR, a kinase that is induced by the cells in response to infection or other forms of stress. Activated PKR phosphorylates the α subunit of the eIF2 translation initiation factor (eIF-2 α), causing a complete block of protein synthesis. Viral γ 34.5 works by activating PP1 phosphatase, that in turn dephosphorylates eIF-2 α and restarts protein synthesis necessary for the virus to complete its lytic cycle. A virus deleted for γ 34.5 cannot replicate in normal cells, but only in cells where the PKR pathway is compromised and non-functional, such as in tumor cells that typically exhibit constitutive activation of the PKR-inhibiting EGFR/Ras/MEK pathway. HSV1716 showed promising results in phase I-III clinical trials. Up to 10^5 infectious units were injected in 12 patients bearing either newly diagnosed or recurrent high grade malignant glioma and were well tolerated, exhibiting no sign of toxicity in the normal tissue surrounding the tumor and showing some evidence of efficacy by increasing the life span of a few patients (respectively 15, 18 and 22 months of life after GBM diagnosis, in three patients) when combined with classical chemo- and radiotherapy after tumor surgery. However, tumor eradication was not observed and none of the patients were cured.^{2,4,18-20}.

G207 is a doubly attenuated vector created to increase tumor specificity and safety for the normal brain by deleting the *UL39* viral gene in addition to both copies of *RL-1*. *UL39* encodes the ICP6 protein, the viral counterpart of the large subunit of mammalian ribonucleotide reductase (RR), an enzyme required for the de-novo synthesis of dNTPs essential for DNA replication. The virus requires ICP6 to infect post-mitotic cells like neurons, where DNA is not replicated and cellular RR is not expressed. In the absence of ICP6 the virus can only infect mitotic cells, such as cancer cells where RR is usually overexpressed because of the constitutive activation of the Rb/p16/EF2 pathway. Thus a virus deleted for both γ 34.5 and ICP6 will grow only in cells that do not express PKR but overexpress RR, a common phenotype of GBM cells but not of normal cells.²¹ G207 has been tested in primates in preclinical studies and in phase I studies on patients with grade IV GBM. The vector was shown to be safe for patients at doses as high as 10^9 infectious particles, much higher than those used with HSV1716.²¹ However, anti-tumor efficacy studies performed by intra-tumor injection of G207 into highly invasive GBM xenografts derived from patient biopsies showed that despite some anti-tumoral effect, specifically a reduction in tumor volume, G207 did not significantly improve animal survival compared to other treatments, indicating that this oHSV had no clinical efficacy by itself.^{22,23}

OncoVEX is a oHSV recently entered into clinical trials for melanoma. It is a doubly attenuated virus that carries deletions of both γ 34.5 and ICP47 along with insertion of a GM-CSF expression cassette. GM-CSF is an immunostimulatory molecule whose expression enhances the tumor-specific immune response against tumor antigens released after lytic replication of the virus, as demonstrated in mouse models. This vector has completed a Phase II clinical study where it was injected into accessible melanoma lesions, resulting in the regression of the injected lesions as a direct oncolytic effect and in the regression of the non-injected lesions as a secondary immune-mediated antitumor effect in 28% of treated patients. A Phase III clinical trial on patients with grades III and IV unresectable melanoma has recently started^{2,3,24}

NV1020 is an attenuated, joint-deleted oHSV vector with only one copy of the *ICP0*, *ICP4* and γ 34.5 genes normally present in two copies in the HSV1 genome. The vector also carries deletions of the *UL24* and *UL56* non-essential genes and expresses the *TK* gene with immediate-early kinetics from the *ICP4* promoter. This set of mutations makes the virus very attenuated and able to grow only in malignant cells that can complement the activities of the deleted viral genes, but not in normal quiescent cells²⁵. NV1020 has completed Phase I and II clinical trials on patients with refractory metastatic colorectal cancer (mCRC) of the liver²⁶. The virus was shown to be safe for the patients at a concentration of up to 1×10^8 infectious units without major adverse effects and demonstrated some effectiveness in reducing tumor size after chemotherapy and in increasing the median survival of the treated patients. A Phase III clinical trial for this virus has been proposed¹⁷.

Despite being safe for patients and showing some tumor killing ability, the oHSV tested so far in clinical trials are too attenuated to efficiently replicate in GBM and eradicate the tumor in the affected patients. To obtain a more effective oHSV that can grow and efficiently kill only tumor cells without affecting the surrounding normal tissue, I created a different kind of vector that is not deleted for any of its genes, but in which the expression of ICP4, one of its essential genes, is controlled by miR124, a neuronal-specific miRNA that is highly expressed in normal brain but not in GBM.

1.3 MiR124 absence is specific for GBM cells

Micro (mi)RNAs, short ~21-23 nucleotide-long non-coding RNAs, are key regulators of almost every cellular pathway in protozoa, metazoa and plants that function by post-transcriptionally repressing gene expression at the mRNA level.

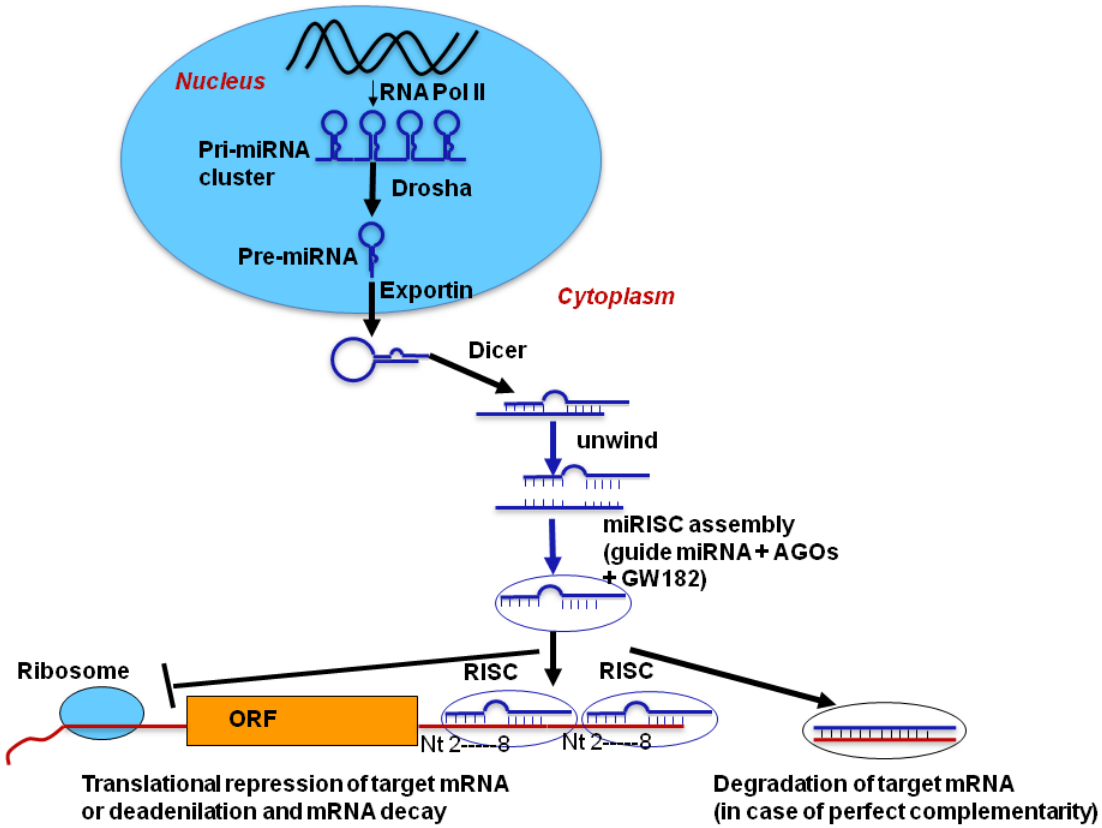


Figure 2: MicroRNAs biosynthesis.

MiRNAs are short ~21-23 nucleotide-long non-coding RNAs that function by post-transcriptionally repressing gene expression at the mRNA level. MiRNAs work in the form of miRISCs, ribonucleoprotein complexes comprised of the guide miRNA strand and several proteins of which AGOs and GW182 are the best-known components. In animals, the main mechanism of interaction between miRNA loaded on the miRISC and its target mRNA involves inexact base-pairing between the two molecules. After recognition of its target mRNA, the miRISC works either by directly inhibiting mRNA translation or by inducing mRNA deadenylation and consequent degradation. Another mechanism of miRNA-mediated mRNA silencing typical of plants but very rare in animals involves exact base-pairing between the entire miRNA and the 3'UTR of its target mRNA that induces mRNA degradation through an endonucleolytic mechanism typical of RNAi.

MiRNAs work in the form of miRISCs (Figure 2), ribonucleoprotein complexes comprised of the guide miRNA strand and several proteins of which AGOs and GW182 (glycine-trypophan protein of 182 kd) are the best-known components^{27,28}. In animals, the main mechanism of interaction between miRNA loaded on the miRISC and its target mRNA involves inexact base-pairing between the two molecules. In fact, the only requirement for an miRNA to work is perfect homology between its seed sequence, the nucleotide stretch between positions 2 and 8, and a complementary region usually in the 3'UTR of the target mRNA²⁹. This characteristic not only allows for the regulation of multiple mRNAs by a single miRNA, but also for the regulation of a

single mRNA by different miRNAs, fine-tuning cell gene expression and increasing the complexity of the system. After recognition of its target mRNA, the miRISC works either by directly inhibiting mRNA translation or by inducing mRNA deadenylation and consequent degradation. There is another mechanism of miRNA-mediated mRNA silencing that is typical of plants but occurs very rarely in animals. In this case, base-pairing between the miRNA and the 3'UTR of its target mRNA is perfect along the entire 20-22 nucleotide length of the miRNA and induces mRNA degradation through an endonucleolytic mechanism typical of RNAi^{30,31}.

According to the miRBase database, 1527 precursors and 1921 mature human miRNAs had been discovered by Nov 2011. Most of these miRNAs are expressed in a tissue-dependent and developmental stage-dependent manner, contributing to the diversity of protein expression in different organs and during different life stages.

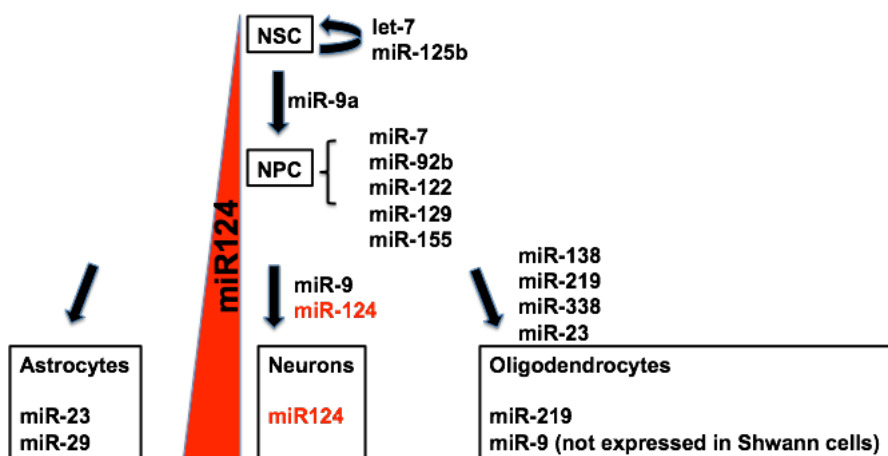


Figure 3: MiRNAs involved in the development of the Central Nervous System (CNS).

During neuronal development, pluripotent embryonic stem cells (ESCs) gradually differentiate first into multipotent neural stem cells (NSCs), then into lineage-specific neuronal progenitors (NPCs), and then into mature neurons and glia (oligodendrocytes and astrocytes). This complex process occurs through a combination of internal and external signaling pathways in which miRNAs play an essential role. MiR124 is a key player in neurogenesis being gradually upregulated during neuronal differentiation. In the mature brain, miR124 is expressed in virtually all post-mitotic neurons but not in glial cells, NPCs or NSCs.

MiR124 is the most abundant miRNA of the adult mammalian central nervous system (CNS), accounting for 25-48% of all miRNAs present in the brain³². The CNS is composed primarily of neurons and glia. During neuronal development, pluripotent embryonic stem cells (ESCs) gradually differentiate first into multipotent neural stem cells (NSCs), then into lineage-specific neuronal progenitors (NPCs), and then into mature neurons and glia. This complex

process occurs through a combination of internal and external signaling pathways in which miRNAs play an essential role³³. As illustrated in Figure 3, miR124 is a key player of neurogenesis being gradually upregulated during neuronal differentiation not only in humans but also in many other species from nematodes to zebrafishes to chicks to mice³⁴. The miR124 stem loop sequence is, in fact, well conserved from nematodes to primates. In the mature brain, miR124 is expressed in virtually all post-mitotic neurons but not in glial cells, NPCs or NSCs^{33,35-37}.

Several *in vitro* studies have shown that overexpression of miR124 in non-neuronal cells like HeLa cells³⁸ or ESCs³⁹ can induce a shift toward neuronal differentiation. Moreover, it has been reported that miR124 is directly involved in modulating the transition from NPCs to mature neurons. During this process the factor RE-1 Silencing Transcription Factor (REST), a negative regulator of *mir124* gene expression, is gradually lost, inducing the upregulation of miR124. MiR124 in turn inhibits the expression of non-neuronal genes⁴⁰ like *SCP1* (small C terminal phosphatase-1), a component of the REST transcription complex, *SOX9* (SRY-box transcription factor), involved in glial cell specification by controlling glial-gene expression in the CNS, *CDK6* (cyclin dependent kinase-6), involved in the cell cycle G1/S transition, and *PTBP1* (polypyrimidine tract binding protein-1), an inhibitor of neuronal specific alternative splicing that allows the expression of neuronal genes to prevail^{41,42}. MiR124 is also important for determining the fate of CNS-cells other than neurons⁴³. It has been demonstrated that in a population of NPCs, miR124 overexpression decreases the rate of glial cell formation by reducing the amount of phosphorylated STAT3, a very important transducer of glial cell differentiation⁴⁴. Human miR124 is encoded by three genes located on three different chromosomes and found often epigenetically silenced through hypermethylation in several precancerous lesions and in different types of leukemia, lymphoma and brain, colon, breast and lung cancer^{45,46}. In particular, miR124 is significantly downregulated in anaplastic astrocytomas (AA WHO grade III) and Glioblastoma Multiforme (GBM WHO grade IV) relative to non-neoplastic tissue, while being 8- to 20-times upregulated during differentiation of cultured mouse NSCs³⁷. Transfection of miR124 into mouse-derived NSCs and mouse and human-derived GBM primary cells has been shown to induce morphological changes consistent with neuronal differentiation. Transfection of miR124 into GBM cell lines U251 and U87 has been shown to induce neuronal differentiation through cell cycle arrest in G1, associated with the downregulation of CDK6 and pRB, both substrates of miR124 post-transcriptional silencing, meaning that expression of miR124 in GBM is incompatible with maintenance of the tumor phenotype and viability^{42,43}.

The lack of current effective therapies for Glioblastoma Multiforme indicates an urgent need for innovative approaches to fight this very aggressive cancer. While existing HSV-based replication-impaired OVs have been shown in clinical trials to be safe for GBM patients at relatively high doses, they are not sufficiently effective to offer a significant benefit to the affected patients. In this study I describe the creation of a novel miR124-regulated replication-competent oncolytic vector called ICP4-miR124t that is able to specifically kill GBM cells without affecting the surrounding normal tissue by taking advantage of the consistent tumor-specific downregulation of miR124 compared to normal brain. An attractive aspect of this strategy is that GBM cells cannot up-regulate miR124, causing resistance to the virus, without losing their malignant phenotype and viability⁴³, thus excluding the possibility of tumor-cell escape from the treatment. In addition, unlike the existing oHSVs, ICP4-miR124t maintains the full complement of viral genes and is therefore able to grow like an unregulated virus in permissive cells that lack miR124. The results of this study indicate that ICP4-miR124t is indeed both selective for the tumor where it maintains its full replication efficiency and non-toxic when injected at high doses into the brains of healthy mice where its replication is repressed. Thus a miR124-controlled oHSV could potentially be a safe and effective therapeutic tool against GBM.

2 METHODS

2.1 Cell lines

All cells utilized in this study were maintained at 37°C with 5% CO₂

Vero African Green Monkey Kidney (CCL-81), U2OS Human Osteosarcoma (HTB-96), HEK 293T/17 Human Epithelial Kidney (CRL-11268) and U87 Human Grade IV Glioblastoma immortalized adherent cell lines were purchased from ATCC (Manassas, VA) and grown in Dulbecco's Modified Minimum Essential Medium (DMEM, HyClone) with 10% Fetal Bovine Serum (FBS, Sigma), 2 mM L-glutamine (Cellgro), 100 U/mL Penicillin (Cellgro), and 100 µg/ml Streptomycin (Cellgro).

SHSY5Y Human Neuroblastoma-derived immortalized adherent cells, generously donated by E.A. Chiocca (Ohio State University), were grown in 1:1 mixture of MEM and F12 medium with 10% FBS (Sigma), 0.1 mM Nonessential amino acids (NEAA, Cellgro), 100 U/mL Penicillin (Cellgro), and 100 µg/ml Streptomycin (Cellgro).

50B11 (Rat-Dorsal Root Ganglia-derived) immortalized adherent cells, generously donated by Dr A. Hoke (Johns Hopkins University, Baltimore, MD, USA)⁴⁷, were grown in Neurobasal medium (Gibco) with 10% FBS (Sigma), 2% B27 supplement (Gibco), 20% glucose (Sigma), 1 mg/ml blasticidin (Lonza), and 2 mM L-glutamine (Cellgro). To induce differentiation, cells were maintained in growth medium with 75 µM Forskolin (Sigma) for 24-48 h⁴⁷.

PC12 (rat pheochromocytoma) cells were grown in DMEM (HyClone) plus 5% FBS (Sigma) and 10% Horse serum (HS), 2 mM L-glutamine (Cellgro), 100 U/mL Penicillin, 100 µg/ml streptomycin, Pen/Strep (Cellgro). To induce differentiation, cells were maintained in growth medium with 1% serum and 50 ng of 2.5s Nerve Growth Factor (NGF) (Sigma) until cells showed neuronal-like phenotype⁴⁸.

GBM30 and Gli68 patient-derived primary glioma spheroids lines, generously donated by E.A. Chiocca (Ohio State University), were grown in Neurobasal medium (Gibco) plus 2% B27 w/o vitamin A, 2 mg/ml amphotericin (Lonza), 100 µg/ml gentamycin (Lonza), 2 mM L-glutamine (Cellgro), plus 10 ng/ml Recombinant Human Epidermal Growth Factor (EGF) (Shenandoah Biotechnology) and 10 ng/ml Human Recombinant Basic Fibroblast Growth Factor βFGF (Shenandoah Biotechnology).

2.2 HSV-1 infection on U2OS and VERO cells

2.2.1 Infection to test viral growth

Vero and U2OS cells were the two established immortalized adherent cell lines routinely used in our laboratory to test viral growth. The day before infection cells were plated as a 70% confluent monolayer. 24 h later 100% confluent wells were infected at an established multiplicity of infection (MOI) in serum free media and incubated at 37°C in 5% CO₂. 2 h after the infection each well was overlaid with DMEM plus 10% FBS and maintained at 33°C in 5% CO₂, a condition that does not interfere with viral growth but stops cells from becoming over-confluent in the plate. At different time-points after initial infection, viral supernatant was collected and titered to quantify viral yield.

2.2.2 High scale viral production

In order to have enough virus to perform both *in vitro* and *in vivo* experiments all viruses used in this study were grown to high titer on U2OS. 24 h before infection U2OS were plated as a 50% confluent monolayer on T150 tissue culture flasks (6 T150 flasks per virus). The day of infection, 100% confluent U2OS were infected with a MOI=0.001 as previously illustrated (see section 2.2.1). 72-96 h after infection, flasks were treated with 5 M NaCl solution to a final concentration of 0.45% to detach the virus from cell membranes and incubated for 30' at RT while slowly shaking. Following Sodium-Chloride (NaCl) treatment both cells and supernatant were collected, sonicated using the Ultrasonic Processor XL sonicator (Misonix Inc.) to free the virus still trapped inside cells and then cleaned from cellular debris through centrifugation at 3000 revolutions per minute (rpm) for 10' followed by filtration through a 0.8 um Versapor filtering membrane (PALL Corporation). The clean viral supernatant was then concentrated by 19,000 rpm centrifugation for 30-45' and the viral pellet resuspended in the minimum possible volume of a 10% Glycerol solution in 1X Phosphate-Buffered-Saline (PBS) by slow overnight shaking at 4°C. The resulting concentrated virus was divided in 10 ul aliquots and stored at -80°C. One aliquot was used for titration in U2OS as described in section 2.2.3.

2.2.3 Viral titration in plaques forming units (p.f.u /ml)

Titration of viral supernatant was performed through infection of a 48 well of either Vero or U2OS with serial 10-fold dilutions of viral supernatant. The day before infection cells were plated as a monolayer on a 48 well dish at a density of 0.8×10^5 cells/well for Vero and 1.5×10^5 cells/well for U2OS. 24 h later cells were infected with serial 10-fold dilutions of each supernatant in 120 μ l of serum-free media and incubated at 37°C in 5% CO₂. 2 h after the infection each well was overlaid with 120 μ l of growth media plus 5% methylcellulose and maintained at 33°C in 5% CO₂. 72-96 h after infection methylcellulose containing supernatant was removed and plates were washed with PBS and incubated for 2 h at room-temperature (RT) in a crystal-violet solution (50% Methanol, 0.1% Crystal-Violet) to stain viral plaques. The staining solution was then removed and each well washed twice with water and allowed to dry. Live cells stained purple; dead cells from viral infection resulted in clear plaques that were counted with an inverted microscope. The titer results were then calculated in p.f.u /ml (plaque forming units per ml of viral preparation). Triplicates were used for statistical analysis.

2.2.4 Viral titration in Viral Genome Copy Number calculated by qPCR

In order to perform in vivo experiments, viral titers calculated in p.f.u /ml, as described in section 2.2.3, were converted into gc /ml through qPCR. Two separated aliquots of virus prepared as described in section 2.2.2 were processed to extract viral DNA using DNAeasy Blood and Tissue Kit (QIAGEN) according to the manufacturer's instructions. qPCR was performed using the StepOne Plus Real Time PCR System (Applied Biosystem) with customized primers (gD-F and gD-R from Applied Biosystems) and probe (FAM-TAMRA TaqMan Probe from Applied Biosystems) for the HSV glycoprotein D (gD) gene (see primer table). The values were then compared to the known number of copies of a pEntr-gD DNA plasmid present in a midi DNA plasmid preparation obtained using the DNAeasy Blood and Tissue Kit (QIAGEN) according to the manufacturer's instructions. The pEntr-gD construct had been previously created in the laboratory by cloning the entire gD gene between two EcoRI restriction sites in the pEntr1A vector (Invitrogen). Viral genome copies were quantified based on a standard curve calculated according to the manufacturer's instructions by qPCR amplification of serial 10-fold dilutions of the pEntr-gD plasmid of known concentration (Standard Curve Method from Applied Biosystems).

2.3 Polymerase Chain Reaction

Table 4: PCR primers used.

	Primer F	Primer R
gD qPCR customized primers to quantify oHSV genome copy number (Section 2.2.4)	gD-Fwr 5'CCCCGCTGAACTACTATGACA3'	gD-Rev 5'GCATCAGGAACCCAGGTT3'
gD qPCR customized TAMRA probe (Section 2.2.4)	gD-Probe TTCAGGCCGTCAAGCGAGGA	
5' Phosphorylated oligos to generate pLuc-124T construct (Section 2.4)	T124-F: 5'PactagtGGCATTACCGCGTGCC TTAtagtaccagGGCATTACCGCGTGCC TAaggatctGGCATTACCGCGTGCC atgactgcGGCATTACCGCGTGCC atgct3'	T124-R: 5'agctcaTAAGGCACGCCGGTGAATGCC gcagtcTAAGGCACGCCGGTGAATGCC tccTAAGGCACGCCGGTGAATGCC TAAGGCACGCCGGTGAATGCC actgt3'
5' Phosphorylated oligos to generate pLuc-Con construct (Section 2.5)	Tcon-F: 5'PactagtATCGAATAGTCTGACTAC AACTtagtaccagATCGAATAGTCTGACTA CAAATaggatctATCGAATAGTCTGACTA CAAATtgactgcATCGAATAGTCTGACTA CAAATctcgagct3'	Tcon-R: 5'agctcgAGTTGTAGTCAGACTATT CGATgcgcgtcatAGTTGTAGTCAGACTATT ATaggatctAGTTGTAGTCAGACTATT ctggactaAGTTGTAGTCAGACTATT tagt3'
Amplification of CS cassette to target gC (Section 2.7.1)	gC-CS F: 5'gcaatcgtgtacgtcgccgacatcacagt cgccagcgtcatggcgGGCCTGGTGATGAT GGCGGGATCG3'	gC-CS R: 5'gagggggacaaactataatagatataaaa aacgggggggtctcgcgTCAGAAGAACTCGTCA AGAAGGGC3'
Diagnostic PCR to check CS cassette insertion and excision in gC (Section 2.7.1)	gC F: 5'atgacgtggaccgcgactcc 3'	gC R: 5'cgccgcaatgtacacaactccc3'
Amplification of eGFP with T2A (Section 2.7.1)	T2A-eGFP-F: 5'GAGGGCAGAGGAAGTCTGCTAA CATGCGGTGACGTCGAGGAGAAC GGCCCAatggtagcaaggcgagga3'	gC-eGFP-R : 5'gagggggacaaactataatagatataaaa aacgggggggtctcgcgTTACTTGACAGCTCGT CC3'
Amplification of T2-eGFP to target gC (Section 2.7.1)	gC-T2A-F: 5'gcaatcgtgtacgtcgccgacatcacagt cgccagcgtcatggcgGAGGGCAGAGGAAGTC TG CTA3'	gC-eGFP-R: 5'gagggggacaaactataatagatataaaa aggtaacg gggggtctcgcgTTACTTGACAGCTCGTCC3'
	Primer F	Primer R
5' Phosphorylated oligos to generate ICP4-4xT124-ICel-Kan-pEntr1A construct (Section 2.7.2.1 step 1)	ICP4 Oligo F: 5'Paagtgtggactgggaaggcgccctggac GAAGACGACGGCGGGTTCGA3'	ICP4 Oligo R: 5'PaattACTAGTttacagcaccccgccccTC <u>GAACGCGCCGCCGTCGTCTTC3'</u>
Amplification of pL-124-ICP4 to	ICP4-F: 5'aagtgtggactgggaaggcgccctggacG	ICP4-R: 5'gctactgcaaaacttaatcagggttgtgcccgtatttg

Table 4: continued

include ICP4polyA after 4x124 element (Section 2.7.2.1 step 4)	AAGACGACGGCGGCCTCGA3'	cgtcttcgggcGAGCTCAAGGCACGCGGTGA ATGCCGCAG3'
Amplification of I-SceI-kan selection cassette to insert flanking direct repeats Section 2.7.2.1 step 7)	I-SceI-Kan-F: 5'taatGAGCTCtaatCGGGCCGtaatATCT ATGTCGGGTGCGGAGAAAGAGGtaatga aatggcaaggatgcgacqa <u>TAAGTAGGGATAA CAGGGTAA3'</u>	I-SceI-Kan-R: <u>5'taatGAGCTCtaatCGGGCCGtaatTGCCAT TTCATTACCTTTCTCCGCACCCCGACA TAGAT</u> caaccaattaaccaattctgattag3'
Amplification of 4xT124 cassette to target ICP4 (Section 2.7.3)	ICP4-F: 5'aagtgtggactggaaaggcgctggacgaaac gacggcggcggtcga3'	ICP4-R: 5'gctactgaaaacttaatcagggttgtccgTTTATTgc gtcttcgggtc3'
Diagnostic PCR to check for correct Cre-mediated excision of the BAC (Section 2.7.5)	UL37-F: 5'CAATAGGCGCTGCATAGGTC 3'	UL38-R: 5'TTCATTGCGACCCCAGAT3'
Amplification of rtTA gene from pgk-rtTA-Sv40polyA (Section 2.8.2 step 1)	BrtTA-F: 5'GAAGATCTatgtctagactggacaagag caaa 3'	NrtTA-R: 5'GCGGCCGCAAttaccggggagcatgtca agg3'
Amplification of Human Pri-miR124 from U87 total DNA (section 2.8.2 step 2)	BmiR124-F: 5'tcgaGGATCCtgcgtgcgcacgcacac 3'	NmiR124-R: 5'tgcaGCTAGCcagaccctccccctcg3'
Amplification of Puro gene from pCDH-CMV-EF1 (Section 2.9.1 step 1)	X-Puro-F: 5'atataatCTAGAatgaccgagtacaagcccac3'	XS-Puro-R: 5'tatatatataatctagaggtagccgtcactcaggcacccgggt tg3'
Amplification of pri-miR137 from U87 total DNA (section 2.9.2)	NmiR137-F: 5'tcgaggatccAAACACCCGAGGAAA TGAAAAG3'	BmiR137-R: 5'tcgagctgcGCTCAGCGAGCAGCAA GAGTTC3'

DNA fragments for subcloning were amplified by Polymerase Chain Reaction (PCR) using either High Fidelity Accuprime PFX DNA Polymerase (Invitrogen) or High Fidelity Accuprime GC-rich DNA Polymerase (Invitrogen). Routine analytical PCR for detection of an amplification product or estimation of a product size was performed using Go-Taq (Promega) according to the manufacturer's instructions. Listed in table 4 are the PCR primers utilized to generate the different constructs.

2.4 Cloning techniques

Listed in table 5 all the constructs described in this study.

Table 5: DNA constructs generated in this study.

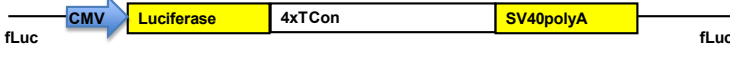
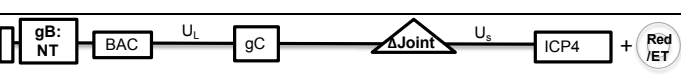
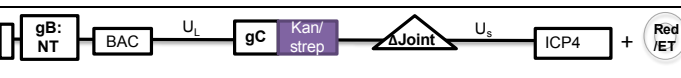
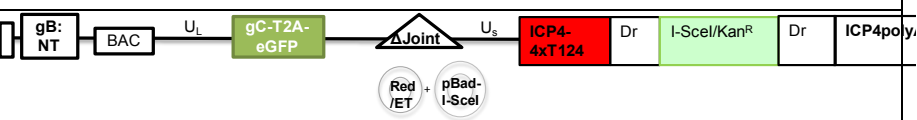
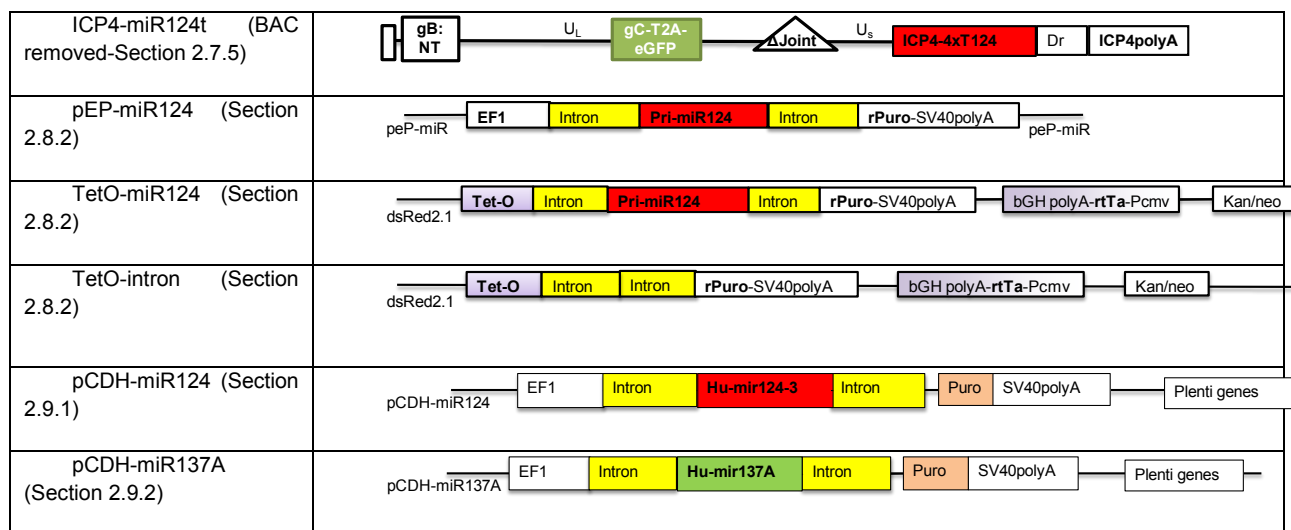
pLuc-T124 (Section 2.5)	
pLuc-Tcon (Section 2.5)	
KB (Section 2.7)	
KBJ (Section 2.7)	
KBBJ (Section 2.7)	
KBBJ-R (Section 2.7.1)	
gC-cs R (Section 2.7.1)	
KBBJ-gC-cs R (Section 2.7.1)	
T2A-eGFP R (Section 2.7.1)	
gC-T2A-eGFP R (Section 2.7.1)	
KBG (Section 2.7.1)	
pEntr-ICP4-T124-kan (Section 2.7.2.1)	
KBG-R (Section 2.7.2.2)	
KBG-ICP4-miR124t-kan plus pRed/ET and pBad (Section 2.7.2.2)	
ICP4-miR124t-BAC (Section 2.7.2.2)	
KG (BAC removed-Section 2.7.5)	

Table 5: continued

2.4.1 DNA restriction digest and purification from agarose gel

Plasmids and PCR products were restriction-digested at 37°C for 1 h, run on a 1% agarose 0.001% Ethidium Bromide (EtBr) gel, and gel purified using the QIAEXII Gel extraction kit (QIAGEN) according to manufacturer's instructions.

2.4.2 Ligation of DNA fragments and transformation of competent bacteria

Linearized vector backbones and DNA inserts were ligated together at a 1:7 backbone: insert ratio using T4 DNA ligase (NEB) according to manufacturer's instructions and incubated at 16°C overnight.

2.4.3 Transformation of competent bacteria cells

Ligation products were transformed into DH10β competent bacteria (NEB) according to the manufacturer's instructions, plated on Luria-Broth (LB) agar plates (1% NaCl, 1% Bacto-Trypton, 0.5% Yeast-Extract, 0.02% NaOH, 1.5% agar) containing the appropriate selection drug and incubated overnight at 37°C.

2.4.4 DNA extraction for screening of transformed bacteria colonies

Transformed bacteria colonies grown on agar plates were picked, expanded overnight in LB broth (1% NaCl, 1% Bacto-Trypton, 0.5% Yeast-Extract, 0.02% NaOH) plus the appropriate selection drug and processed to extract plasmid DNA using the QIAprep Spin Miniprep Kit (QIAGEN) according the manufacturer's instructions.

2.5 Engineering of a firefly-Luciferase expression plasmid carrying the miR124 responsive element, 4xTmiR124

MiRBase (http://www.mirbase.org/cgi-bin/mirna_entry.pl?acc=MI0000443), a miRNA online database, was used to obtain the miR124 target sequence. The miR124-target utilized as a template was a miR124-perfect match to promote degradation of the target mRNA, instead of its translational inhibition. A miR124 responsive element (4xT124) was designed so that four copies of the 22- nucleotides (nt) long miR124 target sequence, each separated from the next by a different 7- or 8- nt random spacer were inserted into the 3' untranslated region (UTR) of the luciferase reporter gene in a firefly-Luciferase (fLuc) expression plasmid (pMIR-Report Luciferase-Promega) as shown in Figure 4. The resulting plasmid was called pLuc-T124. This design has been shown to maximize the effect of the miRNA on the fLuc target gene while minimizing the risk of internal recombination between target sequences⁴⁹⁻⁵². To be used as control, a similar construct called pLuc-Tcon was created using a tandem of four copies of a random miR target sequence (Tcon) that didn't respond to miR124 (Figure 4). To generate pLuc-T124 and pLuc-Tcon constructs, both miR124 and Con responsive elements were designed and purchased as single-stranded 5'-phosphorylated DNA oligonucleotides (oligos) carrying a Spel restriction site at the 5' end and a SacI restriction site at the 3' end. Each oligo was dissolved in water to a final concentration of 3 µg/µl. 1 µl of each oligo was added to 48 µl of annealing buffer (10 mM Tris pH 7.5-8.0, 50 mM NaCl, 1mM TE) and incubated at 95°C for 4', shifted to 70°C for 10' and then shifted to room temperature (RT) for 30' and stored at 4°C. The annealed oligos and pLuc expression plasmid were digested with Spel and SacI (NEB, New England Biolabs) at 37°C for 1 h and gel purified. The linear pLuc backbone was then ligated to each of the annealed oligos and the ligation product was transformed into DH10β competent bacteria (NEB) and selected on LB Ampicillin (amp) (100 µg/ml) agar plates. Amp-resistant colonies were finally screened for correct insertion of either 4xT124 or Tcon oligos by

diagnostic digestion with BamHI, a restriction site present in the inserted fragment. One positive clone was selected for both pLuc-T124 and pLuc-Tcon. Both construct are illustrated in table 4.

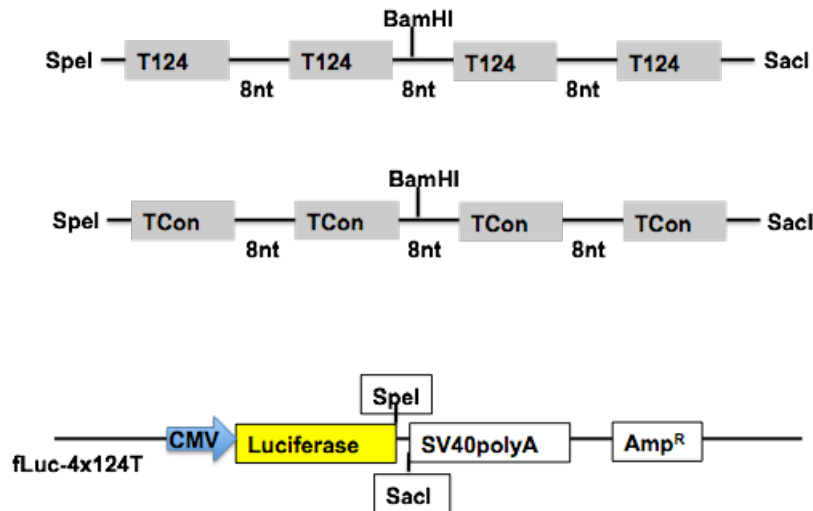


Figure 4: Design of a miR124-controlled Luciferase construct.

A tandem of four 20-nucleotides long miR124 target sequences, each separated from the next by a unique 8 nucleotides spacer (4xT124) was inserted in the 3'UTR of the fLuc reporter gene to create the pLuc-T124 construct. Similarly, a control sequence (Tcon) designed using a random miR target sequence non-responsive to miR124 was inserted in the 3'UTR of the fLuc reporter gene to create the pLuc-Tcon control construct.

2.6 Analysis of MiR124 activity on the 4xT124 response element

To verify that the presence of miR124 effectively blocked luciferase activity in the pLuc-4xmiR124t plasmid and not in the pLuc-Con control, U2OS and HEK293AD cells, which do not express miR124 according to the miRNA.org official website, were transfected with either a pre-miR124 (Ambion AM17100) or a pre-miR21 (Ambion AM17120) as negative control using siPORT-NeoFX transfection agent (Ambion) according to the manufacturer's instructions. Transfection of these synthetic ready-to use double stranded miRNA-mimics resulted in transient production of the desired miRNAs. 24 h post pre-miRNA transfection, the cells were co-transfected with a 1:1 combination of either pLuc-T124 + a renilla luciferase (rLuc) reporter plasmid (pRL-CMV, Promega) or pLuc-con + pRL-CMV using Lipofectamine 2000 transfection reagent (Invitrogen) according to the manifaturer's instructions. 48 h after the second transfection, cells where collected, lysed using a 5X luciferase lysis reagent (Promega) and both

Firefly and Renilla luciferase activities in cell lysates were measured by injecting 100 µl of either Firefly or Renilla luciferase assay buffers (Promega) on 10 µl of total cell lysate using a single-tube luminometer (AutoLumat LB953-EG&G Berthold). Luciferase values (measured on Firefly light units or Flu) were then normalized to Renilla values (measured on Renilla light units or Rlu). Each measurement was done in triplicate to obtain statistically significant results.

2.7 Engineering of the HSV-1 Genome

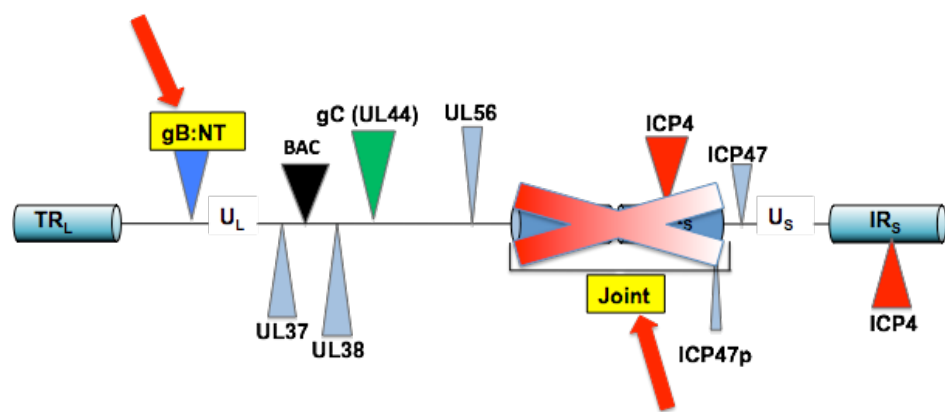


Figure 5: Organization of the KBBJ genome.

The deletion of the joint freezes the HSV genome as one of its isomers with a flipped Us region compared to the isomer conventionally used to represent the HSV-1 genome. The complete deletion of the joint eliminates one copy each of the LAT, ICP0, ICP4 and γ 34.5 genes plus the promoter of ICP47. However the deletion stabilizes the vector against internal recombination events and facilitates accurate engineering without affecting the virus ability to replicate and kill tumor cells in vitro. The region of insertion of the BAC between UL37 and UL38 is depicted as well as the enhancing gB:NT modification in UL27.

To generate the ICP4-miR124t HSV vector, I engineered a modified version, called KBBJ (Figure 5) of a bacterial artificial chromosome (BAC) containing the HSV-1 genome from the strain KOS (KB), originally donated to our lab by Dr. D.A. Leib⁵³. As part of a BAC the HSV-1 genome can autonomously replicate in bacteria, rendering site-specific manipulations easier than in the past. The BAC sequences were located between *loxP* recombination sites in the UL37/UL38 intergenic region of the HSV-1 genome and could therefore be excised by Cre recombinase^{54,55} to eliminate potential negative effects of these sequences on viral replication. In addition to the BAC elements, the region between the two *loxP* sites contained a chloramphenicol-selection gene (CM) to select CM resistant bacteria during BAC modifications, and a *lacZ* reporter gene under control of the SV40 promoter that can be used as marker in eukaryotic cells to detect the presence of the BAC³⁵. All changes to KB and its derivatives were

performed in DH10 β competent bacteria (NEB) using either the Red/ET recombination protocol (Gene Bridges) or a pBad/I-SceI modification adapted in our laboratory from Tischer et al.⁵⁶. The KBBJ vector was previously created in the laboratory by modifying the original KB vector in two locations. KB was first engineered to carry a deletion in the internal repeat region (joint) between UL56 and US12. The deletion of the joint left one copy of each of the HSV-1 diploid *ICP0*, *ICP4* and γ 34.5 genes and deleted the promoter of ICP47, possibly interfering with ICP47 gene expression. However, the deletion of the joint also stabilized the vector against internal recombination events by freezing the HSV genome as one of its isomers. This modification greatly facilitated accurate engineering of the viral genome without affecting virus ability to replicate and kill tumor cells in vitro.

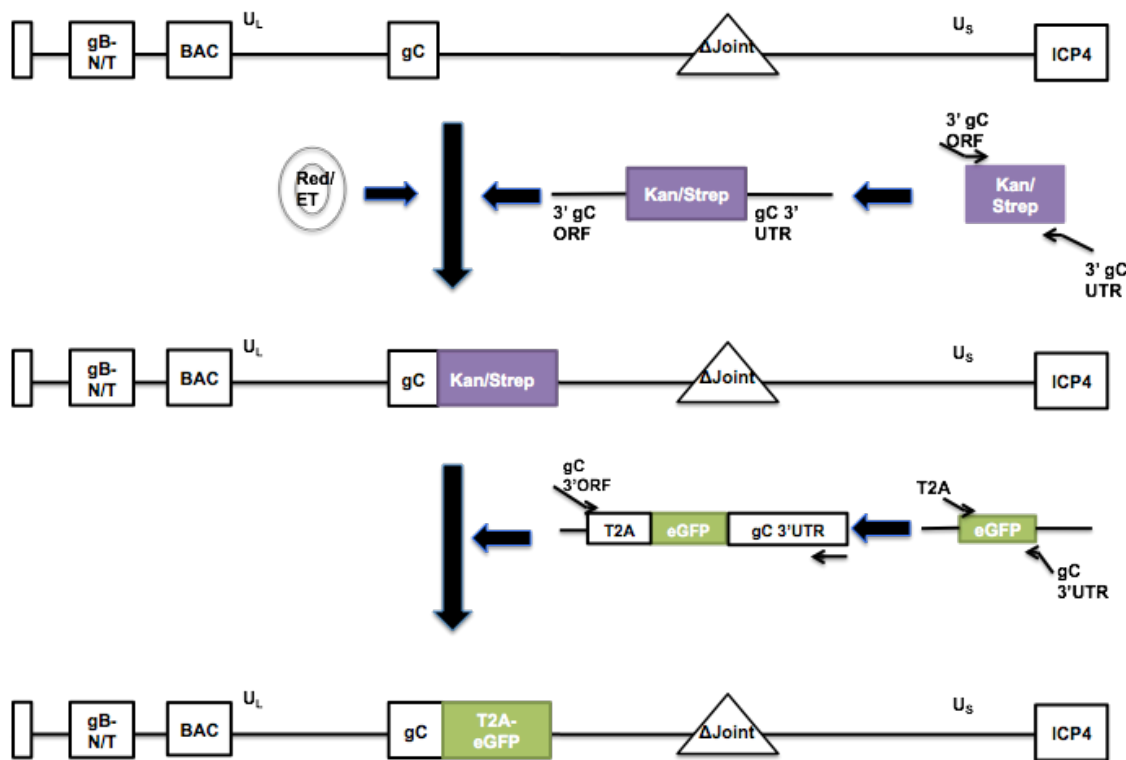


Figure 6: Two steps Gene-Bridges Red/ET temperature-shift-mediated recombination in gC locus.
 Modification of gC using Gene-Bridges Red/ET recombination strategy showing the two steps of Red/ET temperature-shift-mediated recombination in the gC locus. In the first step a Kan-Strep-counter-selection cassette is introduced in front of the gC stop codon. In the second step, the two selectable marker genes are substituted with a cassette containing the T2A-eGFP sequence of interest. The template containing the selectable genes is extended at both ends by PCR to add 50-bp regions of homology to the target region (homology arms).

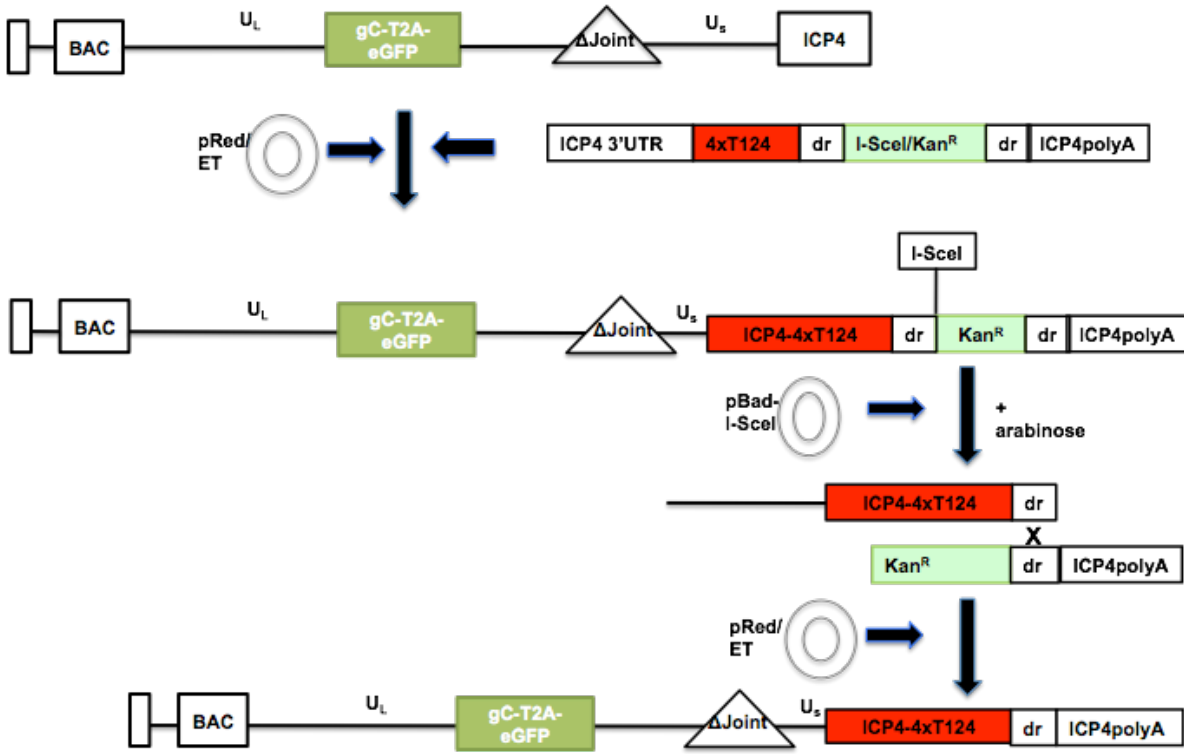


Figure 7: pBad-I-SceI two steps modification of the Gene-Bridges Red/ET temperature-shift-mediated recombination in the ICP4 locus.

In the first step, a DNA fragment containing the sequence of interest (ICP4 3'UTR containing 4xT124), a kanamycin (Kan^R) selection cassette flanked by direct repeats (dr) and an I-SceI restriction site is inserted into a specific region of the HSV-BAC by Red/ET recombinase. In the second step the selected BAC is transformed with a pBad/I-SceI plasmid that codes for the I-SceI restriction enzyme expressed following arabinose induction. Then the induced I-SceI enzyme cuts at its unique site in the Kan-resistant HSV-BAC construct facilitating the Red/ET-mediated recombination between the repeats flanking the Kan cassette, eliminating it from the BAC DNA.

This joint-deleted vector (KBG) was further modified to create the KBBJ backbone by introducing a double mutation in gB, D285N/A549T, (gB:NT). This mutation in the gB glycoprotein was discovered in my laboratory and recently published as enhancing viral entry⁵⁷.

To generate the ICP4-miR124t-BAC I added two additional modifications to the KBBJ parental backbone. The first, illustrated in Figure 6, was the introduction of the enhanced green fluorescent protein (eGFP) gene in-frame with the late viral gC gene to be co-expressed from the native viral gC promoter and used as marker of viral growth and spread both *in vitro* and *in vivo*. The resulting vector was called KBG.

The second, illustrated in Figure 7, was the insertion of the 4xT124 responsive element from the pLuc-T124 construct (section 2.4) into the 3' UTR of the KBG ICP4 gene. The resulting

vector was called ICP4-miR124t. A list of all the BAC constructs schematics is illustrated in Table 5.

2.7.1 Insertion of T2A-eGFP in gC 3'end

The first modification of KBBJ consisted in the insertion of the enhanced green fluorescent protein (eGFP) gene in-frame with the late viral *gC* gene and separated by a 2A translation-pause sequence (T2A)^{58,59}. As a result, the *gC* and eGFP genes were efficiently co-expressed from the native late viral *gC* promoter making eGFP expression a very useful marker of viral growth and spread for both *in vitro* and *in vivo* studies.

The pRed/ET-mediated recombination used to create the backbone relies on the use of a pRed/ET plasmid that contains two λ phage-derived *red* genes under the control of an L-arabinose-inducible promoter and a tetracycline (tet) resistance gene. Protein expression from the *red* genes is induced by L-arabinose and mediates homologous recombination between the BAC and a linear targeting construct. To generate the targeting construct (gC-CS), a counter-selection cassette template (CS) encoding resistance to kanamycin (kan^R) and sensitivity to streptomycin (strep^S) was extended at both ends by PCR to add 50 bp regions of homology (homology arms) to target the 3' end of the *gC* gene (Figure 8A). The PCR reaction was performed using High Fidelity Accuprime Pfx DNA Polymerase (Invitrogen) according to the manufacturer's instructions supplemented with 1 μ l of the counter-selection cassette template (200 ng/ μ l) and 1 μ l of each primer (gC-csF, gC-csR 10 pmol/ μ l). The cycling protocol used was the following: 95°C for 5', 30 cycles x (95°C for 30'', 59°C for 30'', 68°C for 2'), 68°C for 10', 4°C forever. The resulting 1.3-kb gC-CS PCR product shown in Figure 8A was gel-isolated using the QIAEXII Gel extraction kit (QIAGEN) according to manufacturer's instructions, resuspended in double distilled water (ddH₂O) and sent for sequencing to verify the integrity of the amplified sequence. To introduce the targeting construct (Figure 9A), DH10 β bacteria carrying the KBBJ vector containing the CM-resistance gene in the BAC region, were electroporated with pRed/ET expression plasmid containing the tet-resistance gene. Specifically, 24 h before electroporation a single KBBJ overnight culture was inoculated in CM (15 μ g/ml) containing LB medium and grown at 37°C while shaking at 220 rpm. On the day of the electroporation 30 μ l of KBBJ overnight culture were inoculated into 1.4 ml of LB medium and incubated at 37°C for 2 hours while shaking at 220 rpm. Bacteria were then collected and prepared for electroporation by washing them three times with cold double distilled water (ddH₂O) and by resuspending them in

20 μ l of ddH₂O. Bacteria were then electroporated with 1 μ l of pRed/ET plasmid (20 μ g/ μ l) using a Biorad GenePulserXcell electroporator (Voltage 1650 V, Capacitance 25 μ F, Resistance 150 Ω , Cuvette 1 mm).

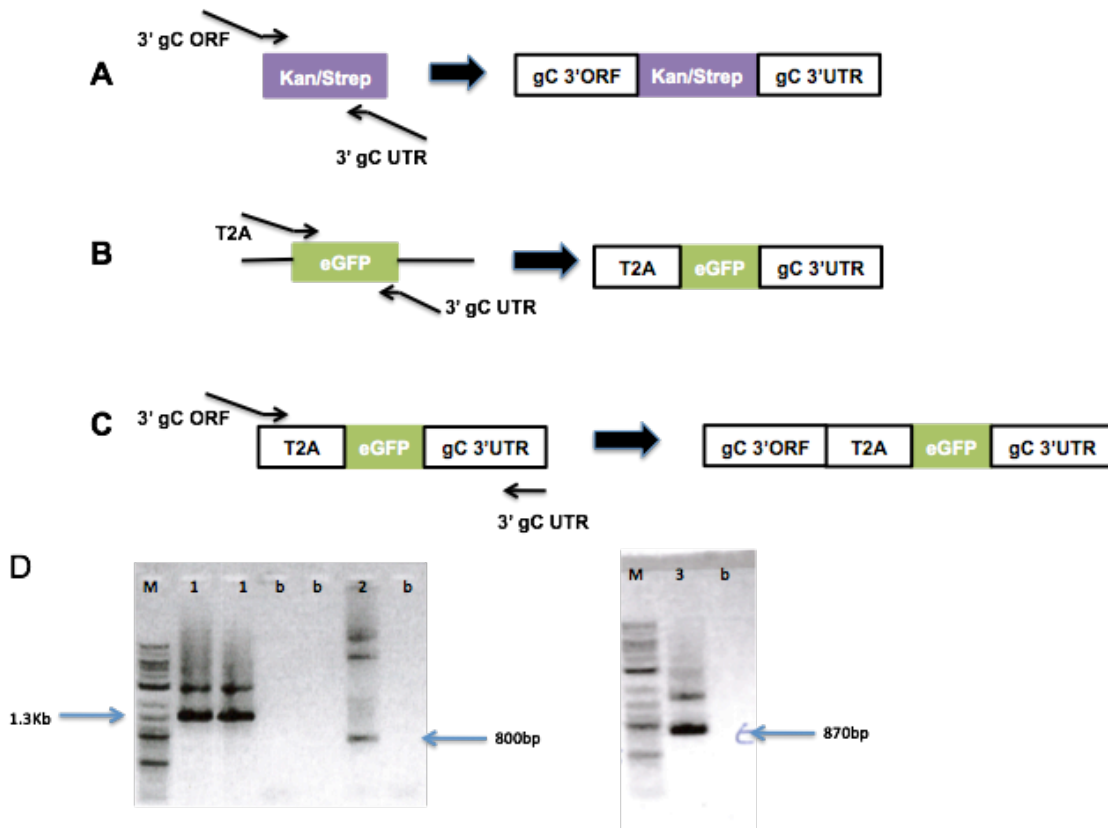


Figure 8: PCR to amplify the counter-selection cassette (CS) with homology arms for gC 3' end

(A) Generation of gC-CS targeting construct. A counter-selection cassette template encoding resistance to kanamycin (kan^R) and sensitivity to streptomycin (strept^S) was extended at both ends by PCR to add 50 bp regions of homology (homology arms) to target the 3' end of the gC gene. (B) Generation of the T2A fragment. The eGFP gene was first extended by PCR with a forward primer containing a T2A sequence (T2A-eGFP-F) and a reverse primer carrying the gC 3'UTR homology arm previously used to target gC (gC-eGFP-R). (C) Generation of a gC-T2A-eGFP targeting construct. The T2A-eGFP fragment was extended with a second round of PCR to add the same 50-bp homology arms previously used to target the 3' end of the gC ORF with the CS-cassette. (D) Agarose gel of the targeting constructs. PCR products were gel-isolated and sent for sequencing to verify the integrity of the amplified sequence.

After electroporation, cells were incubated at 30°C for 70' while shaking at 220 rpm and finally plated on LB agar plates containing CM (15 μ g/ml) and tet (3 μ g/ml) and incubated at 30°C overnight. Due to a temperature sensitive origin of replication, pRed/ET is lost if bacteria are grown at temperatures over 30°C. One pRed/ET positive colony was then randomly

selected to host the recombination reaction in the gC locus of KBBJ (KBBJ-R illustrated in Table 5). gC-CS was then electroporated into KBBJ-R bacteria. 24 h before electroporation, KBBJ-R bacteria were inoculated in CM (15 µg/ml) + tet (3 µg/ml) containing LB media and grown overnight at 30°C while shaking at 220 rpm. On the day of the electroporation, 30 µl of KBBJ-R overnight culture were inoculated into 1.4 mL of LB medium and incubated at 30°C for 2 h with 220 rpm shaking. KBBJ-R bacteria were then induced to express the recombination proteins from pRed/ET through incubation of the 1.4mL culture at 37°C with 0.35% of L-arabinose for 45' with 220 rpm shaking. Bacteria were then collected and prepared for electroporation by washing them three times with ddH₂O and by resuspending them in 20 µl of ddH₂O. Bacteria were then electroporated with 5 µl of the gC-CS fragment using a Biorad GenePulserXcell electroporator (Voltage 1650 V, Capacitance 25 uF, Resistance 150 Ω, Cuvette 1 mm). Following electroporation bacteria were incubated at 37°C for 70' with shaking to allow Red/ET-mediated recombination between the homology arm-flanked selection cassette and the HSV genome in front of the gC stop codon. Cells were finally plated on CM (15 µg/ml) + tet (3 µg/ml) +kan (15 µg/ml) agar plates and incubated at 30°C to avoid loss of Red/ET plasmid. Eight kan-resistant recombinants were selected and checked for strep sensitivity by streaking them on a CM (15 µg/ml) + strep (50 µg/ml) + kan (15 µg/ml) agar plates. Streptomycin sensitivity can indeed be easily lost during the cloning procedure but it is required to complete the Red/ET-mediated recombination. Five kan-resistant-strep-sensitive recombinants were selected and BAC-DNA extracted. The site-specific insertion of the counter-selection cassette was checked in these five isolates by diagnostic PCR using primers outside the region of insertion of the BAC genome as shown in Figure 9B. The diagnostic PCR reaction was performed using High Fidelity Accuprime Pfx DNA Polymerase (Invitrogen) according to manufacturer's instructions supplemented with 2 µl of each BAC-DNA miniprep template and 1µl of each primer (gC-F, gC-R 10 pmol/µl). The cycling protocol used was the following: 95°C for 5', 30 cycles x (95°C for 30", 59°C for 30", 68°C for 2'), 68°C for 10', 4°C forever. All five isolates showed the expected 2.1-Kb PCR band indicating the insertion of the counter-selection cassette when compared to the 800-bp band amplified from the KBBJ parental backbone. All five isolates were then analyzed by FIGE (Field Inversion Gel Electrophoresis) and compared to the original KBBJ backbone after overnight digestion of 20 µl of each BAC-DNA miniprep template with either BglIII or HindIII. As illustrate in Figure 9C, in both digests all 5 isolates showed the expected 1.3 Kb shift of the DNA band containing the site of insertion that went for 17.4-Kb to 18.7-Kb in BglIII digest and from 8.7-Kb to 10-Kb in the HindIII digest, while maintaining intact the remaining pattern of digestion. Two

isolates (KBBJ-CS-A and KBBJ-CS-C illustrated in Table 5) were chosen from the pool and used for the following recombination step.

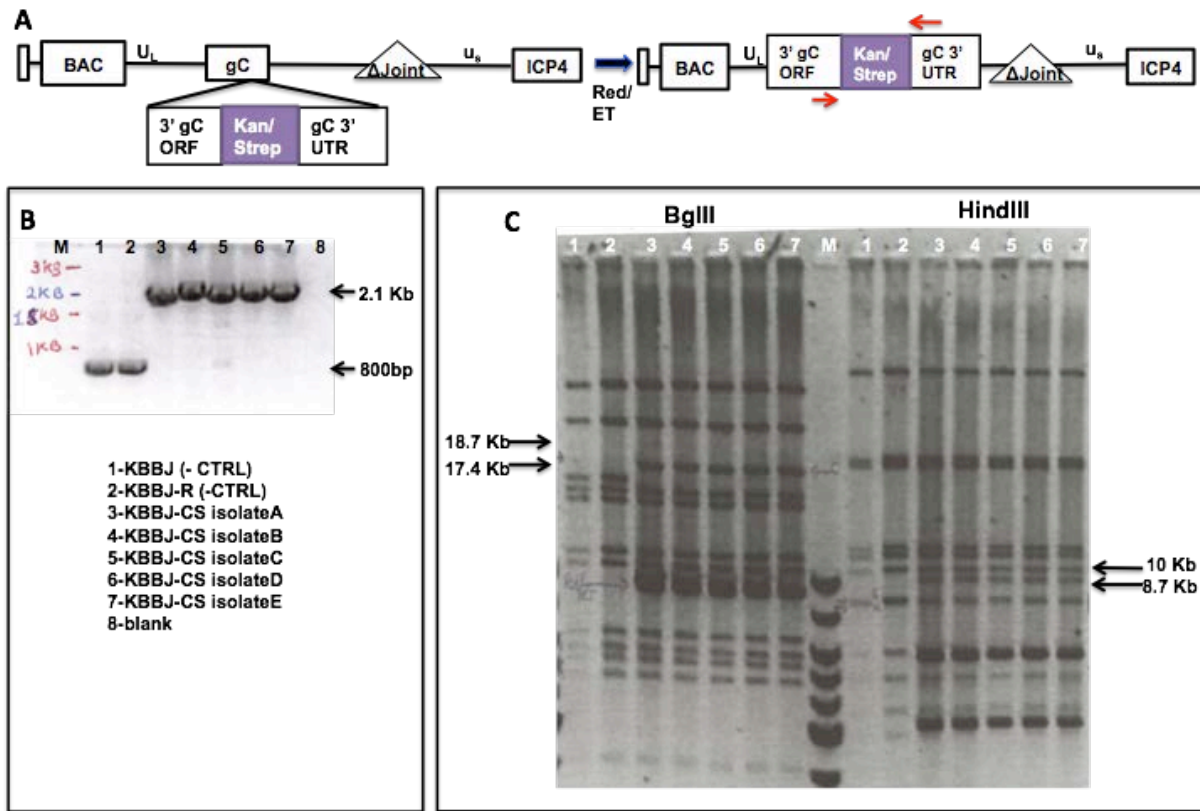


Figure 9: 1st step: counter-selection (CS) cassette insertion in gC 3'UTR.

(A): Schematic of the site-specific insertion of the counter-selection cassette in gC. (B): Diagnostic PCR. Five kan-resistant isolates were checked for correct insertion of the CS cassette by diagnostic PCR using primers outside the region of insertion into the BAC genome. All five isolates were positive showing the expected 1.3-Kb shift from 800-bp to 2.1-Kb due to insertion of the 1.3-Kb large CS cassette. (C): Diagnostic FIGE digest. All five isolates were analyzed by FIGE and compared to the original KBBJ backbone after overnight digestion with either BgIII or HindIII. In both digests all 5 isolates showed the expected 1.3 Kb shift of the DNA band containing the site of insertion that went for 17.4-Kb to 18.7-Kb in BgIII digest and from 8.7-Kb to 10-Kb in the HindIII digest, without changes in other bands.

The next step of the Red/ET temperature-shift-mediated recombination involved the substitution of the counter-selection cassette with a cassette containing the T2A-eGFP sequence flanked by the same homology arms used in step one to target the 3' end of the gC gene (Figure 10A). Two consecutive PCR reactions were used to generate the T2A-eGFP cassette. The eGFP gene was first extended by PCR with an upper primer containing a T2A sequence (T2A-eGFP-F) and a lower primer carrying the 5' gC homology arm previously used to target gC (gC-eGFP-R) as shown in table 4. The PCR reaction was performed using High

Fidelity Accuprime Pfx DNA Polymerase (Invitrogen) according to manufacturer's instructions supplemented with 1 μ l of the eGFP template (200 ng/ μ l) and 1 μ l of each primer (T2A-eGFP-F, gC-eGFP-R 10 pmol/ μ l). The cycling protocol used was the following: 95°C for 5', 30 cycles x (95°C for 30", 59°C for 30", 68°C for 2'), 68°C for 10', 4°C forever. The resulting 800 bp T2A-eGFP PCR product shown in Figure 8B was gel-isolated using the QIAEXII Gel extraction kit (QIAGEN) according to manufacturer's instructions and extended with a second round of PCR to add the same 50 bp homology arms used in the first step to target the 3' end of the gC gene. The PCR reaction was performed using High Fidelity Accuprime Pfx DNA Polymerase (Invitrogen) according to manufacturer's instructions supplemented with 1 μ l of the T2A-eGFP template (200 ng/ μ l) and 1 μ l of each primer (gC-T2A-F and gC -eGFP-R 10 pmol/ μ l). The cycling protocol used was the following: 95°C for 5', 30 cycles x (95°C for 30", 59°C for 30", 68°C for 2'), 68°C for 10', 4°C forever. The 870 bp gC-T2A-eGFP PCR product shown in Figure 8C was gel-isolated using the QIAEXII Gel extraction kit (QIAGEN) according to manufacturer's instructions and resuspended in ddH₂O. The gC-T2A-eGFP fragment was then electroporated into KBBJ-CS-A and KBBJ-CS-C electrocompetent bacteria for Red/ET mediated recombination to substitute the counter-selection cassette with the T2A-eGFP gene in front of the gC stop codon.

One day before electroporation KBBJ-CS-A and KBBJ-CS-C bacteria, still carrying the pRed/ET plasmid, were inoculated in CM (15 μ g/ml)+ tet (3 μ g/ml) + kan (15 μ g/ml) LB media and grown overnight at 30°C with 220 rpm shaking. On the day of the electroporation 30 μ l of KBBJ-CS-A and KBBJ-CS-C overnight cultures were inoculated into 1.4 mL of LB medium and incubated at 30°C for 2 h with 220 rpm shaking. KBBJ-CS-A and KBBJ-CS-C bacteria were then induced to express the recombination proteins from pRed/ET through incubation for 45' at 37°C with 0.35% of L-arabinose while shaking at 220 rpm. Bacteria were then collected and prepared for electroporation by washing them three times with ddH₂O and by resuspending them in 20 μ l of ddH₂O. Bacteria were then electroporated with 5 μ l of the gC-T2A-eGFP fragment using a Biorad GenePulserXcell electroporator (Voltage 1650 V, Capacitance 25 μ F, Resistance 150 Ω , Cuvette 1 mm). Following electroporation, bacteria were incubated for 70' at 37°C with shaking to allow Red/ET mediated recombination between the homology arm-flanked selection cassette and the KBBJ-CS genome in front of the gC stop codon. Cells were finally plated on CM (15 μ g/ml) + strep (50 μ g/ml) agar plates and incubated at 37°C to allow loss of Red/ET plasmid. 18 Strep-resistant recombinants (9 derived from the KBBJ-CS-A and 9 from the KBBJ-CS-C) were selected and BAC DNA. The site-specific insertion of T2A-eGFP gene was checked on these 18 isolates by PCR using the gC-F and gC-R primers outside the region of

insertion of the BAC genome. The PCR reaction was performed using High Fidelity Accuprime Pfx DNA Polymerase (Invitrogen) according to manufacturer's instructions supplemented with 1 μ l of the BAC-DNA template (200 ng/ μ l) and 1 μ l of each primer (gC-F and gC-R 10 pmol/ μ l). The cycling protocol used was the following: 95°C for 5', 30 cycles x (95°C for 30", 59°C for 30", 68°C for 2'), 68°C for 10', 4°C forever. The two isolates (KBBJ-T2A-eGFP-A6 and KBBJ-T2A-eGFP-C9) that showed the expected 1.7-Kb PCR amplification band shown in the Figure 10B were then compared by FIGE to the original KBBJ and the KBBJ-CS-A and KBBJ-CS-C backbones after overnight digestion of 20 μ l of each BAC-DNA template with either BgIII or HindIII.

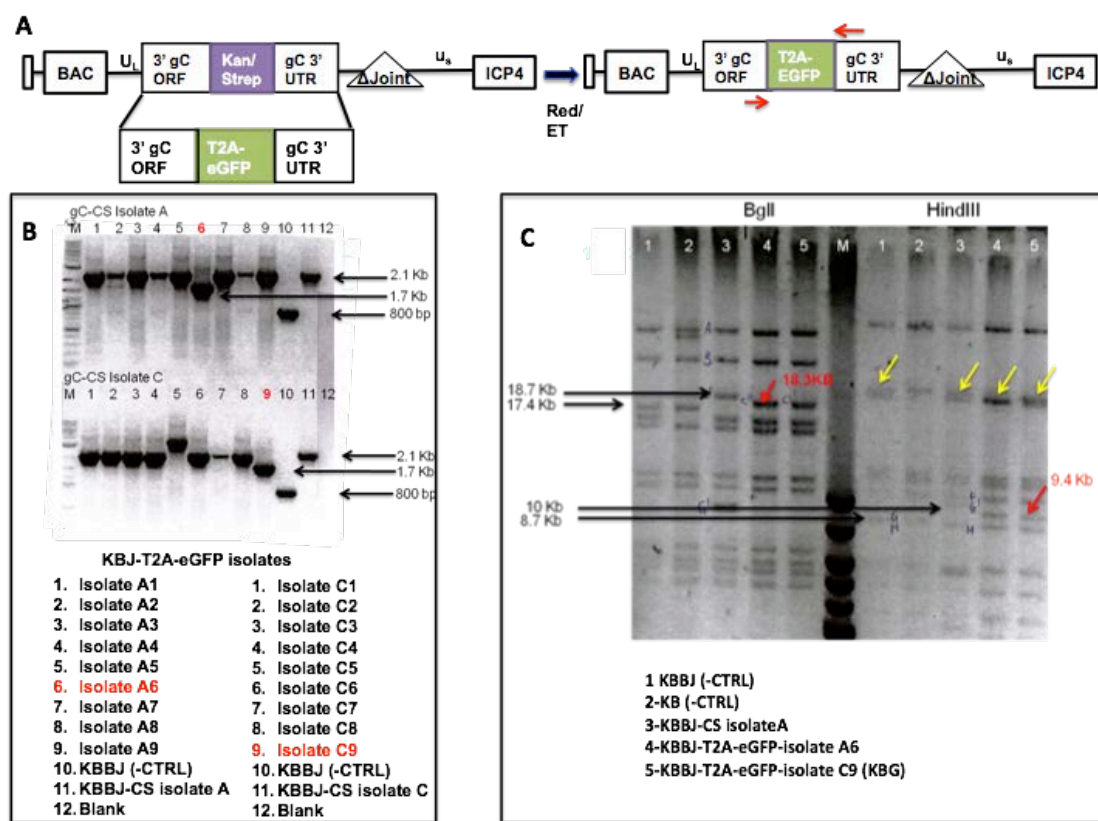


Figure 10: 2nd step: counter-selection (CS) replacement with T2A-eGFP in gC 3'UTR.

(A): Schematic of the site-specific substitution of the CS- cassette in gC with a T2A-eGFP cassette. (B): Diagnostic PCR. The site-specific insertion of T2A-eGFP gene was checked on 18 isolates by PCR using primers outside the region of insertion into the BAC genome. Two isolates, A6 and C9, showed the expected 1.7-Kb PCR amplification band. (C): Diagnostic FIGE. A6 and A9 were compared to the original KBBJ and the KBBJ-CS-A and KBBJ-CS-C backbones by FIGE. A6 showed a shift-down in the HindIII pattern of digestion of its 20.5-Kb band towards the 19.5-Kb band, evidence of an unexpected secondary recombination event in the BAC (yellow arrows). C9 instead showed for both digestions only the desired 400-bp shift of the gC-containing DNA band, while the remaining digestion pattern remained intact.

As shown by the yellow arrows in the Figure 10C, KBBJ-T2A-eGFP-A6 showed a shift-down in the HindIII pattern of digestion of its 20.5-Kb band towards the 19.5-Kb band, evidence of an unexpected incorrect secondary recombination event in the BAC. KBBJ-T2A-eGFP-C9 instead showed for both digestions only the correct 400-bp shift of the gC-containing DNA band, while the remaining digestion pattern remained intact. The KBBJ-T2A-eGFP-C9 isolate (renamed KBGillustrated in Table 5) was then selected and transfected into U2OS cells to ensure the ability of the BAC-DNA to produce virus as described in section 2.7.4.

2.7.2 Insertion of 4xT124 responsive element in ICP4-3'UTR

2.7.2.1 Generation of pEntr-ICP4-T124-Kan

To insert the 4xT124 responsive element from the pLuc-T124 construct (section 2.5) into the 3' UTR of the *ICP4* gene, I had to generate an intermediate construct called pEntr-ICP4-T124-Kan. The pEntr-ICP4-T124-Kan construct was generated in eight steps summarized in Figures 11-13.

In step one, two partially overlapping single-strand 5'-phosphorylated DNA oligos including the ICP4 stop codon, the 3'-end of the *ICP4* gene and an Spel restriction site were designed (see Table 4). The two lyophilized oligos were dissolved in water to a final concentration of 3 ug/ μ l. To anneal the two oligos, 1 μ l of each oligo was combined with 48 μ l of annealing buffer (10 mM Tris Ph 7.5-8.0, 50 mM NaCl, 1 mM TE) and incubated at 95°C for 4', shifted to 70°C for a 10' incubation, shifted to room temperature (RT) for a 30' incubation, and then stored at 4°C. The annealed, partially overlapping oligos were then elongated using Accuprime Pfx DNA polymerase (Invitrogen) for 30' at 68°C to close the gaps generating a perfectly annealed 93-bp long double-stranded ICP4 DNA fragment (Figure 11-Step 1).

In step two, 1 μ l of the annealed ICP4 DNA fragment was ligated into the pZero-blunt vector (Invitrogen), transformed into DH10 β competent bacteria (NEB), plated on kanamycin (100 μ g/ml) agar plates and incubated overnight at 37°C. Following selection the DNA extracted from the kan-resistant ICP4-pZero colonies was screened for insertion of the annealed oligo between two EcoRI sites through diagnostic EcoRI (NEB) digest. Two ICP4-pZero clones were selected and sent for sequencing to verify the integrity of the amplified sequence (Figure 11-Step 2). In step three, one selected ICP4-pZero isolate and the pLuc-T124 construct (described in section

2.5.2) were digested with EcoRI + Spel (NEB) for 1 h at 37°C. The ICP4-pZero 81-bp fragment (insert) and 5-Kb pLuc-T124 backbone were gel purified and ligated together.

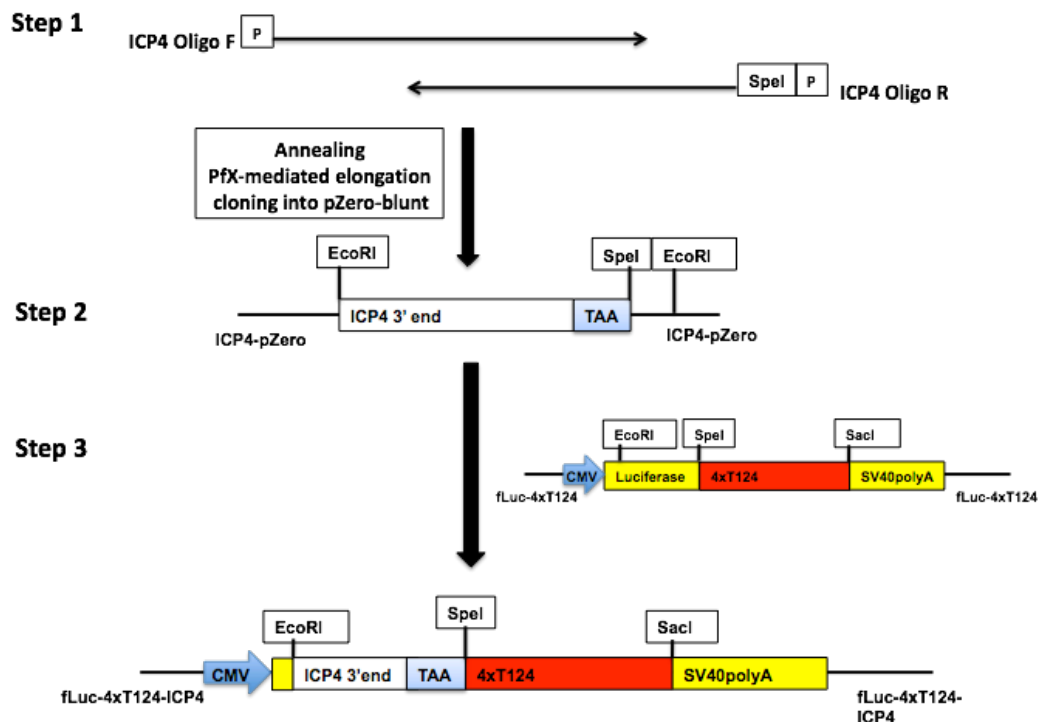


Figure 11: Schematic of pEntr-ICP4-T124-kan generation, Steps 1-3.

Step 1. Two partially overlapping single-strand 5'-phosphorylated DNA oligos including the ICP4 stop codon, the 3'-end of the *ICP4* gene and an Spel restriction site were designed, annealed and elongated, generating a perfectly annealed 93-bp long double-stranded ICP4 DNA fragment. Step 2. The annealed ICP4 DNA fragment was ligated into the pZero-blunt vector. Following cloning in bacteria and diagnostic digest for correct insertion of the oligo, two ICP4-pZero clones were selected and sent for sequencing to verify the integrity of the amplified sequence. Step 3. One selected ICP4-pZero isolate and the fLuc-4xT124 construct (described in Figure 4) were digested with EcoRI + Spel and ligated together. Following cloning into bacteria, fLuc-4xT124-ICP4 colonies were screened for insertion of the ICP4 fragment into the fLuc-4xT124 vector through EcoRI + SacI diagnostic digest.

The ligation product was then transformed into DH10 β competent bacteria (NEB), plated on ampicillin (100 μ g/ml) agar plates and incubated overnight at 37°C. Following selection, the DNA from pLuc-T124-ICP4 amp-resistant colonies was screened for insertion of the ICP4 fragment into the pLuc-T124 vector through EcoRI + SacI diagnostic digest (Figure 11-Step 3).

In step four, the 4xT124-ICP4 portion of the pLuc-T124-ICP4 plasmid generated in step 3 was extended by PCR with an ICP4 upper primer (ICP4-F) that overlapped the ICP4-oligo-F used in step one, and a lower primer (ICP4-R) containing a SacI restriction site and the polyA

region of ICP4. The PCR reaction was performed using Thermo Scientific® Phusion High-Fidelity DNA Polymerase (NEB) according to the manufacturer's instructions supplemented with 1 μ l of the pLuc-T124-ICP4 plasmid as template (200 ng/ μ l) and 1 μ l of each primer (ICP4-F, ICP4-R 10 pmol/ μ l). The cycling protocol used was the following: 98°C for 30'', 25 cycles x (98°C for 10'', 58°C for 10'', 72°C for 15''), 72°C for 10', 4°C forever (Figure 12- Step 4).

In step five, the 237-bp 4xT124-ICP4polyA product was gel-purified and 1 μ l of it was ligated into pZero-blunt vector (Invitrogen), transformed into DH10 β competent bacteria (NEB), plated on kanamycin (100 μ g/ml) agar plates and incubated overnight at 37°C. Following selection, DNA from kan-resistant 4xT124-ICP4polyA-pZero colonies were screened for insertion of 4xT124-ICP4polyA between two EcoRI sites through diagnostic EcoRI (NEB) digest. Two pZero-4xT124T-ICP4polyA clones were selected and sent for sequencing to verify the integrity of the amplified sequence (Figure 12-Step 5).

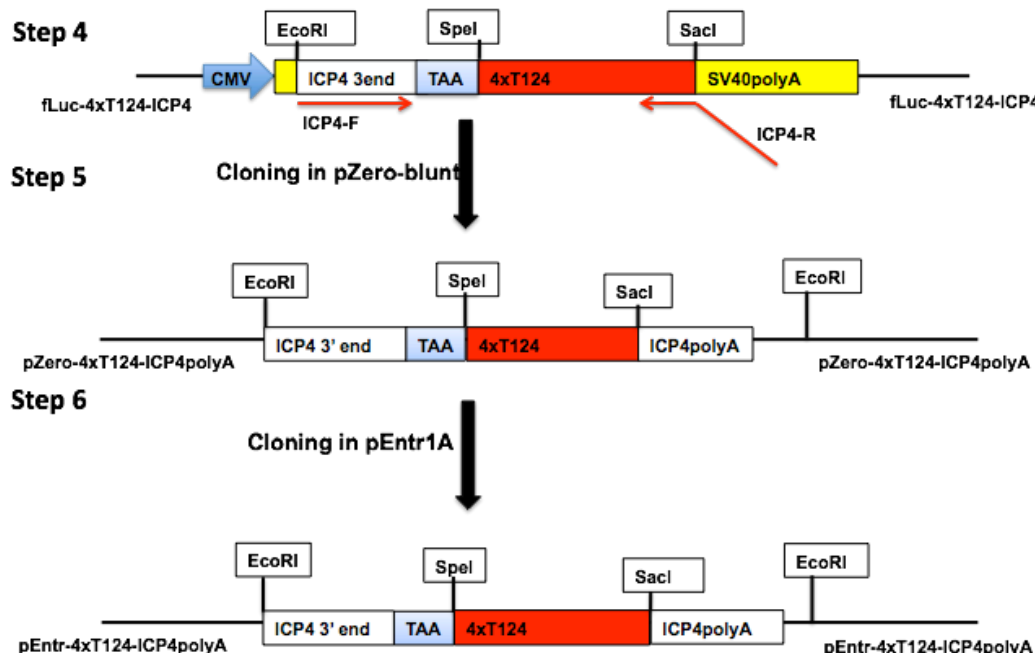


Figure 12: Schematic of pEntr-ICP4-T124-kan generation, Steps 4-6.

Step 4. The 4xT124-ICP4 portion of the fLuc-4xT124-ICP4 plasmid generated in step 3 was extended by PCR with an ICP4 forward primer (ICP4-F) that overlapped the ICP4-oligo-F used in step one, and a reverse primer (ICP4-R) containing a SacI restriction site and the polyA region of ICP4. **Step 5:** The 237-bp 4xT124-ICP4polyA PCR product was ligated into pZero-blunt vector. Following cloning into bacteria and EcoRI diagnostic digest for correct insertion of 4xT124-ICP4polyA fragment between two EcoRI sites, two pZero-4xT124-ICP4polyA clones were selected and sent for sequencing to verify the integrity of the amplified sequence. **Step 6:** One pZero-4xT124-ICP4polyA isolate and the pEntr1A plasmid were digested with EcoRI and ligated together. Following cloning into bacteria, pEntr-T124-ICP4polyA kan-resistant colonies were screened for insertion of the 4xT124-ICP4polyA fragment into pEntr1A through EcoRI diagnostic digest.

In step six, one of the sequenced pZero-4xT124-ICP4polyA isolates and the pEntr1A plasmid (Invitrogen) were digested with EcoRI (NEB) for 1 h at 37°C. The 4xT124-ICP4polyA 250-bp fragment (insert) and 3.4-Kb pEntr1A backbone were gel purified, ligated together and transformed into DH10β competent bacteria (NEB), plated on kanamycin (100 µg/ml) agar plates and incubated overnight at 37°C. Following selection, pEntr-T124-ICP4polyA kan-resistant colonies were screened for insertion of the 4xT124-ICP4polyA fragment into pEntr1A through EcoRI diagnostic digest (Figure 12-Step 6).

In step seven, a plasmid containing the I-SceI restriction site next to a kanamycin resistance gene (I-SceI-kan cassette), kindly donated by Dr N. Osterrieder (Cornell University, Ithaca, NY, USA), was PCR amplified with I-SceI-Kan-F and I-SceI-Kan-R primers to insert two direct repeats (dr) on both sides of the cassette.

The direct repeats were designed to contain a combination of three restriction sites for pI-SceI, NotI and SacI enzymes. The PCR reaction was performed using Thermo Scientific® Phusion High-Fidelity DNA Polymerase (NEB) according to the manufacturer's instructions supplemented with 1 µl of the I-SceI-kan cassette containing plasmid as template (200 ng/µl) and 1 µl of each primer (I-SceI-Kan-F and I-SceI-Kan-R 10 pmol/µl). The cycling protocol used was the following: 98°C for 30'', 25 cycles x (98°C for 10'', 63°C for 10'', 72°C for 15''), 72°C for 10', 4°C forever (Figure 13-Step 7).

In step eight, both the I-SceI-Kan-dr (insert) from step seven and the pEntr-T124-ICP4polyA (backbone) from step six were digested with SacI for 1 h at 37°C, gel purified and ligated together. The ligation product was then transformed into DH10β competent bacteria (NEB), plated on kanamycin (100 µg/ml) agar plates and incubated overnight at 37°C. Following selection the pEntr-ICP4-T124-kan kan-resistant colonies were screened for insertion of the I-SceI-kan-dr fragment into pEntr-T124-ICP4polyA through Xhol diagnostic digest. The pEntr-ICP4-T124-kan construct (illustrated in Table 5) was used for the pBad/I-SceI-Red/ET mediated insertion of 4xT124 in ICP4 3'UTR (Figure 13- Step 8).

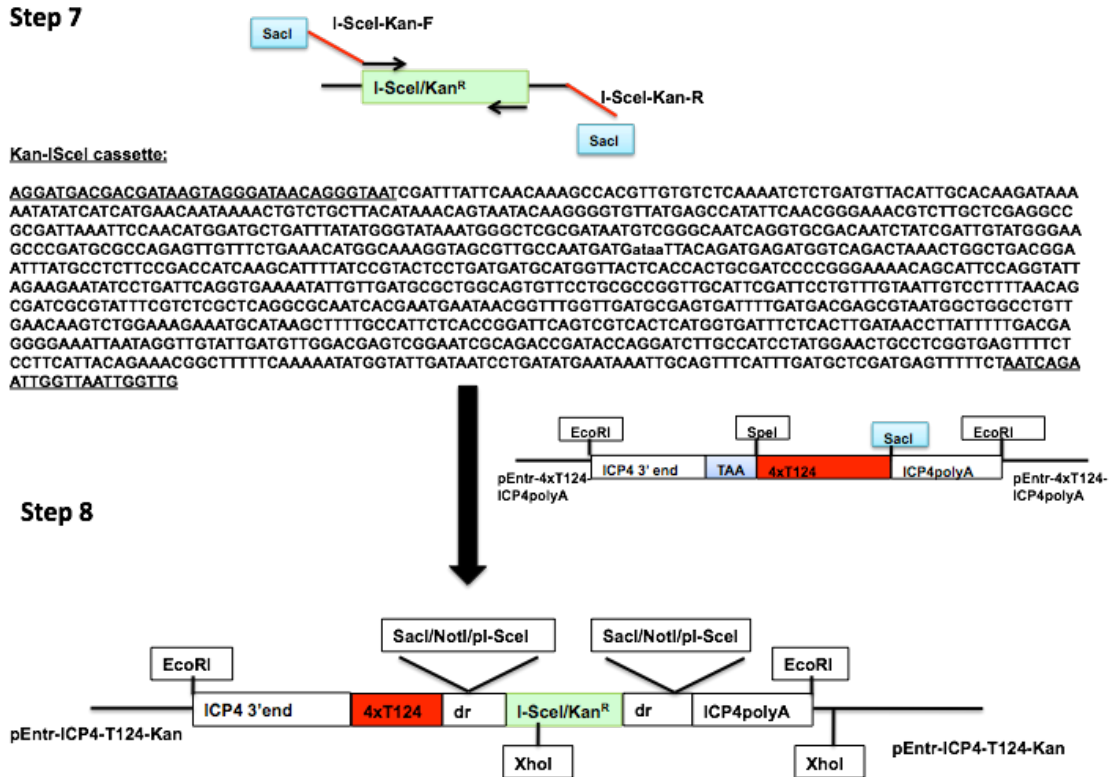


Figure 13: Schematic of pEntr-ICP4-T124-kan generation Step 7-8.

Step 7. A plasmid containing the I-SceI restriction site next to a kanamycin resistance gene (I-SceI-kan cassette), was PCR amplified with I-SceI-Kan-F and I-SceI-Kan-R primers to insert two direct repeats (dr) on both sides of the cassette designed to contain a combination of three restriction sites for pl-SceI, NotI and SacI enzymes. Illustrated is the sequence of the I-SceI/ Kan selection cassette with underlined the position of the amplification primers and the I-SceI restriction site in bold. Step 8: Both the I-SceI-Kan-dr (insert) from step 7 and the pEntr-T124-ICP4polyA (backbone) from step six were digested with SacI and ligated together. Following cloning into competent bacteria, pEntr-ICP4-T124-kan kan-resistant colonies were screened for correct insertion of the I-SceI-kan-dr fragment through Xhol diagnostic digest.

2.7.2.2 pBad/I-SceI modified Red/ET protocol to insert 4xT124 in ICP4-3'UTR

The Red/ET recombination protocol works very poorly in HSV regions that are extremely repetitive and very GC rich like the *ICP4* locus of HSV-1. To overcome this problem, our laboratory adapted a pBad/I-SceI modification to the original Red/ET protocol⁵⁶. As illustrated in Figure 7, using this modified protocol I was able to insert a tandem array of four miR124 target sequences (4xT124), previously generated and tested by luciferase assay (see section 2.5), into the 3' UTR of the ICP4 gene.

In the first step of the pBad/I-SceI modified Red/ET protocol KBG containing bacteria were electroporated with pRed/ET plasmid and selected on CM +Tet plates at 30°C as previously described (see KBBJ bacteria pRed/ET electroporation in section 2.7.1). One pRed/ET positive colony was then randomly selected to host the recombination reaction in the ICP4 locus of KBG (KBG-R illustrated in Table 5). A 1.3-Kb DNA fragment containing the 4xT124 sequence in the 3'UTR of ICP4, a kanamycin selection cassette flanked by direct repeats and an I-SceI restriction site was then amplified by PCR from the previously generated pEntr-ICP4-T124-Kan construct (see section 2.7.2) as illustrated in Figure 14. The PCR reaction was performed using High Fidelity Accuprime GC-rich DNA Polymerase (Invitrogen) according to the manufacturer's instructions supplemented with 1 µl of the ICP4-4xT124-ISceI-Kan template (200 ng/µl) and 1 µl of each primer (ICP4-F and ICP4-R 10 pmol/µl). The cycling protocol used was the following: 95°C for 5', 25 cycles x (95°C for 30'', 60°C for 30'', 72°C for 1'20''), 72°C for 10', 4°C forever. The resulting 1.3-Kb 4xT124-ICP4-ISceI-Kan PCR product shown in Figure 14 was gel-isolated using the QIAEXII Gel extraction kit (QIAGEN) and resuspended in ddH₂O.

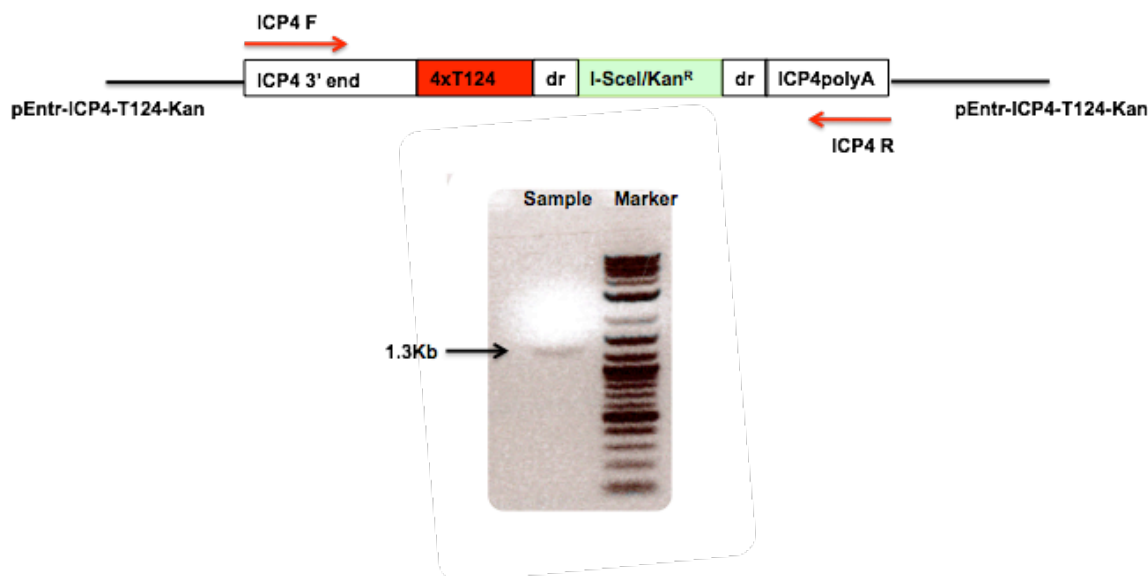


Figure 14: PCR amplification of 4xT124-ICP4-ISceI-Kan selection-cassette to be inserted in ICP4 3'UTR.
A 1.3-Kb DNA fragment containing the 4xT124 sequence in the 3'UTR of ICP4, a kanamycin selection cassette flanked by direct repeats and an I-SceI restriction site was amplified by PCR from the previously generated pEntr-ICP4-T124-Kan construct illustrated in Figure 13, purified and sent for sequencing to verify the integrity of the amplified sequence.

The PCR purified fragment was then electroporated into KBG-R bacteria to recombine in the ICP4 locus as described in Figure 15A.

For the electroporation, one KBG-R bacteria colony was inoculated in CM (15 µg/ml) + tet (3 µg/ml) LB medium and grown overnight at 30°C with 220 rpm shaking. 30 µl of KBG-R overnight culture was inoculated into 1.4 mL of LB medium and incubated at 30°C for 2 h with 1100rpm shaking. KBG-R bacteria were induced to express the recombination proteins from pRed/ET through incubation of the 1.4 mL culture at 37°C with 0.35% of L-arabinose for 45' while shaking at 220 rpm. Bacteria were then collected and prepared for electroporation by washing them 3 times with ddH₂O and by resuspending in 20 µl of ddH₂O. Bacteria were electroporated with 5 µl of the 4xT124-ICP4-IScel-Kan fragment using a Biorad GenePulserXcell electroporator (Voltage 1650 V, Capacitance 25 uF, Resistance 150 Ω, Cuvette 1 mm). Following electroporation, bacteria were incubated for 70' at 37°C with 220 rpm shaking to allow Red/ET mediated recombination between the homology arm-flanked selection cassette and the KBG genome in front of the 3'UTR of ICP4. Cells were finally plated on CM (15 µg/ml) + tet (3 µg/ml) + kan (15 µg/ml) agarose plates and incubated at 30°C to avoid loss of Red/ET plasmid. 16 kan-resistant recombinants were selected and BAC DNA was extracted.

The site-specific insertion of the 4xT124-ICP4-IScel-Kan cassette was checked by PCR on 16 kan-resistant recombinants, using the same ICP4-F and ICP4-R previously employed to amplify the 4xT124-ICP4-IScel-Kan cassette from the pENTR1A construct (see table 4). The ICP4 region is very GC-rich and it is very hard to find primers able to amplify it, that why the ICP4-F and ICP4-R primers, which are internal to the inserted fragment, were used for the diagnostic PCR too. The PCR reaction was performed using High Fidelity Accuprime GC-rich DNA Polymerase (Invitrogen) according to the manufacturer's instructions supplemented with 2 µl of BAC-DNA template (200 ng/µl) and 1 µl of each primer (ICP4-F and ICP4-R 10 pmol/µl). The cycling protocol used was the following: 95°C for 5', 25 cycles x (95°C for 30", 60°C for 30", 72°C for 1'20"), 72°C for 10', 4°C forever. As shown in Figure 15B, eight of the 16 isolates amplified 2 bands, the expected 1.3-Kb band plus one 130-bp band identical to the band amplified from the ICP4 3'UTR region of the KBG control without the 4xT124-ICP4-IScel-Kan insertion. Of the 8 isolates that showed only the correct PCR band at 1.3-Kb, two (ICP4-miR124t-kan-B and ICP4-miR124t-kan-C illustrated in Table 5) were selected and compared to the original KBG backbone by FIGE analysis after overnight digestion of 20 µl of each BAC-DNA miniprep template with either MfI, AflII or HindIII restriction enzymes. As shown in Figure 15C both isolates showed a 1.3-Kb shift up of the 20.7-Kb band in the MfI digest, a break of the 27.4-Kb band in a 17.4-Kb + 11.3-Kb bands in the AflII digest and a break of the 20.2-Kb

band in a 16.5-Kb + 6.5-Kb bands in the HindIII digest. No other non-specific changes in the pattern of digestion were found and both isolates were used for the following step.

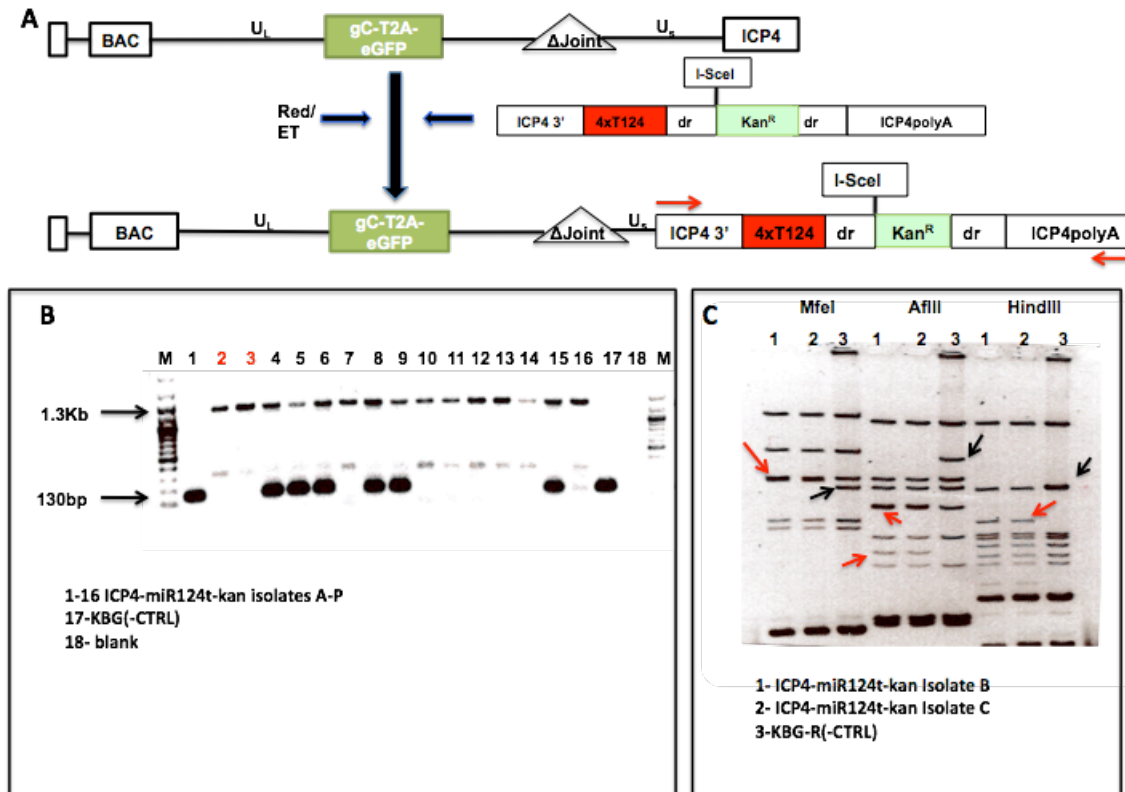


Figure 15: 1st step: I-SceI-kan selection cassette insertion in ICP4 3'UTR.

(A): Schematic of the I-SceI-kan selection cassette insertion in ICP4 3'UTR. (B) Diagnostic PCR. The site-specific insertion of the 4xT124-ICP4-I-SceI-Kan cassette was checked by PCR on 16 kan-resistant recombinants, using the same ICP4-F and ICP4-R used to generate the cassette in Figure 14. Eight of the 16 isolates amplified 2 bands and were discarded. Of the 8 isolates that showed only the correct PCR band at 1.3-Kb, two (ICP4-miR124t-kan-B and ICP4-miR124t-kan-C) were selected and analyzed by FIGE. (C): Diagnostic FIGE. ICP4-miR124t-kan-B and ICP4-miR124t-kan-C were compared to the original KBG backbone by FIGE analysis after overnight digestion with Mfcl, Aflll or Hindlll restriction enzymes. Both isolates showed a 1.3-Kb shift up of the 20.7-Kb band in the Mfcl digest, a break of the 27.4-Kb band in a 17.4-Kb + 11.3-Kb bands in the Aflll digest and a break of the 20.2-Kb band in a 16.5-Kb + 6.5-Kb bands in the Hindlll digest.

In the second step, both KBG-ICP4-miR124t-kan-B and KBG-ICP4-miR124t-kan-C bacterial colonies, still carrying the pRed/ET plasmid, were electroporated with the pBad/I-SceI expression plasmid (kindly provided by K. Osterrieder^{53,56}) coding for the I-SceI restriction enzyme driven by the pBad arabinose-inducible promoter and for ampicillin (Amp) resistance. The electroporation procedure was identical to the one used to electroporate the pRed/ET (see section 2.7.1). Transformed bacteria were plated on CM (15 µg/ml) + tet (3 µg/ml) + kan (15

$\mu\text{g/ml}$) + Amp (50 $\mu\text{g/ml}$) agarose plates and incubated at 30°C to avoid loss of Red/ET plasmid. One pBad positive colony for both KBG-ICP4-miR124t-kan-B and KBG-ICP4-miR124t-kan-C was then randomly selected to host the recombination reaction and kan-selection cassette removal in the ICP4 locus (Figure 16A).

One day before electroporation ICP4-miR124t-kan-B and ICP4-miR124t-kan-C bacteria were inoculated and grown overnight in CM (15 $\mu\text{g/ml}$) + tet (3 $\mu\text{g/ml}$) + Amp (50 $\mu\text{g/ml}$) containing-medium without kan at 30°C with 220 rpm shaking. On the day of the electroporation 100 μl of ICP4-miR124t-kan-B and ICP4-miR124t-kan-C overnight cultures were inoculated into 2.0 mL of LB medium and incubated at 30°C for 2 h with 220 rpm shaking. To induce KBG-ICP4-miR124t-kan-B and KBG-ICP4-miR124t-kan-C to express the recombination proteins from pRed/ET and the I-SceI enzyme from pBad the 2.0 ml bacteria culture were mixed with 2 mL of LB media containing 2% of L-arabinose and incubated at 30°C for 60' with shaking. Bacteria cultures were then shifted to 37°C for 45' and then incubated again for 60' at 30°C to allow both the I-SceI-mediated cleavage at its unique site in the kan-resistant construct and the internal Red/ET-mediated recombination between the repeats flanking the kanamycin selection cassette to eliminate the cassette from the BAC DNA. Bacteria were then grown overnight on CM (15 $\mu\text{g/ml}$) agar plates at 37°C to allow loss of the pRed/ET plasmid, but not of the pBad plasmid that remains when bacteria are grown at 37°C. CM-resistant colonies were then picked and tested for kan-sensitivity by replica-plating on CM (15 $\mu\text{g/ml}$) + kan (15 $\mu\text{g/ml}$). Six CM-resistant, Kan-sensitive recombinants (KBG-ICP4-miR124t-B1-4 and KBG-ICP4-miR124t-C5-6) were selected and BAC-DNA extracted. The site-specific elimination of the I-SceI-kan selection cassette from the ICP4 locus was checked by PCR using the same ICP4-F and ICP4-R primers previously employed to detect the insertion of the 4xT124-ICP4-ISceI-Kan cassette inside the ICP4 region. The PCR reaction was performed using High Fidelity Accuprime GC-rich DNA Polymerase (Invitrogen) according to the manufacturer's instructions supplemented with 2 μl of the BAC-DNA template (200 ng/ μl) and 1 μl of each primer (ICP4-F and ICP4-R 10 pmol/ μl). The cycling protocol used was the following: 95°C for 5', 25 cycles x (95°C for 30", 60°C for 30", 72°C for 1'20"), 72°C for 10', 4°C forever. As shown in Figure 16B, four isolates (KBG-ICP4-miR124t-B2, B3, B4, and C1) out of six showed the expected 300-bp PCR amplification band indicative of the elimination of the I-SceI cassette when compared to the 1.3-Kb band amplified from the parental KBG-ICP4-miR124t-kan-B and KBG-ICP4-miR124t-kan-C BACs.

The four positive isolates were then analyzed by FIGE and compared to both parental KBG and KBG-ICP4-miR124t-kan-C BACs backbones after overnight digestion of 20 μl of each BAC-DNA miniprep template with MfeI, AflII or HindIII.

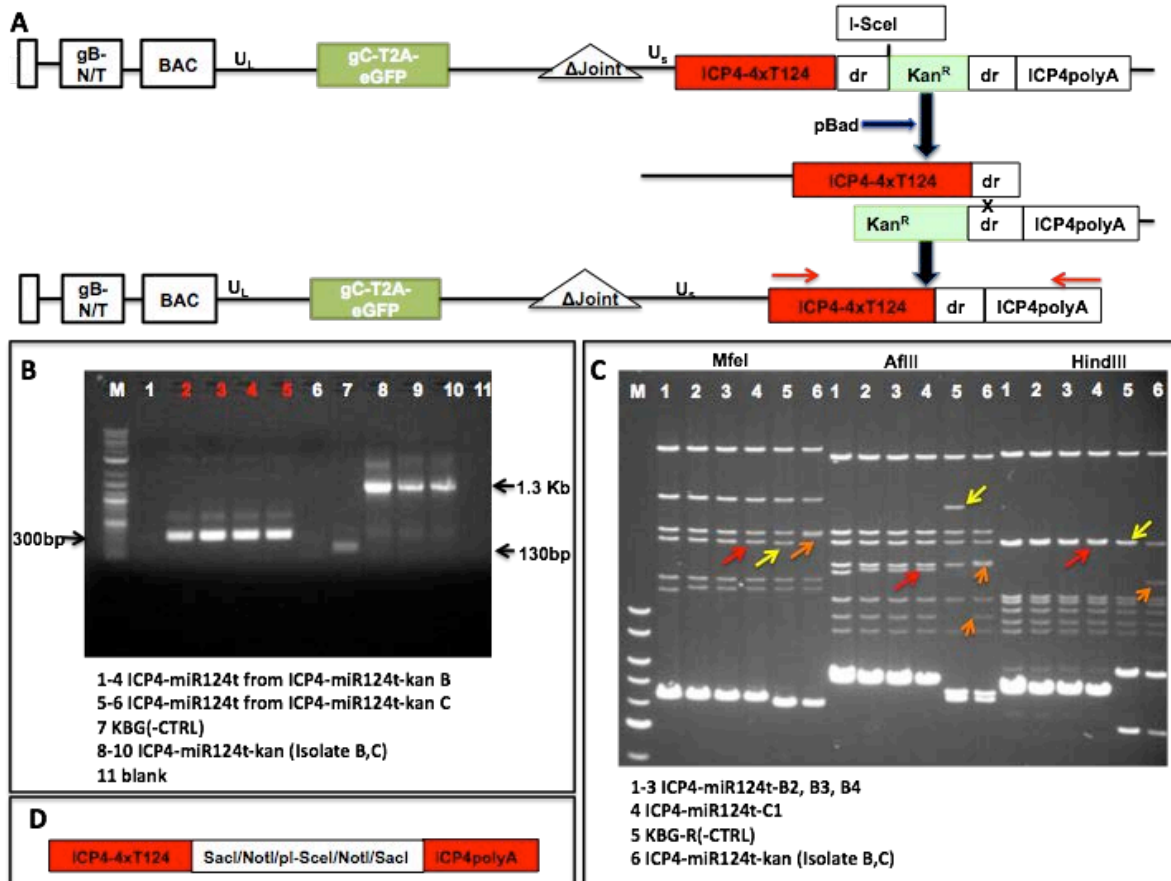


Figure 16: pBad-induced I-SceI-kan selection cassette removal in ICP4 3'UTR.

(A): Schematic of the I-SceI-kan selection cassette removal in ICP4 3'UTR. (B) Diagnostic PCR. The site-specific elimination of the I-SceI-kan selection cassette from the ICP4 locus was checked by PCR using the same ICP4-F and ICP4-R primers used in the previous step. Four isolates (KBG-ICP4-miR124t-B2, B3, B4, and C1) showed the expected 300-bp PCR amplification band indicative of the elimination of the I-SceI cassette when compared to the 1.3-Kb band amplified from the parental BACs. (C): Diagnostic FIGE. The four positive isolates were compared to both parental KBG and KBG-ICP4-miR124t-kan-C BACs backbones after overnight digestion with MfeI, AflII or HindIII. Three isolates (KBG-ICP4-miR124t-B3, B4, C1) showed the right pattern of digestion: in the MfeI digest, the band that shifted from 20.7-Kb up to 22-Kb with the insertion of the I-SceI-kan, shifted down to 20.8-Kb ; in the AflII digest, the 17.4-Kb band formed by the breakage of the 27.4-Kb band, shifted down to 16.3-Kb ; and in the HindIII digest, the 15-Kb band plus a 6.5-Kb band fused to form a 20.4-Kb band, forming a doublet on the gel with a preexisting 20.2-Kb band. (D): Schematic of the structure of the ICP4-miR124t after sequencing.

As shown in Figure 16C, three isolates out of four (KBG-ICP4-miR124t-B3, B4, C1) showed the right pattern of digestion: in an MfeI digest, the band that shifted from 20.7-Kb up to 22-Kb with the insertion of the I-SceI-kan, shifted down to 20.8-Kb ; in an AflII digest, the 17.4-Kb band formed by the breakage of the 27.4-Kb band, shifted down to 16.3-Kb ; and in a HindIII digest, the 15-Kb band plus a 6.5-Kb band fused to form a 20.4-Kb band, forming a doublet on the gel with a preexisting 20.2-Kb band. No other non-specific changes in the pattern of digestion were

found. BAC DNA from all three isolates was then sent for sequencing to verify the integrity of the ICP4-3'UTR region (Figure 16D). To clean the bacteria from the ampicillin-containing pBad plasmid, responsible for the presence of extra-bands on the FGE restriction digest between 4-Kb and 6-Kb, the DNAs from the three positive recombinants KBG-ICP4-miR124t-B3, B4, C1 were re-electroporated into fresh DH10 β electrocompetent cells (NEB) that were then plated on CM (15 μ g/ml) agar plates in the absence of amp to select for BAC-containing isolates without pBad plasmid. Briefly, frozen DH10 β electrocompetent cells (NEB) were quickly thawed in ice and electroporated with 5 μ l of KBG-ICP4-miR124t-B3, B4, C1 DNA using a Biorad GenePulserXcell electroporator (Voltage 1650 V, Capacitance 25 μ F, Resistance 150 Ω , Cuvette 1 mm).

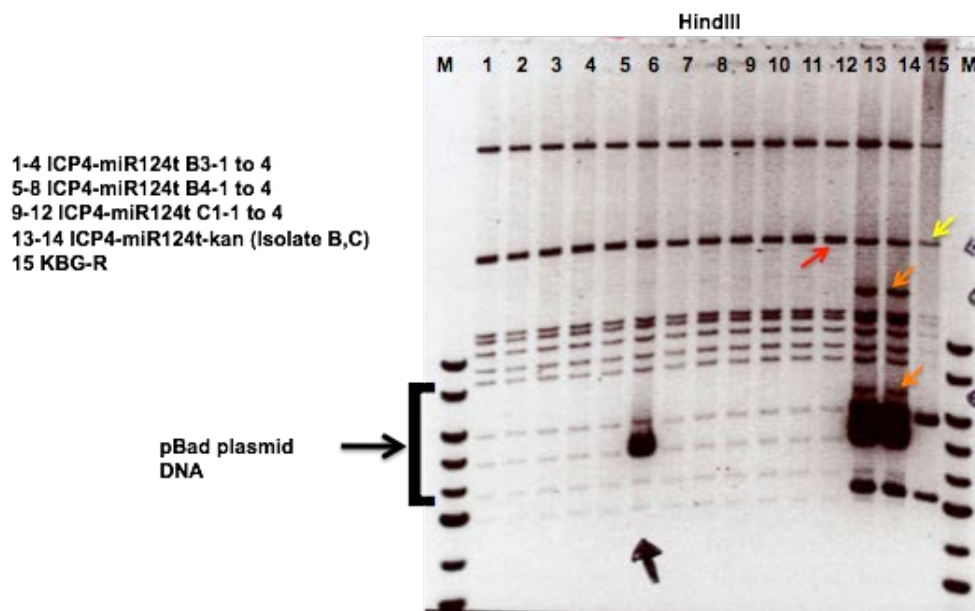


Figure 17: pBad plasmid removal.

10 isolates were analyzed by overnight digestion with HindIII and FGE analysis for loss of the pBad plasmid. 9 out of 10 isolates lost pBad while maintaining the BAC-DNA integrity.

Following electroporation bacteria were incubated for 45' at 37°C with shaking then plated on CM (15 μ g/ml) agarose plates and grown at 37°C overnight. Ten CM-resistant isolates were picked and BAC-DNA extracted. The 10 isolates were then re-analyzed by FGE for loss of the pBad plasmid after overnight digestion of 20 μ l of each BAC-DNA miniprep template with HindIII. As shown in Figure 17, 9 out of 10 isolates lost pBad while maintaining the BAC-DNA integrity. The DNA from isolate KBG-ICP4-miR124t-C1-10 (renamed ICP4-miR124t-BAC

illustrated in Table 5) was randomly selected to be transfected in U2OS cells to ensure the ability of the BAC-DNA to produce eGFP expressing virus

2.7.3 BAC minipreps

Following electroporation and selection on agar plates BAC-transformed bacteria cells were picked and BAC-DNA extracted following the “Miniprep-Alkaline Lysis for BACs” protocol from Untergasser’s

Lab (http://untergasser.de/lab/protocols/miniprep_alkaline_lysis_for_bacs_v1_0.htm). The BAC-DNA was then checked for correct manipulation using both diagnostic PCR and FIGE analysis.

2.7.4 Transfection of BAC-DNA into U2OS to produce KBG and ICP4-miR124t-BAC oHSV-1 viruses

KBG and ICP4-miR124t-BAC were transfected into U2OS cells to ensure the ability of the BAC-DNA to produce virus. On the day before transfection cells were plated at a density of 1.2×10^6 cells /well. 24 h later 80% confluent cells were transfected with 40 μ l of either KBG or ICP4-miR124t-BAC DNA using Lipofectamine LTX (Invitrogen) following the manufacturer’s instructions. Cells were incubated at 37°C in 5% CO₂ and observed by fluorescence microscopy for eGFP expression every 24 h up to 72 h post transfection. Fluorescent pictures of either KBG or ICP4-miR124t-BAC infected cells were taken using a Nikon Diaphot fluorescent microscope.

2.7.5 Transfection of BAC-DNA into U2OS-Cre cells to produce BAC-free KG and ICP4-miR124t oHSV-1 viruses

To eliminate the *loxP*-flanked BAC, which has been shown to negatively affect viral growth ⁵³ both KBG and ICP4-miR124t BAC DNAs were converted into virus by transfection into U2OS-Cre cells already available in the laboratory ^{55,56}. Loss of the BAC region, which also contained the LacZ reporter gene, was determined by staining the infected cells for X-gal. On the day before transfection cells were plated as a 50% confluent monolayer on 2 wells of a 6 well dish at a density of 1.2×10^6 cells/well. 24hrs later, 80% confluent cells were transfected with 40 uL of either KBG or ICP4-miR124t-BAC DNA using Lipofectamine LTX (Invitrogen) following the

manufacturer's instructions and then incubated at 37°C in 5% CO₂. 72 h post transfection viral supernatant was collected, titered and used to perform a viral limiting dilution on regular U2OS cells as follows: 1x10⁶ cells were infected with 30 plaque forming units (p.f.u) of virus, plated in a 96 well dish, and incubated at 37°C for 5-7 days to allow plaque formation. Virus from wells with single plaques was collected, expanded, and used to infect U2OS cells. 48 h after infection cells were fixed with 1% glutaraldehyde solution for 1', then washed twice with PBS and incubated for 30'-1 h at 37 °C with X-gal solution (X-gal 1 mg/ml, 0.25% deoxycholate, 0.8% NP40, 200 mM MgCl₂, 5 mM potassium-ferricyanide, 5 mM potassium-ferrocyanide). After X-gal staining, cells were washed twice with PBS and checked for presence or absence of blue color in the infected cells; viral clones in which no color change could be observed indicated Cre-recombinase mediated removal of the DNA region between the loxP sites. One *lacZ*-negative viral clone was then selected for both KG (BAC removed illustrated in Table 5) and ICP4-miR124t (BAC removed illustrated in Table 5) and checked by PCR with primers outside the BAC region for clean removal of the region between the *loxP* sites. The PCR reaction was performed using High Fidelity Accuprime GC-rich DNA Polymerase (Invitrogen) according to the manufacturer's instructions supplemented with 2 µl of the viral DNA template (200 ng/µl) extracted using the DNAeasy Blood and Tissue Kit (QIAGEN) according to the manufacturer's instructions and 1 µl of each primer (UL-37-F and UL38-R 10 pmol/µl).

The cycling protocol used was the following: 95°C for 5', 25 cycles x (95°C for 30'', 60°C for 30'', 72°C for 1'20''), 72°C for 10', 4°C forever. The PCR in Figure 18 shows a 600-bp band expected after correct removal of the BAC in both KG and ICP4-miR124t. The two primers couldn't amplify the expected 10-kb band in the control sample KGB because the extension time of the PCR cycle was not long enough

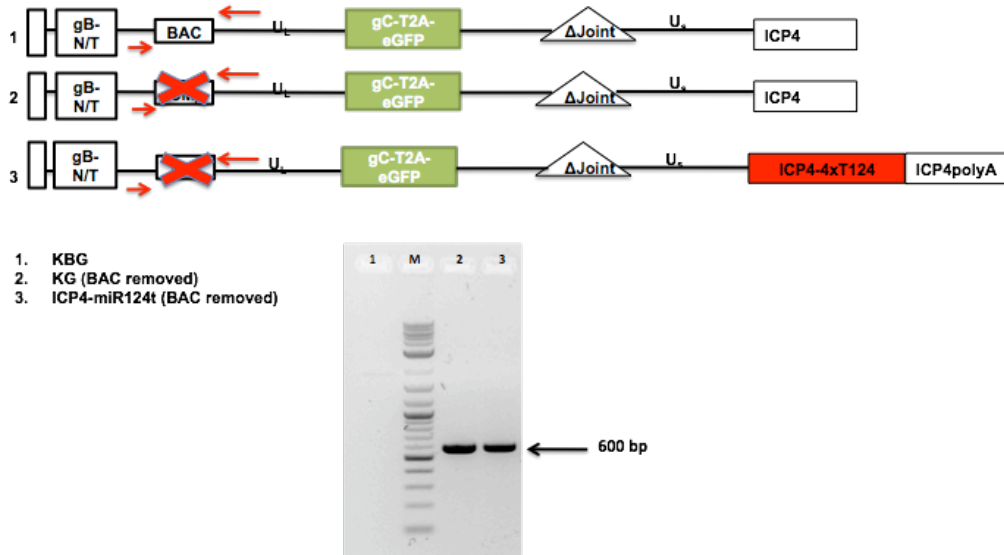


Figure 18: PCR to verify correct removal of the BAC after infection of U2OS-Cre cells.

After X-gal staining one *lacZ*-negative viral clone was selected for both KG and ICP4-miR124t and checked by PCR with primers outside the BAC region for clean removal of the region between the *loxP* sites. Both KG and ICP4-miR124t isolates showed a 600-bp band expected after correct removal of the BAC. The two primers couldn't amplify the expected 10-kb band in the control sample KGB.

2.8 Creation of Tet-on-miR124 stable cell line

2.8.1 Extraction of total DNA from U87 cells

Both human *pri-miR124* and *pri-miR137* sequences were PCR amplified using the genomic DNA extracted from U87 (human grade IV glioblastoma cell line) as a template. To extract DNA from U87 cells, 9×10^6 cells were first incubated in a Proteinase K (Sigma) digestion cocktail (10 mM Tris pH=7.5, 100 mM NaCl, 10 mM EDTA, 0.5% SDS, 0.2 mg/ml Proteinase K) at 50°C for 4 h with light vortexing every 45'. The digestion mixture was then combined with one volume of (25:24:1 v/v) Phenol/Chloroform/Isoamyl Alcohol solution (solution) and centrifuged at maximum speed for 15'. The top layer was then combined with one volume of Chloroform and centrifuged at maximum speed for 10'. The top layer was then combined with 2.5 volumes of 100% EtOH (ethyl alcohol) and left at -20°C overnight to allow precipitation of DNA. The DNA then was centrifuged 10' at maximum speed, the pellet washed twice with 70% EtOH and finally resuspended in ddH₂O.

2.8.2 Engineering of a Tet-On-miR124 construct

To generate an inducible cell line expressing miR124, I generated a Tet-On-miR124 construct in two steps. In the first step, illustrated in Figure 19, the rtTA gene was PCR amplified from a pgk-rtTA-Sv40polyA plasmid (kindly donated By Dr. Richard Chaillet, University of Pittsburgh) with BrtTA-F and NrtTA-R primers, designed to carry a BgIII and a NotI restriction sites. The rtTA PCR reaction was performed using High Fidelity KOD DNA Polymerase (Millipore) according to manufacture instructions supplemented with 0.5 ul of pgk-rtTA-Sv40polyA template (200 ng/ul) and 1 ul of each primer (BrtTA-F and NrtTA-R 10 pmol/ul). The cycling protocol used was the following: 95°C for 1', 25 cycles x (95°C for 30'', 60°C for 30', 72°C for 40''), 72°C for 10', 4°C forever. The 750-bp rtTA PCR product was ligated into pZero-blunt vector (Invitrogen). One rtTA-pZero positive clone was selected and sent for sequencing to verify the integrity of the amplified sequence. The rtTA gene was then inserted between BamHI and NotI sites in a pCDNA3.1 expression plasmid (Invitrogen) between the CMV promoter (pCMV) and the bovine growth hormone polyadenylation (bGH-polyA) signal. The BamHI and Nhel sites from the pCDNA-rtTA construct were eliminated to facilitate the future cloning steps by digesting with BamHI and Nhel and blunting with Klenow DNA polymerase (NEB). The expected 6.7-Kb band was gel purified, re-ligated, and screened through BamHI and Nhel diagnostic digest to ensure that both restriction sites had been eliminated (Figure 19A) The TetO promoter was isolated from TetO-pks construct (kindly donated By Dr. R. Chaillet, University of Pittsburgh) and inserted into pDsRed2.1 expression plasmid (Clonetech) between Xhol and EcoRI restriction sites (Figure 19B). The resulting construct, called DsRed-TetO, was used as backbone to create DsRed-TetO-rtTA by digestion with XmaI and AflII and blunting by Klenow DNA polymerase (NEB). pCMV-rtTA-bGH-polyA was excised from the previously generated pCDNA-rtTA with Bpu10I and PvuII, blunted by Klenow DNA polymerase and insterted into the DsRed-TetO backbone (Figure 19C).

In the second step, illustrated in Figure 20, using as template the genomic DNA extracted from U87 as described in section 2.8.1, the human *pri-miR124* sequence was PCR amplified from the *hsa-mir124-3* gene (located on chromosome 20q13.33) with primers Bmir124-F and NmiR124-R designed to carry a BamHI and a Nhel restriction sites to simplify the cloning procedure. The pri-miR124 PCR reaction was performed using High Fidelity Accuprime GC-rich DNA Polymerase (Invitrogen) according to manufacture instructions supplemented with 2.5 ul of U87 total DNA template (100 ng/ul) and 1ul of each primer (miR124-F and miR124-R 10 pmol/ul).

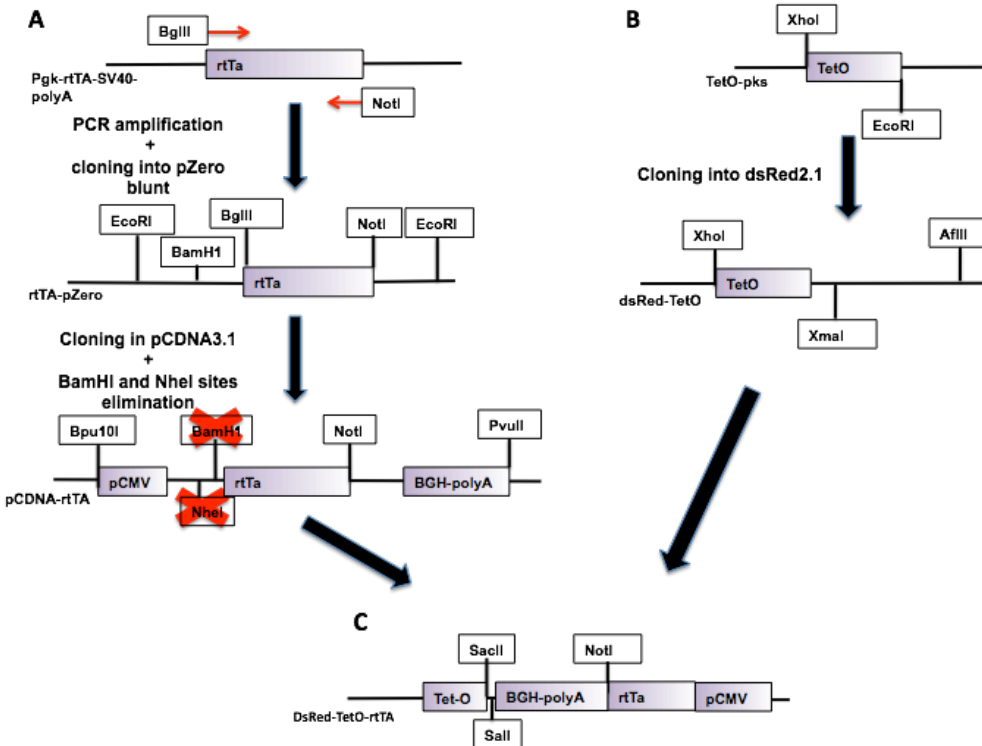


Figure 19: Generation of the TetO-inducible miR124-expressing construct: Step 1.

(A): cloning of the rtTA gene. The rtTA gene was PCR amplified from a pgk-rtTA-Sv40polyA plasmid with BrtTA-F and NrtTA-R primers. The 750-bp rtTA PCR product was ligated into pZero-blunt vector. The rtTA gene from one selected and sequenced rtTA-pZero clone was then inserted between BamHI and NotI sites in a pcDNA3.1 expression plasmid between the CMV promoter (CMVp) and the bovine growth hormone polyadenylation (bGH-polyA) signal. The BamHI and Nhel sites from this pcDNA-rtTA construct were then eliminated. **(B): Cloning of the TetO promoter.** The TetO promoter was isolated from TetO-pks and inserted into pDsRed2.1 expression plasmid between Xhol and EcoRI restriction sites. The construct was called DsRed-TetO. **(C): Cloning of TetO promoter and rtTA gene together in the same plasmid.** pCMV-rtTA-bGH-polyA was excised from the pCDNA-rtTA with Bpu10I and Pvull, blunted and inserted in DsRed-TetO used as backbone after digestion with XmaI and Afll and blunting. The construct was called DsRed-TetO-rtTA.

The cycling protocol used was the following: 95°C for 5', 32 cycles x (95°C for 1', 55°C for 1', 72°C for 30"), 72°C for 10', 4°C forever. The 320-bp pri-miR124 PCR product was inserted into pZero-blunt vector and a pZero-miR124 positive clone was selected and sent for sequencing to verify the integrity of the amplified sequence (Figure 20A). The pri-miR124 fragment was then inserted in the miRNASElect pEP-miR Cloning and Expression Vector (Cell Biolabs Inc.) between BamHI and Nhel cloning sites, designed to insert pri-miR sequences within an intron in the 5' UTR of the rPuro (Puromycin-resistance) gene. The resulting construct was called pEP-miR124 (Figure 20B and Table 5). The intron-miR124-rPuro cassette was removed from pEP-miR124 by Acc65I and AcII digest and was placed behind the TetO-inducible promoter in the DsRed-TetO-rtTA by blunt end cloning into a SacII site.

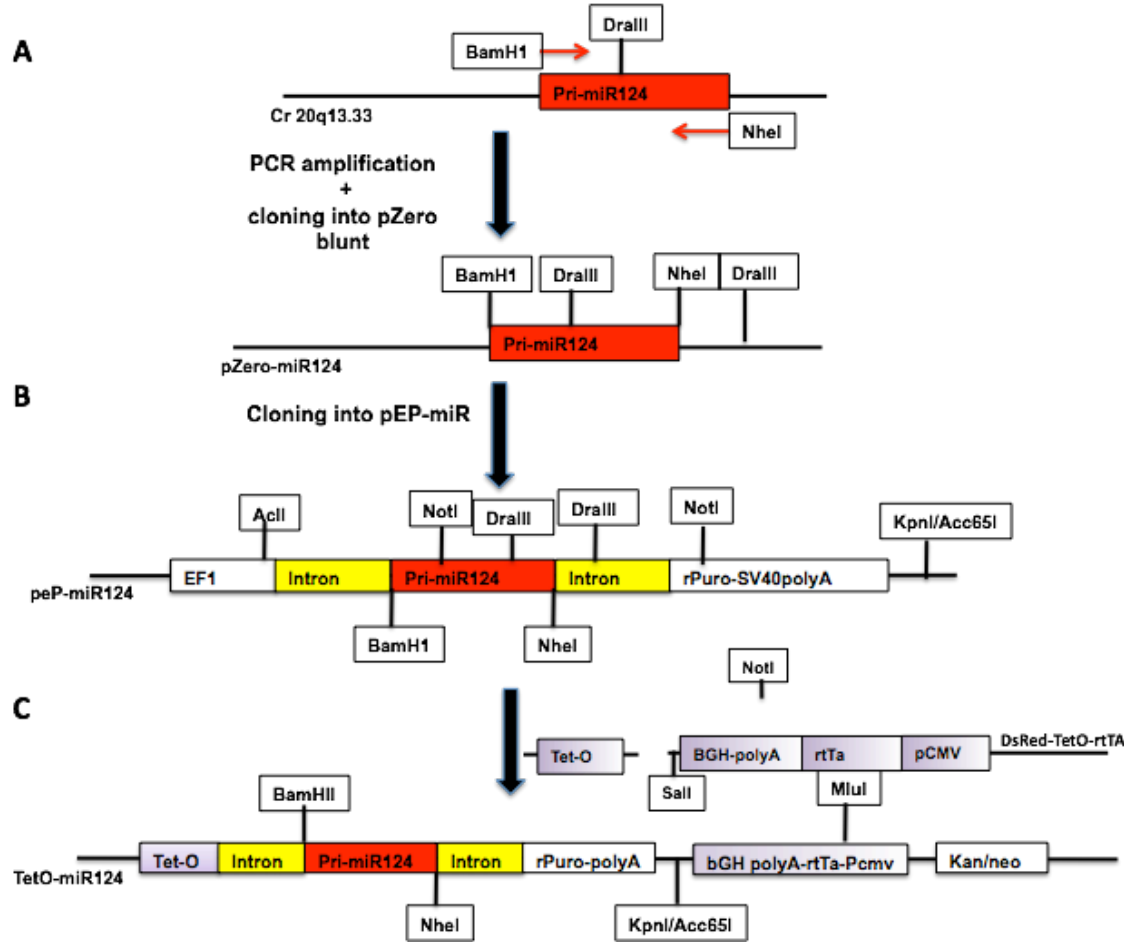


Figure 20: Generation of the TetO-inducible miR124-expressing construct Step 2.

(A): The human *pri-miR124* sequence was PCR amplified from the *hsa-mir124-3* gene (located on chromosome 20q13.33) of the U87 cells total DNA with primers Bmir124-F and NmiR124-R. The 320-bp *pri-miR124* PCR product was inserted into pZero-blunt vector. One positive pZero-miR124 clone was selected and sent for sequencing. (B): The *pri-miR124* fragment was then cloned from pZero-miR124 to a miRNASElect pEP-miR Cloning and Expression Vector between BamHI and NheI cloning sites, within an intron in the 5' UTR of the *rPuro* (Puromycin-resistance) gene. (C): The intron-miR124-rPuro cassette was removed from pEP-miR124 by Acc65I and AcII digest and was placed behind the TetO-inducible promoter in the DsRed-TetO-rtTA by blunt end cloning into a SacII site. The resulting construct was called TetO-miR124.

The resulting construct was called TetO-miR124 (Figure 20C and Table 5). To be used as control for TetO-miR124, a TetO-intron (Table 5) inducible construct without miRNA was created by digesting TetO-miR124 with BamHI and NheI (NEB) to remove the miR, then blunting through Klenow DNA polymerase (NEB) and religating.

2.8.3 U2OS transfection and selection of stable clones

The TetO-miR124 and TetO-intron constructs, which express the neomycin (neo) resistance gene, were transfected in U2OS cells to make a TetO inducible stable cell lines. On the day before transfection cells were plated as monolayer at 50% confluence on 2 wells of a 6 well plate at a density of 0.5×10^6 cells /dish. 24 h later 80% confluent cells were transfected with either TetO-miR124 or TetO-intron using Lipofectamine 2000 (Invitrogen) following the manufacturer's instructions. Cells were than incubated at 37°C in 5% CO₂. 24 h after transfection cells were treated with 0.75 mg/ml G-418 (50 mg/mL, Gemini), obtaining a mixed population of U2OS cells expressing Tet-inducible miR124 (U2OS-Tet-miR124 cells) or Tet-inducible control cells (U2OS-Tet-control). Single clones of stably transfected U2OS-Tet-miR124 and U2OS-Tet-control cells were then isolated through limiting dilution in G418 selection. 60 U2OS-Tet-miR124 and 10 U2OS-Tet-control cell clones were then tested for miR124 expression after doxycycline (Dox, Sigma) induction. One day before treatment each clone was plated on 2 wells of a 48 well plate at a density of 0.5×10^5 cells/dish. 24 h later cells were treated with (1 µg/ml) of Dox and incubated at 37°C in 5% CO₂ for 48 h. Total RNA was collected from each clone using Trizol (Invitrogen) according to the manufacturer's instructions. RT-qPCR on the total RNA extracted was then performed as described in section 2.8.4. The miR124 expression was calculated relative to the expression of RNU-43 a small RNA used as internal control.

2.8.4 RT-qPCR for miR124 quantification

RT-qPCR was performed on total RNA reverse transcribed from cell sample using the TaqMan Small RNA Assay kit (Applied Biosystems), that included both the RT primers and the qPCR primers for both hsa-miR-124a and hsa-RNU-43, a small RNA used as internal control, following the manufacturer's instructions. The RT primers were used together with the TaqMan MicroRNA Reverse Transcription kit (Applied Biosystems) to reverse-transcribe 10 ng of Trizol-extracted total RNA, while the qPCR primers were used to measure the amount of miR124 and RNU-43 present using StepOne Plus Real Time PCR System (Applied Biosystem). The thermal cycling conditions used were the following: 50°C for 2', 95°C for 10', 40 cycles x (95°C for 15'', 60°C for 1'). Mir124 expression relative to RNU-43 expression was then calculated using the comparative C_T method according to the manufacturer's instructions (Applied Biosystems).

2.8.5 oHSV-1 infection of U2OS TetO stable lines, SHSY5Y, 50B11, PC12 following miR-124 inducing drug treatment with either doxycycline (Dox), Forskolin or Nerve Growth Factor (NGF)

To examine potential effects of induced miR124 expression on oHSV-1 activity, both KG and ICP4-miR124t viruses were tested in Tet-miR124-10, Tet-miR124-84 and Tet-negative-7 in presence or absence of a 48 h long doxycycline (Dox) treatment, 50B11 in presence or absence of a 48 h long Forskolin treatment, PC12 after a 7-14 days long NGF treatment and naïve SHSY5Y. One day before drug treatment, cells were plated at a 50% confluent monolayer. 24 h later cells were treated with either 10 µg/ml Dox (Sigma), 75 µM Forskolin (Sigma), 50 ng/ml NGF(Sigma) or left untreated and incubated at 37°C in 5% CO₂ for as long as required by the specific treatment. Following treatments, cells were divided in two groups. On the first group total RNA was collected using Trizol (Invitrogen) according to the manufacturer's instructions and RT-qPCR for miR124 expression was performed as described in section 2.8.4. The second group of cells was instead infected with either KG or ICP4-miR124t at the appropriate MOI (MOI= 0.01 and 0.001 for TetO stable clones; MOI= 0.1 for 50B11; MOI= 0.3 and 3 for PC12; MOI= 0.1, 0.01 and 0.001 for SHSY5Y cells). At different timepoint after infection (24, 48, and 72 h PI for TetO clones; 24, 48, 72, 120, 196 h PI for 50B11; 48 and 120 h PI for PC12; 24, 48, 96 h PI for SHSY5Y), cells and supernatants were collected and sonicated using the Ultrasonic Processor XL sonicator (Misonix Inc.) to free the virus still trapped inside cells. Viral supernatants were then cleaned from cellular debris through centrifugation at 3000 rpm for 10' and titered on U2OS cells in p.f.u /ml to measure HSV replication (see Section 2.2.3).

2.9 Creation of a transiently expressing Lenti-miR124 and Lenti-miR137A Primary Glioma Cells

2.9.1 Engineering of pCDH-miR124 expression construct

The pCDH-miR124 construct used to generate the Lenti-miR124 virus was engineered from the original lentiviral expression vector pCDH-CMV-EF1 (System Biosciences), as illustrated in Figure 21A.

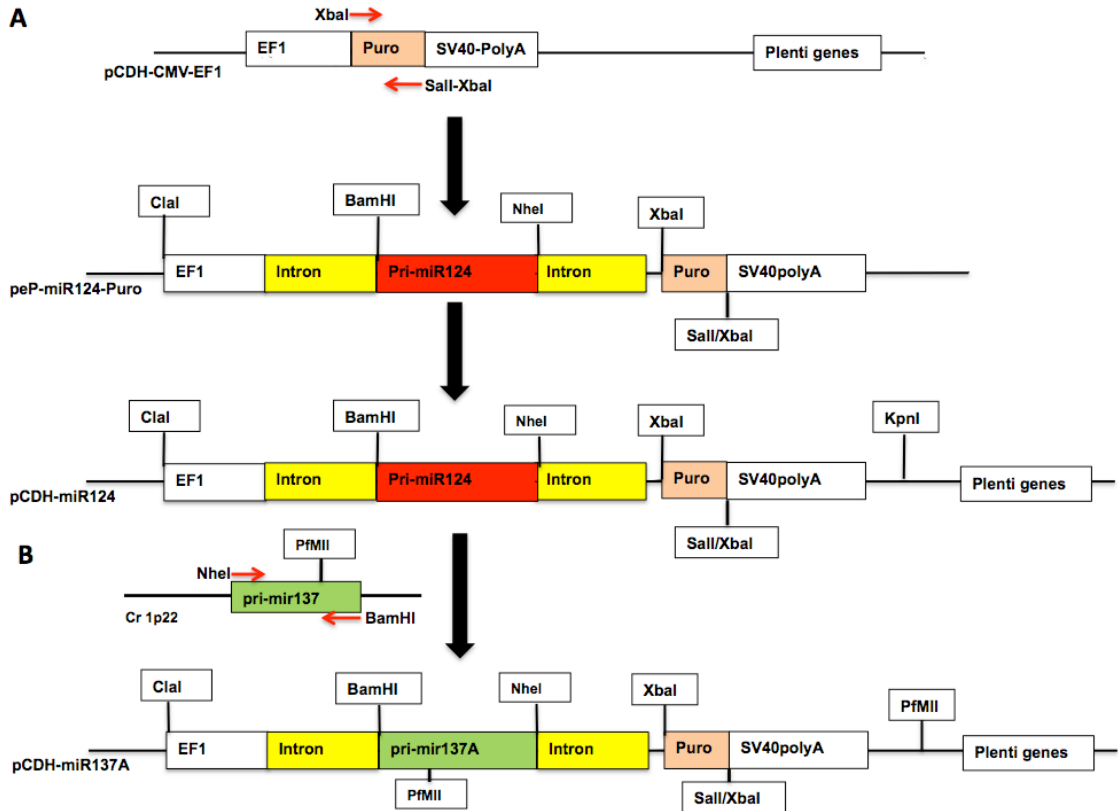


Figure 21: Generation of pCDH expression constructs.

(A): Engineering of pCDH-miR124. the Puromycin (Puro) gene was PCR amplified using an upper primer (X-Puro-F) carrying a XbaI restriction site and a lower primer (XS-Puro-R) carrying a Sall and a XbaI restriction sites and inserted into pEP-124 construct (Figure 19) between two XbaI sites. The resulting construct was called pEP-miR124-Puro. The EF1-intron-miR124-Puro expression cassette was excised from the Pep-miR124-Puro plasmid and inserted into the pCDH-CMV-EF1 lentiviral expression vector between Clal and Sall sites. The resulting lentiviral construct was called pCDH-miR124. (B): Engineering of pCDH-miR137A. The human pri-mir137 sequence was PCR amplified with two primers, Nmir137-F carrying a NheI site and BmiR137-R carrying a BamHI restriction site, from the *hsa-mir137* gene of U87 cells total DNA, located on chromosome 1p22. The pCDH-miR124 construct and the pri-miR137 PCR product were digested with BamHI + NheI, gel purified and ligated together to create pCDH-miR137A with the miR137 sequence positioned in the reverse (anti-sense) orientation.

First, the Puromycin (Puro) gene was PCR amplified using an upper primer (X-Puro-F) carrying a XbaI restriction site and a lower primer (XS-Puro-R) carrying a Sall and a XbaI restriction sites, to be inserted into pEP-124 construct (see section 2.8.2 step 2) between two XbaI sites. The PCR reaction was performed using High Fidelity Accuprime GC-Rich DNA Polymerase (Invitrogen) according to manufacture instructions supplemented with 1uL of the pCDH-CMV-EF1 (200 ng/ul) and 1ul of each primer (X-Puro-F, XS-Puro-R 10 pmol/ul). The cycling protocol used was the following: 95°C for 5', 30 cycles x (95°C for 30", 57°C for 30", 72°C for 1'), 72°C for 10', 4°C forever. The resulting construct was called pEP-miR124-Puro. The EF1-intron-

miR124-Puro expression cassette was excised from the Pep-miR124-Puro plasmid to be inserted into the pCDH-CMV-EF1 lentiviral expression vector between Clal and Sall sites. The resulting lentiviral construct was called pCDH-miR124 (Table 5).

2.9.2 Engineering of pCDH-miR137A control expression construct

To have a control lentivirus to use during Lenti-miR124 infection, the pCDH-137A construct was created from the pCDH-miR124 construct by substituting the miR124 sequence with a miR137 sequence cloned in opposite orientation as illustrated in Figure 21B.

First, the human pri-miR137 sequence was PCR amplified with two primers, Nmir137-F carrying a Nhel site and BmiR137-R carrying a BamHI restriction site, from the *hsa-mir137* gene, located on chromosome 1p22, using as template the genomic DNA extracted from U87 cells as described in section 2.8.1. The pri-miR137 PCR reaction was performed using High Fidelity Accuprime GC-rich DNA Polymerase (Invitrogen) according to manufacturer instructions supplemented with 2.5 uL of hES total DNA template (100 ng/uL) and 1uL of each primer (NmiR137-F and BmiR137-R 10 pmol/uL). The cycling protocol used was the following: 95°C for 5', 32 cycles x (95°C for 1', 55°C for 1', 72°C for 30"), 72°C for 10', 4°C forever. The 297-bp pri-miR137 PCR product was then gel purified and resuspended in ddH₂O. The pCDH-miR124 construct created in section 2.9.1 and the pri-miR137 PCR product were digested with BamHI + Nhel, gel purified and ligated together to create pCDH-miR137A (Table 5).

2.9.3 Production of Lenti-miR124 and Lenti-miR137 viruses

To produce all lentiviruses, the pCDH expression constructs were cotransfected with three pLenti packaging plasmids (PLP1, PLP2, PLP-VSVG) into 293T cells, the cell line of choice to produce high lentiviral titer. The day of transfection 10x10⁶ cells were plated on two 10 cm dishes coated with poly-lysine (Sigma). 6 h later attached cells were co-transfected with 3 µg of either pCDH-miR124 or pCDH-miR137A plus a mixture of three pLenti packaging plasmids (1.5 µg of pLP1, 1.0 µg of pLP2 and 1.5 µg of pLP-VSVG from Invitrogen) using Lipofectamine 2000 reagent (Invitrogen) according to the manufacturer's instructions and incubated overnight at 37°C in 5%CO₂. 24 h after infection cell medium was changed and cells were incubated at 33°C in 5% CO₂ for additional 48 h, a condition that blocks cells from overgrowing without interfering with viral replication. 72 h after transfection the cell supernatants containing the viruses were

collected, filtered through a 0.45 µm filter (Millipore) to clean it from impurities and centrifuged at 7500 rpm for 16 h. Each viral pellet was then resuspended in DMEM and titered on 293T cells to assess lentivirus concentration for the subsequent transient expression assays.

2.9.4 Lentivirus titration calculated in colony forming units (c.f.u. /ml)

The day before lentivirus titration 80% confluent 293T cells were plated on a 6 well dish and incubated overnight at 37°C in 5% CO₂. 24 h later cells were infected with serial 10-fold dilutions of viral supernatant plus 8 µg/ml polybrene (Sigma), an enhancer of lentivirus infection, and incubated overnight at 37°C in 5% CO₂. 24h after infection cell medium was changed and cells were incubated with 8 µg/ml of puromycin (puro, Sigma), whose resistance gene was expressed from the pCDH backbone. Colonies of puromycin resistant pCDH expressing cells were counted 10-15 days after initial infection and viral titer calculated in colony forming units (c.f.u. /ml).

2.9.5 Lenti-miR124 infection of primary glioma cells

To examine potential effects of lentiviral miR124 expression on primary glioma cells, such as neuronal differentiation or reduced cell viability, Gli68 and GBM30 primary glioma cells were infected with either Lenti-miR124 or Lenti-miR137A viruses. On the day of the infection both cells, which were grown as spheroid aggregates, were broken up into single cells to allow viral infection. 2 x 10⁵ cells/ virus were then counted and infected with either Lenti-miR124 or Lenti-miR137A viruses at MOI of 5.0 based on 293T cells titration calculated in c.f.u /ml (see section 2.9.4) in 1.5 ml of regular growth media plus 8 µg/ml polybrene. Cells were incubated with gentle rotation in 2.0 ml eppendorf tubes at 37°C for 90' and then plated on 2 wells of a 6 well plate. 24 h after infection cell medium was replaced with fresh medium and cells were selected with 30 µg/ml of puromycin whose resistance gene was jointly expressed with miR124 from the pCDH plasmid. At 72 h after puromycin selection (96 hours after initial lentivirus infection), part of the cells was collected and total RNA was extracted using Trizol (Invitrogen) according to the manufacturer's instructions to measure miR124 expression by RT-qPCR (see Section 2.8.4). Another part of the cells instead was super-infected with either ICP4-miR124t or KG virus at an MOI of 0.01 to test oHSVs response to miR124 expression (see Section 2.9.6)

2.9.6 KG and ICP4-miR124t oHSV infection of primary glioma cells

On the day of the infection both GBM30 and Gli68 primary glioma cells, which were grown as spheroid aggregates, were broken up into single cells to allow viral infection. 2×10^5 cells were then counted and infected with either ICP4-miR124t or KG virus at MOI of 0.01 in 1.5 ml of regular growth media. Cells were then incubated with gentle rotation in eppendorf tubes at 37°C for 90' and then plated on a 48 well plate (2 wells per timepoint per virus). At 72 and 96 h post infection, cells and supernatants were collected and sonicated using the Ultrasonic Processor XL sonicator (Misonix Inc.) to free the virus still trapped inside cells. Viral supernatants were then cleaned from cellular debris through centrifugation at 3000 rpm for 10' and titered on U2OS cells in p.f.u /ml to measure HSV replication (see section 2.2.3).

2.10 In Vivo Toxicity Testing

The ICP4-miR124t viral response to endogenous levels of miR124 was assessed *in vivo* by toxicity studies performed to evaluate potential immunologic and pathogenic effects on normal brain in tumor-free, immunodeficient NUDE BALB/c mice and in tumor free immunocompetent BALB/c mice.

2.10.1 Viral injections in immunocompetent mice

Either KG or ICP4-miR124t virus was administered by intracranial stereotactic injection into the right temporal lobe (cortex) of 3 weeks old female regular BALB/c mice for a total of 3 mice per virus. A single dose of 4.8×10^9 genome-copies (gc) of each virus was tested by injecting each mouse with 4 µl of viral prep. Two animals, one for each virus, were sacrificed 3 hours after injection (hpi), while the remaining animals were left alive and monitored for general health (weight, activity, clinical signs) every other day after injection. At 5 days post injection (dpi) the first KG animal started giving signs of vector related pathology, specifically more than 30% weight loss, loss of activity, arched back, no grooming, and it was sacrificed together with one mouse injected with the ICP4-miR124t virus. The second KG animal was instead sacrificed at 7dpi because, after being sick for the first 5 dpi, it started to show signs of recovery, possibly indicating of a change in viral yield in its brain. On the contrary, the second ICP4-miR124t injected virus was not sacrificed at that time, but was left alive to these days where it continues

to be monitored for general health. All animals were first sacrificed by saturating a sealed chamber with CO₂ for 2 minutes, and then their entire brain was collected and stored in PBS. At this point, total DNA was extracted from each brain using the DNAeasy Blood and Tissue Kit (QIAGEN) according to manufacturer's instructions. To determine the amount of viral genomes present in each brain compared to the amount of virus injected on day 0, qPCR for the HSV glycoprotein D (gD) gene was performed as described in section 2.2.4.

2.10.2 Viral injections in immunocompromised mice

Either KG or ICP4-miR124t virus was administered by intracranial stereotactic injection into the right temporal lobe (cortex) of 3 weeks old female nu/nu nude BALB/c mice for a total of four mice per virus. A single dose of 1.5x10⁹ gc of each virus was tested by injecting each mouse with 4 µl of viral prep. The animals that survived from viral injection were sacrificed at 5, 14, 21 and 33 dpi by saturating a sealed chamber with CO₂ for 2 minutes and their entire brain collected and stored in PBS. At this point, total DNA was extracted from each brain using the DNAeasy Blood and Tissue Kit (QIAGEN) according to manufacturer's instructions. To determine the amount of viral genomes present in each brain compared to the amount of virus injected on day 0, qPCR for the HSV glycoprotein D (gD) gene was performed as described in section 2.2.4.

3 RESULTS

3.1 Validation of the use of a joint deleted HSV-1 as backbone to create a GBM oncolytic vector

The 152-kb HSV-1 genome is organized into a Unique Long (U_L) and a Unique Short (U_S) region, each flanked by inverted repeats as shown in Figure 1. The junction between the internal repeats is called Joint and contains one copy of *ICP0*, *ICP4* and $\gamma 34.5$ genes; the unique regions can flip back and forth, creating four possible HSV isomers and making the HSV genome unstable and prone to internal recombination^{15,16}. The deletion of the joint freezes the HSV genome as one of its isomers, maintaining one copy of each of its diploid genes, *ICP0*, *ICP4* and $\gamma 34.5$, and stabilizing the vector against internal recombination events, facilitating accurate engineering without affecting virus ability to replicate and kill tumor cells *in vitro*.

Previous *in vitro* studies have demonstrated that deletion of the joint region of HSV-1 produces a viable virus that can be grown in cell culture, meaning that this region is dispensable for viral replication *in vitro*⁶⁰. Vectors described in this study were derived from KOS-BAC (KB illustrated in Table 5), a complete HSV-1 strain KOS genome cloned on a bacterial artificial chromosome (BAC) and kindly donated by Dr. D.A. Leib⁵³. To facilitate vector engineering and stabilize the HSV genome, a joint deleted version of KB, KOS-BAC-ΔJ (KBJ illustrated in Table 5), was previously created in our laboratory by deleting the KB internal repeat (Joint) region between UL56 and US12 including the portion corresponding to the ICP47 promoter. I examined the growth of KB and KBJ on two immortal cell lines routinely used in our laboratory for HSV propagation, Vero and U2OS, to confirm previous reports that the joint is dispensable for virus replication *in vitro*⁶⁰. 24 hours (h) and 48 h after initial infection at a multiplicity (MOI) of 1, viral supernatants were collected and titered to quantify viral yields. As shown in Figure 22, both KB and KBJ exponentially replicated in both cell lines with a difference in titer between the two viruses of only about 4 times in U2OS and 10 times in Vero cells at 48 h post- infection (hpi), demonstrating that the deletion of the joint region of HSV-1 does not dramatically decrease the ability of the virus to replicate in tumor cells *in vitro*.

These results show that a joint-deleted HSV-1 virus constitutes a good platform for the development of an oncolytic virus against GBM because it is comparable to its non-deleted

counterpart in terms of replication in immortalized cells *in vitro*, while more stable and easier to engineer than its deleted counterpart.

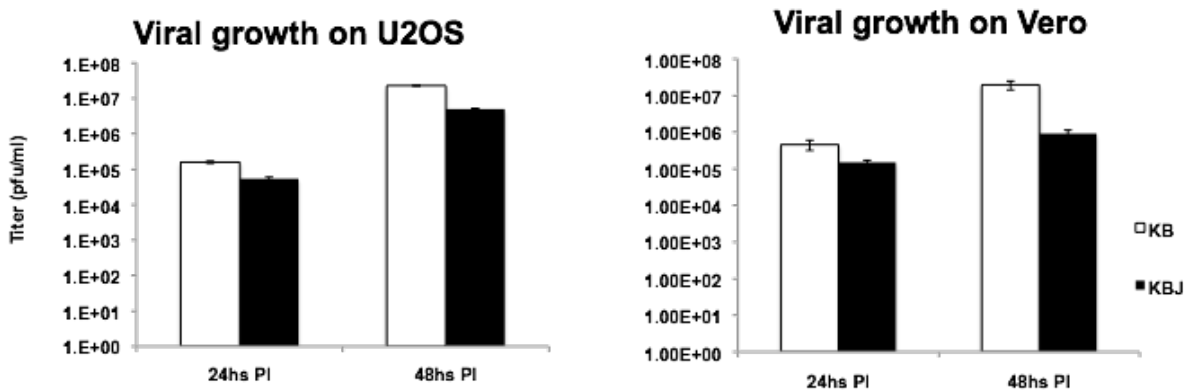


Figure 22: Replication efficiency of Joint deleted KOS-BAC (KBJ) *in vitro*

Both Vero and U2OS cells were infected with either KOS-BAC (KB) or KOS-BAC- Δ J (KBJ) viruses. At 24hrs and 48hrs after initial infection viral supernatants were collected and titered on Vero cells. Plates were then fixed and stained with crystal-violet. Viral plaques were counted and viral titer was calculated. The mean value \pm standard deviations from three determinations are illustrated. The chart shows no difference in viral growth between the two viruses

3.2 Testing of a firefly-Luciferase expression plasmid (pLuc) carrying the miR124 responsive element 4xT124

To test the ability of a miR124 responsive element (T124) to efficiently block protein expression when inserted in the 3'UTR of a target gene, a tandem of four copies of the miR124 target sequence (4xT124) obtained from the miRBase online database (http://www.mirbase.org/cgi-bin/mirna_entry.pl?acc=MI0000443) was inserted in the 3'UTR of the luciferase reporter gene in a firefly-Luciferase (fLuc) expression plasmid (pLuc-T124), as shown in Figure 4 (see Section 2.5 for construct description). A similar construct called pLuc-Tcon was created using a tandem of 4 copies of a random sequence without complementarity to miR124 to be used as control. To verify that the presence of miR124 effectively blocked luciferase activity, both constructs were co-transfected with a renilla luciferase (rLuc) internal control plasmid into U2OS and HEK293AD cells transiently expressing either miR124 or an unrelated control miRNA (miR21) transfected

24h earlier as pre-miRNAs. Cells were collected 48h after the second transfection, lysed, and luciferase activity in cell lysates was measured using a luminometer.

The results in Figure 23, normalized to rLuc activity, show a miR124-dependent 96% decrease in fLuc activity in HEK293AD expressing pLuc-T124 and an 89% decrease in U2OS cells. In contrast, no difference in fLuc activity was detected in either cell line expressing pLuc-Tcon or in miR21-transfected cells. These results demonstrated that the 4xT124 element is specifically responsive to miR124 expression, suggesting it could be introduced in the 3'UTR of the ICP4 gene to impede HSV-1 replication in miR124-expressing cells such as normal neurons.

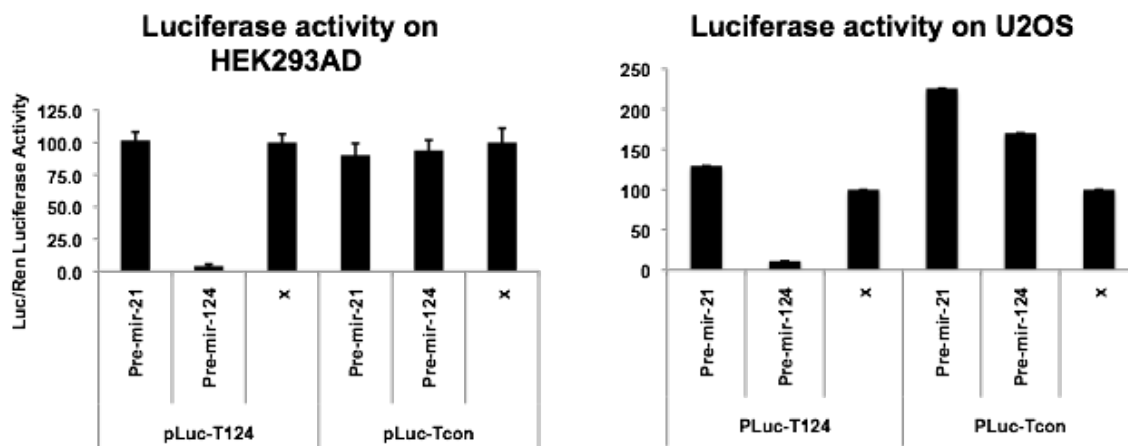


Figure 23: MiR124-controlled Luciferase Activity.

Both pLuc-T124 and pLuc-Tcon constructs were co-transfected with a renilla luciferase (rLuc) internal control plasmid into two different cell lines, HEK293AD and U2OS, transfected 24 h earlier with synthetic pre-miR124 or pre-miR21. 48 h after the Luc transfections cells were collected, lysed and luciferase activity in cell lysates was measured using a luminometer. The results normalized to rLuc activity represent the mean value \pm standard deviations from three determinations. Charts show strong inhibition of the luciferase activity only in cells expressing both pLuc-124 and pre-miR124.

3.3 Engineering and Production of a ICP4-miR124T oHSV-1 Oncolytic Vector

3.3.1 Engineering of the HSV-1 genome.

To generate the final ICP4-miR124t-BAC construct I added two modifications to the parental KOS-BAC-gB_{N/T}-ΔJ (KBBJ), as described in section 2.7 (Figure 5). KBBJ was derived from the

joint-deleted KBJ backbone by introducing a double mutation in gB, D285N/A549T, named (gB:NT)⁵⁷. All the schematics of the described BAC constructs are illustrated in Table 5.

The parental KBBJ was first modified by in-frame fusion of an eGFP gene preceded by a 2A translation-pause sequence with the last residue of the resident late viral gC gene (Figure 6). This first modification was generated to use eGFP green expression as a marker for viral replication and spread in infected cells both in vitro and in vivo. Using Red/ET recombination, a kan/strep counter-selection cassette was initially inserted in front of the gC stop codon. This cassette was then replaced with the T2A-eGFP sequence to create KOS-BAC-gB_{N/T}-ΔJ-gCeGFP (KBG). Both Red/ET mediated recombination steps were confirmed by PCR using primers flanking the insertion site and by FIGE to ensure that recombination had occurred correctly without major rearrangements elsewhere in the HSV genome. Compared to the parent KBBJ, PCR analysis of 5 isolates from the first recombination step showed the expected 1.3-Kb increase in the size of the amplified product caused by the counter-selection cassette insertion (Figure 9B), and FIGE analysis showed a 1.3-Kb upward shift of a HindIII fragment containing the intended insertion site (Figure 9C). After the second recombination step, only 2 isolates showed the 400-bp decrease in the size of the PCR product expected for correct replacement of the counter-selection cassette by the shorter T2A-eGFP sequence (isolates A6, C9, Figure 10B).

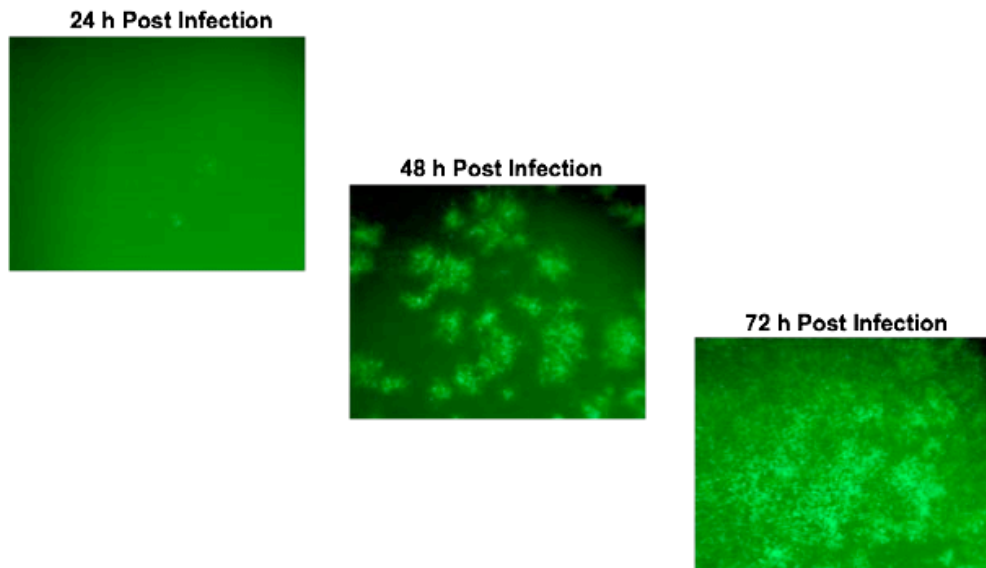


Figure 24: KBG BAC-DNA transfection into U2OS to verify BAC-DNA ability to generate virus.

Following transfection, cells were incubated at 37°C in 5% CO₂ and observed by fluorescence microscopy for eGFP expression every 24 h up to 72 h post transfection. Fluorescent pictures of actively replicating and spreading KBG into infected cells were taken using a Nikon Diaphot fluorescent microscope.

Although FIGE analysis of *Bgl*III digests seemed to indicate that both of these isolates were correct, *Hind*III digests revealed an aberrant deletion in isolate A6 (Figure 10C). The DNA of isolate C9 was then transfected into U2OS cells to ensure that the modified vector genome remained capable of virus production. As shown in Fig 24, transfection produced an increasing number of green cells over time, indicating active virus production and spread.

KBG isolate C9 was further modified to create KBG-ICP4-4xT124, abbreviated as ICP4-miR124t, by inserting the previously validated miR124 response element (4xT124, Section 3.2) into the 3' UTR of the *ICP4* gene, as illustrated in Figure 7. In this instance I used a modification of the Gene Bridges-Red/ET protocol to facilitate the second step, removal of the selection cassette⁵⁶. A DNA fragment consisting of (i) the 3'UTR of the *ICP4* gene with the insertion of 4xT124, (ii) a kanamycin-selection cassette preceded by an I-SceI restriction site and flanked by direct repeats, and (iii) *ICP4* 3' flanking sequence, was assembled and PCR amplified for replacement recombination with the homologous region of the *ICP4* gene. Following kanamycin selection and confirmation of recombinants, removal of the selection cassette was performed by introduction of the arabinose-inducible I-SceI expression plasmid pBAD-/SceI into confirmed colonies, arabinose-induced linearization of the BAC DNA, and Red/ET-mediated recombination between the direct repeats flanking the kan gene. Intermediate (kan^R) and final (kan^S) products were confirmed by PCR and FIGE. BAC DNAs from kan^R colonies selected in the first step were examined by PCR using primers at the ends of the recombination fragment. The results showed that only eight of the 16 selected isolates (B, C, G, J, K, L, M, N, P) showed the expected 1.3-Kb band, while one isolate (A) amplified one 130-Kb band identical to the band amplified from the ICP4 3'UTR region of the KBG control without the 4xT124-I-SceI-Kan insertion and five other isolates (4, 5, 6, 8, 9, 15) amplified both bands, the expected 1.3-Kb band plus the parental 130-bp band (Figure 15B). Of the 8 positive isolates two (ICP4-miR124t-kan-B and ICP4miR124t-kan-C) were selected and compared to the original KBG backbone by FIGE analysis of *Msp*I, *Afl*III or *Hind*III restriction digests. Restriction analysis of isolates B and C by FIGE indicated that both were correct (Figure 15C) and thus both were used for removal of the kan cassette. PCR analysis of isolates from this second step showed a band of the expected size (0.3 kb) in 4 isolates (ICP4-miR124t-B2, B3, B4, C1) out of six analyzed (Figure 16B). All 4 isolates were then examined by FIGE of restriction digests, showing the anticipated patterns for 3 of the 4 (ICP4-miR124t-B3, B4, C1) (Figure 16C). Sequencing of these fragments confirmed their structure illustrated in Figure 16D. To clean the bacteria from the pBad plasmid, which presence could have interfered with the ability of the ICP4-miR124t-B3, B4, C1 BAC-DNAs to make virus, the DNAs from the three positive recombinants ICP4-miR124t-B3, B4, C1

were re-electroporated in fresh DH10 β electrocompetent cells and re-analyzed by FUGE restriction analysis after digestion with HindIII. As shown in Figure 17, 9 out of 10 isolates lost the pBad The DNA from isolate n10 was randomly selected and transfected into eukaryotic cells to make virus. Transfection of isolate KB-ICP4-miR124t-C1-2 (sample n°10 on the FUGE image, renamed ICP4-miR124t-BAC) into miR124-negative U2OS cells demonstrated that the vector modifications were compatible with virus growth (Figure 25).

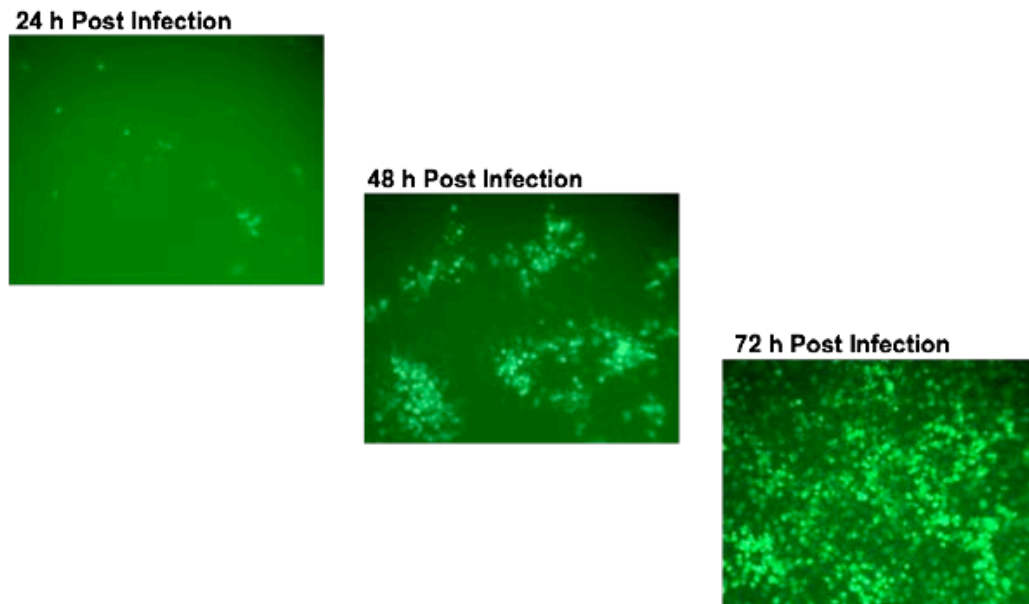


Figure 25: ICP4-miR124t BAC-DNA transfection into U2OS to verify BAC-DNA ability to generate virus.
Following transfection, cells were incubated at 37°C in 5% CO₂ and observed by fluorescence microscopy for eGFP expression every 24 h up to 72 h post transfection. Fluorescent pictures of actively replicating and spreading ICP4-miR124t into infected cells were taken using a Nikon Diaphot fluorescent microscope.

3.3.2 Production of KG and ICP4-MIR124t viruses

To generate the final oHSV-1 viruses to use for in-vitro and in-vivo testing, both KBG and ICP4-miR124t BAC DNA were transfected into U2OS-Cre cells (generated in our laboratory by Dr. Y. Miyagawa) to eliminate the *loxP*-flanked BAC sequence [36,37] known to negatively affect viral growth ⁵³. Loss of the BAC region, which also contains the *lacZ* reporter gene, was determined by staining the infected cells with X-gal. After limiting dilution of the U2OS-Cre derived viral supernatant on regular U2OS cells, one *lacZ*-negative viral clone was selected for both KBG-

BAC removed (now referred to as KG) and ICP4-miR124t-BAC-removed (now referred to as ICP4-miR124t) viruses. Each viral clone was checked for clean removal of the region between the *loxP* sites by PCR with primers outside the *LoxP* region (Figure 18) and grown to high titer in regular U2OS cells.

3.4 In Vitro Testing of ICP4-miR124T Vector for Growth Selectivity

3.4.1 ICP4-miR124t replication efficiency in transiently miR124-transfected cells

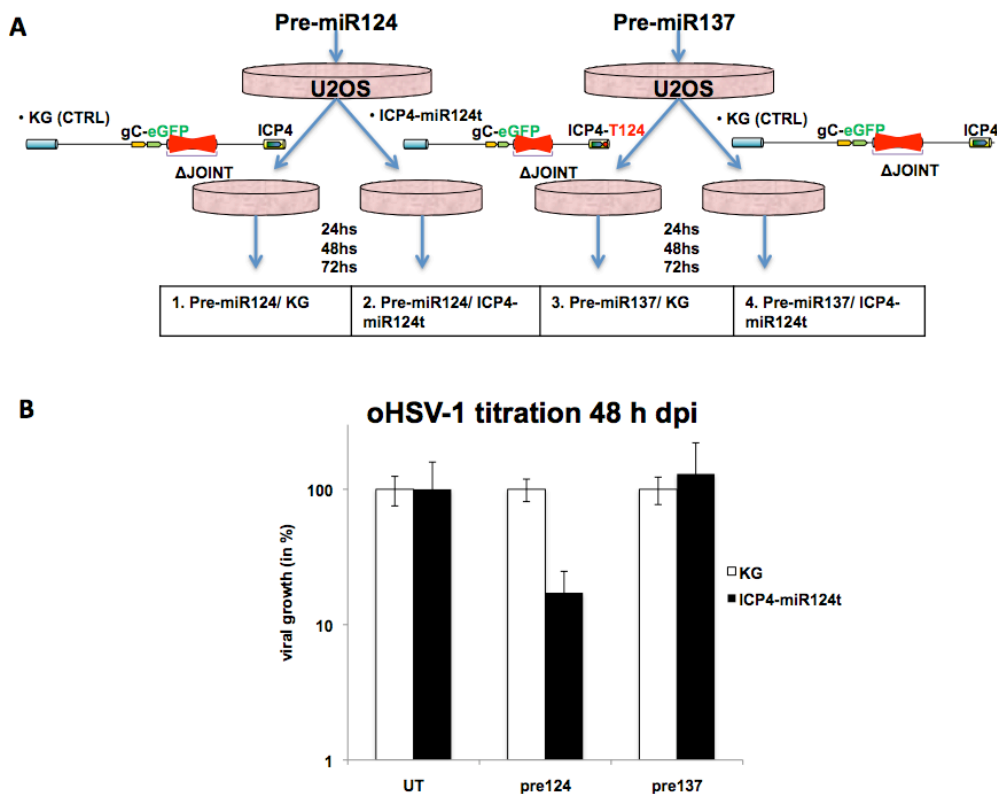


Figure 26: ICP4-miR124t oHSV-1 replication efficiency after miR124 transient transfection.

(A): **Experiment schematic.** Human U2OS cells were left untransfected or were transiently transfected either with pre-hu-pre-miR124-3 (Ambion) or hu-pre-miR137 (Ambion). 48 h later transfected and untransfected cells were infected with either KG or ICP4-miR124t. 48 h after infection the viral supernatant was collected and titered on regular U2OS to quantify virus yield. (B): **oHSV-1 titration.** ICP4-miR124t viral growth was first normalized to the growth of the control KB virus in untransfected, pre-miR124 transfected and pre-miR137 transfected cells. Data were then normalized to the growth of ICP4-miR124t in untransfected cells. The mean value \pm standard deviations from four determinations are illustrated. The chart shows ICP4-miR124t inhibition in the presence of miR124 expression, but not of miR137, with a decrease in growth of six times compared to the growth of the same virus in the absence of miR124.

The efficiency of replication of ICP4-miR124t was compared to that of KG in the presence or absence of miR124 as summarized in Figure 26A. Human U2OS cells (negative for miR124) were left untransfected or were transiently transfected either with pre-hu-miR124-3 (Ambion AM17100-PM10691) or pre-hu-miR137 (Ambion AM17100-PM10513), a neuronal-specific miRNA for which the ICP4-miR124t virus had no responsive elements. 48 h later transfected and untransfected cells were infected with either KG or ICP4-miR124t. 48 h after infection, supernatants were collected and titered on U2OS cells to quantify virus yields. The experiment was done in quadruplicate to obtain statistically significant results. ICP4-miR124t viral growth was first normalized to the growth of the control KB virus in untransfected, pre-miR124 transfected and pre-miR137 transfected cells. Data were then normalized to the growth of ICP4-miR124t in untransfected cells. As shown in Figure 26B, ICP4-miR124t growth was reduced approximately 6-fold by miR124 expression. Moreover, ICP4-miR124t growth inhibition was miRNA specific as the expression of miR137 in the infected cells did not impair ICP4-miR124t viral growth.

3.4.2 ICP4-miR124t replication efficiency in miR124-inducible stable cell lines

To better quantify the miR124-dependent difference in viral growth between ICP4-miR124t and the KB control vector, stable miR-124-inducible cell lines were generated. An expression construct was created in which the promoter that controls miR124 synthesis is activated in response to treatment with tetracycline (Tet) or doxycycline (Dox).

As shown in Figure 27, the Tet-On inducible system was comprised of a recombinant, tetracycline controlled transcription activator (rtTA) expressed from the *rtTA* gene that, following binding of Tet or Dox, interacted with tet operator (tetO) elements in an rtTA responsive promoter (Ptet) and induced the expression of the gene of interest under the control of this promoter. In the absence of Tet or Dox, rtTA was not able to bind to Ptet and the gene of interest was not expressed⁶¹.

The structures of the Ptet-miR124-rtTA construct and a related control construct expressing no miRNA are shown in Table 5. The Tet-miR124 and Tet-intron control constructs were transfected into U2OS cells to generate Tet-inducible miR124 expressing and control clones. Real-time RT-qPCR demonstrated different levels of miR124 in the highest miR124-expressing clones Tet-miR124-10 and Tet-miR124-84, with the former expressing 8.5 times more miR124

than the latter at 48 h after Dox treatment (Figure 28). Expression of miR124 in the control clone (Tet-negative-7) was several orders of magnitude lower and uninducible.

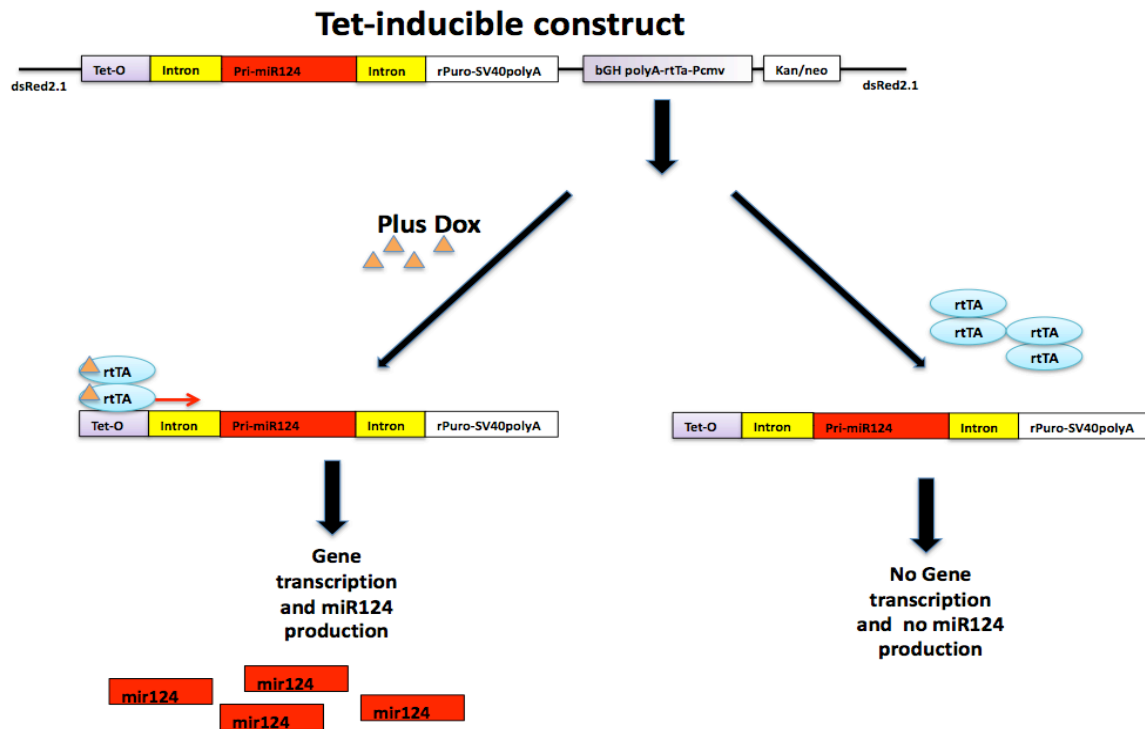


Figure 27: Tet-inducible construct for Hu-mir124-3 expression.

The Tet-On inducible system is comprised of a recombinant, tetracycline controlled transcription activator (rTta) expressed from the *rTta* gene that, following binding of tetracycline or its analog doxycycline, interacts with tet operator (tetO) elements in an rTta responsive promoter (Ptet) and induces the expression of the gene of interest, in this case pri-miR124, under control of Ptet. In the absence of tetracycline (or doxycycline), rTta cannot bind to Ptet and the gene of interest is not expressed. Specifically in TetO-miR124 construct, the addition of doxycycline activates rTta that binds to the TetO promoter and induces both pri-miR124 and puromycin resistance expression. Expression of both pri-miR124 and Puro can be modulated by Dox addition and depletion.

The growth of KG and ICP4-miR124t viruses was tested in uninduced and induced Tet-miR124-10, Tet-miR124-84 and Tet-negative-7 cells. As outlined in Figure 29, the cells were first treated with Doxycycline for 48 h or left untreated, and were then infected with KG or ICP4-miR124t viruses at an MOI of 0.01 or 0.001. At 24, 48, 72 h post infection (hpi), viral supernatants were collected and titrated on U2OS cells to quantify viral growth.

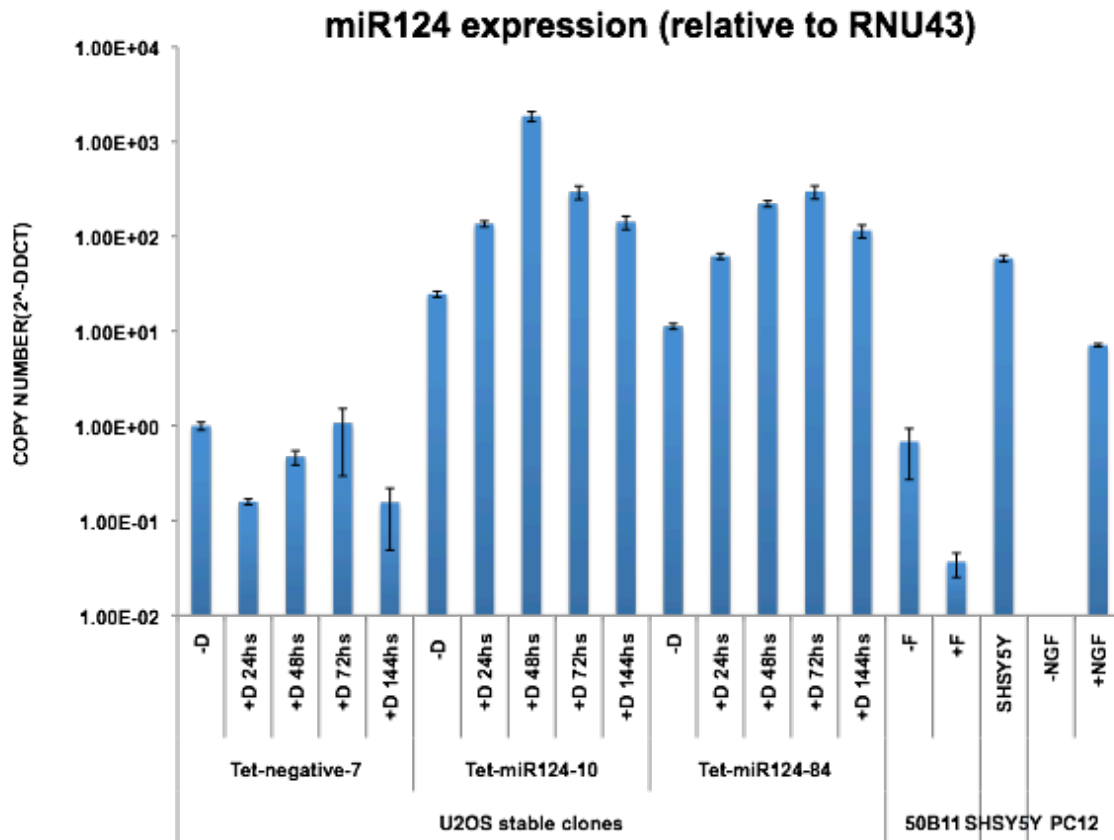


Figure 28: RT-qPCR for mir124 expression in U2OS TetO clones and in cells expressing endogenous miR124. The TetO-miR124 and TetO-intron constructs, which express the neomycin (neo) resistance gene, were transfected in U2OS cells to make a TetO inducible stable cell line. Single clones of stably transfected U2OS-Tet-miR124 and U2OS-Tet-control cells were then isolated through G418 selection and limiting dilution. Tet-miR124-10, Tet-miR124-84 and Tet-negative-7 cell clones were tested for miR124 expression after doxycycline induction by RT-qPCR from total RNA extracted 48 h after Dox induction. 50B11 and PC12 were differentiated into neuronal cells through overnight Forskolin (F) treatment (50B11) or through a two weeks Nerve Growth Factor (NGF) treatment (PC12). Following treatment, cells were collected and tested for miR124 expression by RT-qPCR from total RNA extracted in presence or absence of the differentiating treatment. RT-qPCR from total RNA extracted from untreated SHSY5Y was also performed. The mean value \pm standard deviations from three determinations are illustrated. The two different Tet-miR124 clones showed different levels of miR124 expression after Dox treatment, with clone Tet-miR124-10 expressing 8.5 times more miR124 than Tet-miR124-84. Tet-negative-7 expressed no miR124 with or without Doxycycline treatment. Neither 50B1, nor PC12 nor SHSY5Y showed level of endogenous miR124 expression comparable to either doxycycline- induced Tet-miR124-10 or Tet-miR124-84.

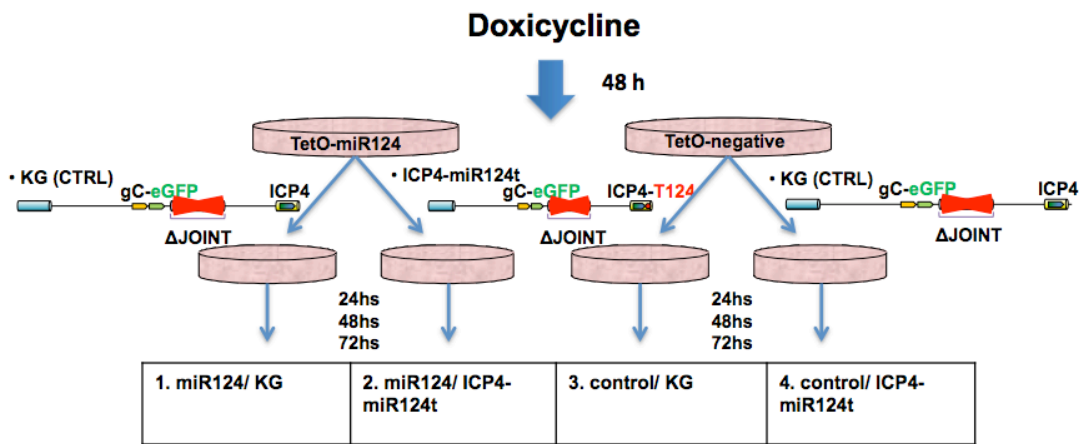


Figure 29: ICP4-mir124t replication efficiency in TetO-mir124 stable cell lines.

To examine potential effects of doxycycline-induced miR124 expression on oHSV-1 activity, both KG and ICP4-miR124t viruses were tested in Tet-miR124-10, Tet-miR124-84 and Tet-negative-7 in presence or absence of a 48 h long doxycycline (Dox) treatment. One day before Dox treatment, Tet-miR124-10, Tet-miR124-84 and Tet-negative-7 cells were plated as 50% confluent monolayers. 24 h later cells were treated with 10 µg/ml Dox for 48 h. Cells were then infected with either KG or ICP4-miR124t at two different MOIs, MOI= 0.01 or MOI= 0.001. At 24, 48, and 72 h post infection, cells and supernatants were collected and sonicated. Viral supernatants were then titrated on U2OS cells to measure HSV replication.

Both viruses grew at comparable rates in the Tet-negative-7 clone at both MOIs in the presence or absence of Dox (Figure 30A), as expected because no miR124 was expressed. The two viruses also grew at similar rates in both Tet-miR124-10 and Tet-miR124-84 cells in the absence of Dox treatment because no miR124 was expressed (Figures 30B-C). However, after Dox treatment, ICP4-miR124t viral growth was impaired in these cells while the growth of KB control virus was unaffected, indicating that the presence of miR124 specifically interfered with ICP4-miR124t replication (Figures 30B-C). Consistent with the RT-qPCR data (Figure 28), ICP4-miR124t viral replication was blocked up to 72 h after infection at both MOIs in clone Tet-miR124-10, which expressed the highest levels of miR124, but not in clone Tet-miR124-84 where, 72 h after infection at the higher MOI (MOI=0.1), miR124 expression was clearly not sufficient to inhibit ICP4-miR124t replication. However, 72 hpi at the lower MOI (MOI=0.01), ICP4-miR124t replication was still inhibited in clone Tet-miR124-84. These results indicated that there was a correlation between the amount of miR124 expressed by each clone and the degree of interference with ICP4-miR124t viral replication, with the stronger inhibition of ICP4-miR124t virus associated with the higher expression of miR124 in clone Tet-miR124-10.

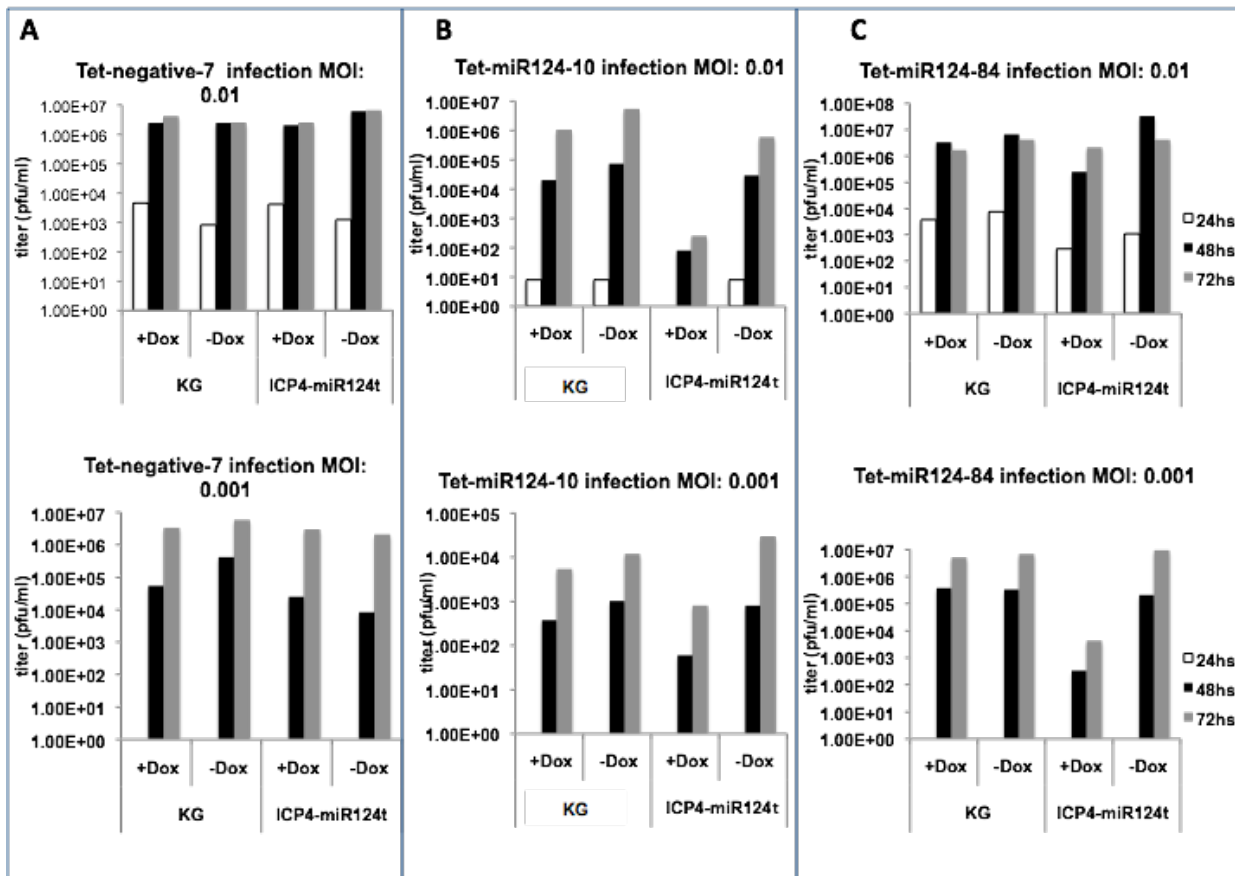


Figure 30: ICP4-miR124t oHSV-1 replication efficiency in TetO inducible clones.

(A): Viral replication in Tet-negative-7 control cells. Both ICP4-miR124t and KG viruses were able to grow at comparable rate at both MOI= 0.01 and MOI= 0.001 in presence or absence of doxycycline because no miR124 was expressed. (B): Viral replication in tet-miR124-10 cells. Both ICP4-miR124t and KG viruses were able to grow at comparable rate at both MOIs in absence of doxycycline because no miR124 was expressed. After doxycycline treatment the presence of miR124 in Tet-miR124-10 was able to interfere with ICP4-miR124t viral growth without affecting KB control virus at both MOI. (C): Viral replication in tet-miR124-84 cells. Both ICP4-miR124t and KG viruses were able to grow at comparable rate at both MOIs in absence of doxycycline because no miR124 was expressed. After doxycycline treatment the presence of miR124 in Tet-miR124-84 clone was able to interfere with ICP4-miR124t viral growth without affecting KB control virus at the lower MOI = 0.001, but not at the higher MOI = 0.01 where both ICP4-miR124t and KG viruses could replicate at the same rate. No standard deviation is available for this experiment.

3.4.3 ICP4-miR124t replication efficiency in cells expressing endogenous miR124

Human neuroblastoma SHSY5Y, rat DRG-derived 50B11 and rat pheochromocytoma PC12 cells were chosen to test the replication efficiency of ICP4-miR124t virus in the presence of endogenous levels of miR124. SHSY5Y cells reportedly express elevated levels of miR124 compared to many other cell lines

(<http://www.microrna.org/microrna/getExprData.do?matureName=hsa-miR-124&organism=9606>), while 50B11 and PC12 cells may induce miR124 expression during differentiation into neuronal cells through overnight forskolin treatment (50B11) or through two weeks of NGF treatment (PC12). It should be noted that human and rat miR124 are identical in sequence and thus it was expected that ICP4-miR124t would be responsive to rat miR124.

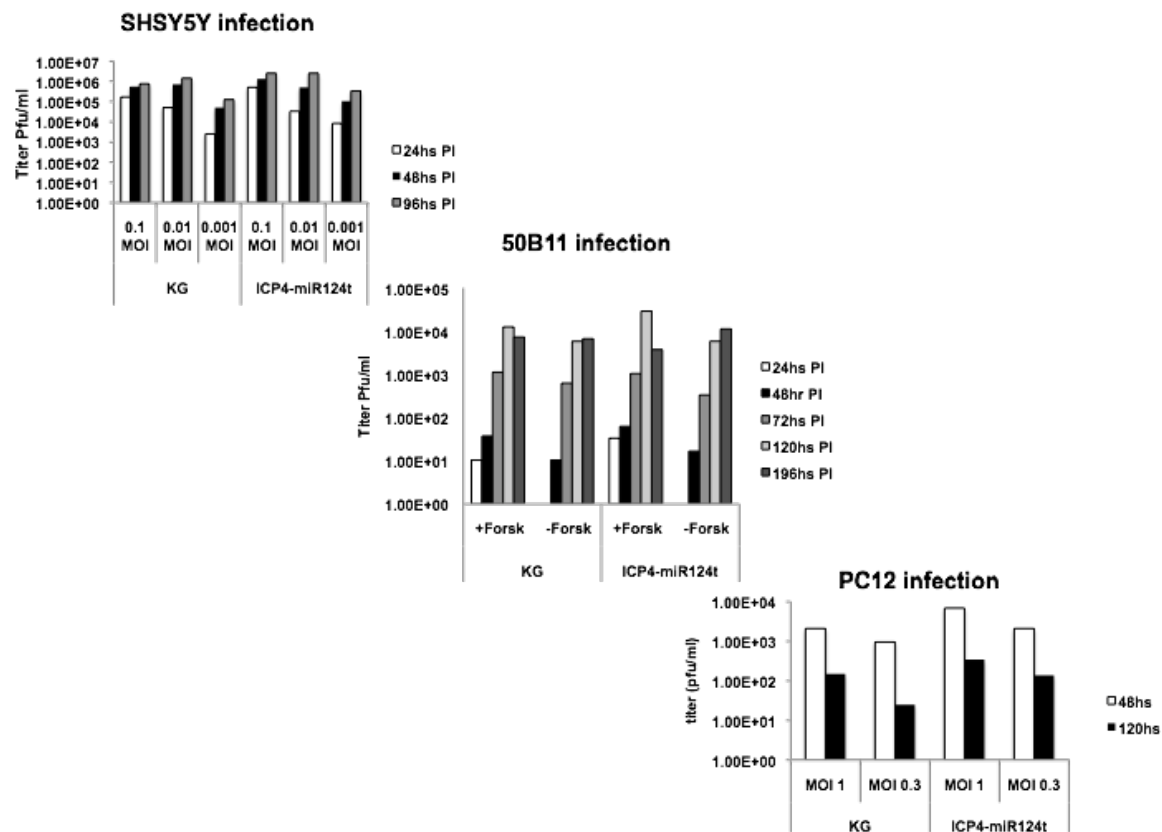


Figure 31: ICP4-mir124t oHSV-1 replication efficiency in cells expressing endogenous miR124.

To examine potential effects of endogenous miR124 expression on oHSV-1 activity, both KG and ICP4-miR124t viruses were tested in 50B11, PC12 and SHSY5Y. One day before drug treatment, cells were plated at a 50% confluent monolayer. 24 h later cells were treated with either 75 μ M Forskolin (Sigma), 50 ng/ml NGF (Sigma) or left untreated and incubated at 37°C in 5% CO₂ for as long as required by the specific differentiating treatment. One portion of the treated cells was used to quantify miR124 expression through RT-qPCR (Fig 28), while the rest of the cells were infected with either KG or ICP4-miR124t at the appropriate MOI (MOI= 0.1 for 50B11; MOI= 0.3 and 3 for PC12; MOI= 0.1, 0.01 and 0.001 for SHSY5Y cells). At different time-points after infection (24, 48, 72, 120, 196 h dpi for 50B11; 48 and 120 h dpi for PC12; 24, 48, 96 h dpi for SHSY5Y), cells and supernatants were collected and sonicated. Viral supernatants were then titered on U2OS cells to measure HSV replication. No standard deviation is available for this experiment. No difference in viral replication between KG and ICP4-miR124t was detected in any of the three cell lines.

SHSY5Y, 50B11 and PC12 were either left untreated or treated with the appropriate drugs to induce neuronal differentiation. Following treatment, cellular RNA was extracted to measure miR124 expression by RT-qPCR. As shown in Figure 28, endogenous miR124 levels in these cells were at least 1-2 orders of magnitude lower than the highest levels observed in Dox-induced Tet-miR124-10 or Tet-miR124-84 cells. A viral growth experiment was then performed to determine if these relatively low levels of endogenous miR124 could interfere with ICP4-miR124t replication. SHSY5Y cells were infected with either KG or ICP4-miR124t at MOIs of 0.1, 0.01 and 0.001, and supernatants were collected at 24-72 hpi and titered on U2OS cells. Differentiated and undifferentiated 50B11 cells were infected at an MOI of 0.1 and supernatants collected at 24-120 hpi. Differentiated PC12 cells were infected at MOIs of 0.3 or 1.0 and supernatants collected at 48 and 120 hpi.

As shown in Figure 31, there was no detectable difference in viral replication between KG and ICP4-miR124t in any of the three cell lines, indicating that the low levels of miR124 in these cell lines were not sufficient to control ICP4-miR124t replication. However, since miR124 expression reduces the viability of cells in culture and the levels of miR124 in individual cells of the brain *in vivo* are not known, these results mainly pointed out that *in vitro* experiments couldn't properly predict the behavior of ICP4-miR124t at the levels of miR124 existing in the brain.

3.4.4 ICP4-miR124t replication efficiency in patient-derived primary glioma spheroid lines (GICs) in the presence or absence of induced miR124 expression

To test if ICP4-miR124t virus could replicate like KG control virus in GBM-derived cells, ICP4-miR124t and KG viruses were used to infect two unrelated patient-derived primary glioma lines cultured as spheroids (GICs), GBM30 and Gli68 kindly donated by E.A. Chiocca (Ohio State University). Both cell lines were previously characterized by OSU colleagues for the absence of miR124 expression and their ability to form invasive tumors when injected into the brains of nude mice. These studies determined that animals injected with 2×10^5 cells of either line had an MST (mean survival time) between 20 and 30 days, meaning that both lines grew at approximately the same rate *in vivo*, allowing for better comparison of ICP4-miR124t viral growth between the two.

Since these cells were propagated as spheroid aggregates, the aggregates needed to be broken up into single cells to allow viral infection. The cells were then infected with either KG or ICP4-miR124t virus in suspension at an MOI=0.01 for two hours at 37°C and plated as single cell suspensions. Supernatants were collected at 24, 48 and 72 hpi and titered on U2OS cells..

As shown in Figure 32, ICP4-miR124t grew nearly as well as the KG control virus in both cell lines, reaching a titer that was 4.6 times lower than that of KG in Gli68 cells and only 2.6 times lower than that of KG in GBM30 cells.

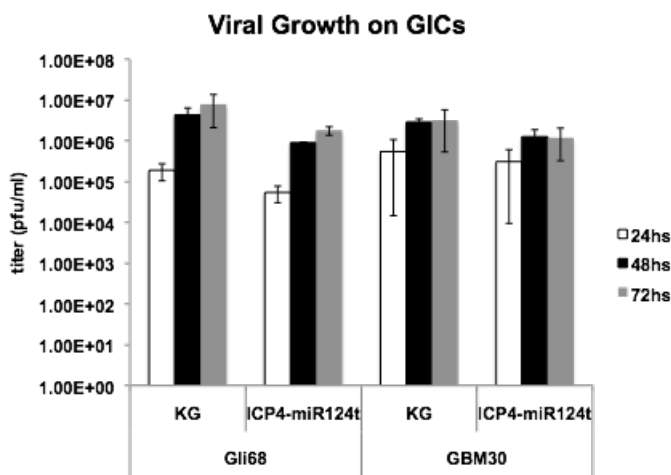


Figure 32: ICP4-miR124t oHSV replication efficiency in patient-derived mir124-negative (GICs).

On the day of the infection both GBM30 and Gli68 primary glioma spheroid cells aggregates, were broken up into single cells to allow viral infection. 2×10^5 cells were then counted and infected with either ICP4-miR124t or KG virus at MOI of 0.01. At 24, 48 and 72 h post infection, cells and supernatants were collected, and titered on U2OS cells. ICP4-miR124t grew nearly as well as the KG control virus in both cell lines, reaching a titer 4.6 times lower than KG in Gli68 and only 2.6 times lower in GBM30 at 72 h dpi.

To confirm that ICP4miR124t replicated in these cells like the KG control virus because of the absence of miR124t, GBM30 and Gli68 cells were infected with lentiviruses expressing miR124 (Lenti-miR124) or miR137-antisense (Lenti-miR137A) as a control before superinfection with either KG or ICP4-miR124t viruses, as illustrated in Figure 33A; lentiviral infection is a convenient method to express high levels of a transgene in poorly transfectable spheroid lines. The Lenti-miR124 virus was generated by cloning the intron-miR124-rPuro cassette derived from the earlier Tet-miR124 construct (see Figure 21 and table 5 for schematics) into a pCDH expression vector, transfection of the pCDH-miR124 plasmid together with three lentivirus packaging plasmids (PLP1, PLP2, PLP-VSVG) into 293T cells, and collection and

concentration of the supernatant. Plasmid pCDH-miR137A for expression of miR137-antisense (no response elements in ICP4-miR124t) was constructed in parallel and used to produce the control lentivirus.

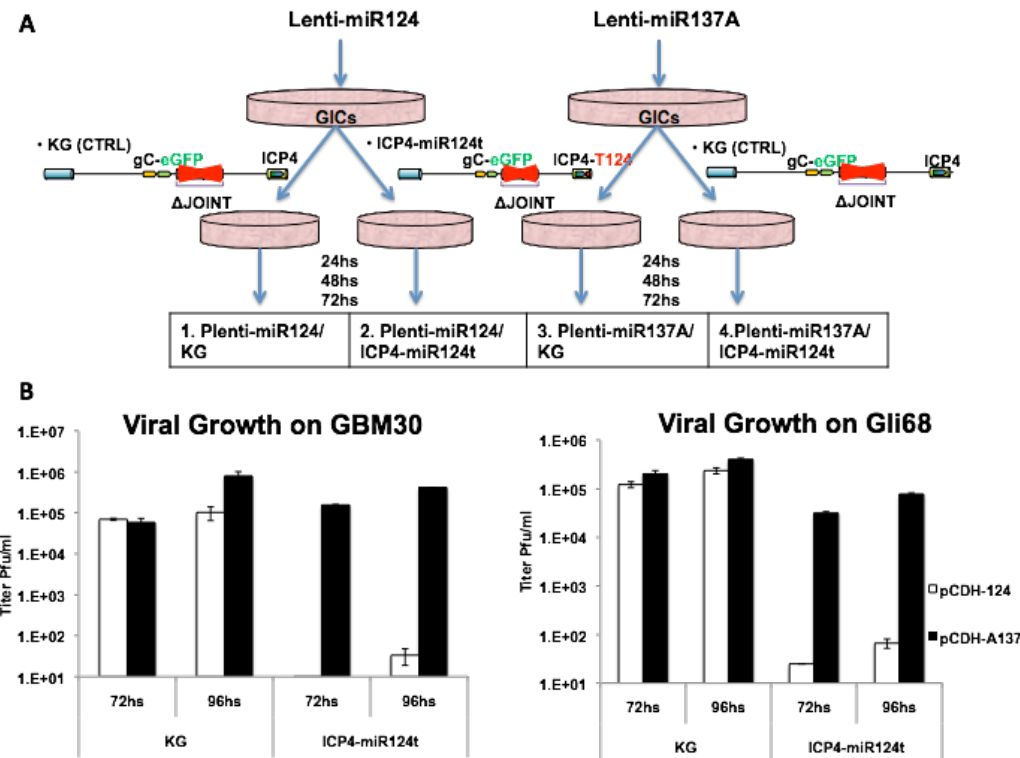


Figure 33: ICP4-miR124t oHSV replication efficiency in (GICs) following plenti-induced miR124 expression.
(A): Experiment schematic. On the day of infection both GBM30 and Gli68 primary glioma spheroid cells aggregates, were broken up into single cells to allow viral infection. 2×10^5 cells were then counted and infected with either Lenti-miR124 or Lenti-miR137A viruses at MOI of 5.0 before super-infection with either KG or ICP4-miR124t viruses. 24 h after infection cell medium was replaced with fresh medium and cells were selected with 30 μ g/ml of puromycin expressed with miR124 from the lentivirus. At 72 h after puromycin selection both cells were super-infected with either ICP4-miR124t or KG virus at an MOI of 0.01. At 48 and 96 h post infection, cells and supernatants were collected, and titered on U2OS cells. **(B): Viral titrations.** ICP4-miR124t virus was completely inhibited by expression of miR124, in both GBM30 and Gli68 cells, without being affected by the presence of miR137A, while KG control virus could replicate with no difference both in presence or absence of either miR124 or miR137A.

To examine potential effects of lentiviral miR124 expression on the cells, such as neuronal differentiation or reduced cell viability, one of the cell lines, Gli68, was initially infected with Lenti-miR124. 24 h after infection, cells were selected with puromycin whose resistance gene was jointly expressed with miR124 from the pCDH plasmid. Cells maintained their spheroid phenotype without any sign of change, continuing to replicate well throughout the length of the experiment. At 72 h after puromycin selection (96 hours after initial Lenti-virus infection), cells

were collected and total RNA was extracted to measure miR124 expression by RT-qPCR. The results were normalized to miR124 expression levels in U2OS cells that do not express miR124 (Figure 28). As shown in Figure 34, there was a very strong 3.5 logs increase in miR124 expression in Lenti-miR124 infected Gli68 cells compared to uninfected cells, demonstrating the feasibility of lentivirus-mediated exogenous miRNA expression in primary GICs.

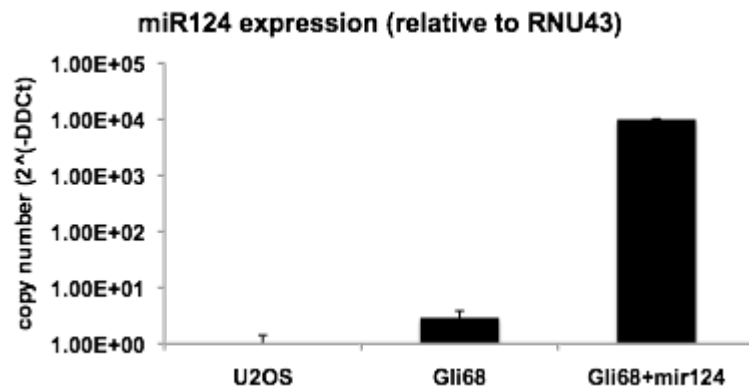


Figure 34: RT-qPCR of miR124 expression in Lenti-miR124 infected Gli68.

On the day of the infection Gli68 primary glioma spheroid cells aggregates, were broken up into single cells to allow viral infection. 2×10^5 cells were then counted and infected with Lenti-miR124 at MOI of 5.0. 24 h after infection cell medium was replaced with fresh medium and cells were selected with 30 μ g/ml of puromycin which resistance was expressed together with the miR124 gene from the lentivirus. At 72 h after puromycin selection cells were collected and total RNA was extracted to measure miR124 expression relative to RNU43, a small RNA used as internal control, through RT-qPCR. Data were normalized by miR124 expression in U2OS, which didn't express any miR124 as illustrated in Figure 28. The mean value \pm standard deviations from three determinations are illustrated. The chart shows a very strong 3.5 logs increase in miR124 expression in Lenti-miR124 infected Gli68 cells.

Both GMB30 and Gli68 cells were then infected with either Lenti-miR124 or Lenti-miR137A at an MOI of 5 to ensure that most of the cells would get infected. Puromycin selection was initiated 24 hours after infection and 72 h later (96 h after lentivirus infection), cells were super-infected with either ICP4-miR124t or KG virus at an MOI of 0.01. Supernatants were collected at 72 and 96 h post super-infection and titered on U2OS cells to measure HSV replication. As shown in Figure 33B, in both cell lines ICP4-miR124t viral growth was completely inhibited by miR124 expression, while remaining unaffected in the presence of miR137A. KG control virus instead replicated equally efficiently in presence and absence of either miR124 or miR137A. At 96 h after HSV infection, the ICP4-miR124t titer was 3×10^3 times lower in miR124-expressing GBM30 cells than in the miR137 control cells. A very similar result was evident in Gli68 where

the titer of ICP4-miR124t at 96 h after infection was 3.5×10^3 times lower in miR124 expressing cells than in the miR137A expressing cells.

In conclusion, these data show that ICP4-miR124t virus can grow and replicate like KG virus in GBM-derived cells in vitro, but its growth is completely inhibited when these same CNS-derived tumor cells are induced to express miR124.

3.5 In Vivo Testing of ICP4-miR124T Virus for Growth Selectivity

The ICP4-miR124t viral response to endogenous levels of miR124 was assessed in vivo, a preferred read-out as the diversity of normal brain cells cannot be faithfully recapitulated in vitro.

Toxicity studies were performed to evaluate potential immunologic and pathogenic effects on normal brain in both tumor-free, immunocompetent BALB/c mice and tumor-free immunocompromised nu/nu nude BALB/c mice.

3.5.1 Toxicity testing for virus safety in immunocompetent mice

In the first *in vivo* experiment, either KG control virus or ICP4-miR124t virus was administered into the brains of 3 weeks old female immunocompetent BALB/c mice for a total of three mice per virus (Figure 35A).

For each virus one single dose containing 4.8×10^9 genome copies (gc) was tested through injection of each mouse with 4 μ l of viral prep. Two animals, one for each virus, were sacrificed 3 h post injection (hpi), while the remaining animals were left alive and monitored for general health. The 3 hpi timepoint was taken to measure how much of the viral DNA injected as virus particles could be recovered by DNA extraction from total mouse brain. As illustrated in Figure 35B, the first KG treated mouse was sacrificed at day 5 after injection because of extreme weight loss and signs of discomfort. One ICP4-miR124t injected mouse was also sacrificed at the same time. The second KG injected mouse was sacrificed at day 7 after injection, while its ICP4-miR124t injected counterpart was left alive and continues to be monitored for general health. DNA was extracted from whole brain of the sacrificed animals and qPCR was performed using primers and probe specific for the viral glycoprotein D (gD) gene to determine the number of viral genome copies compared to input virus. The 7 dpi timepoint was chosen because after being sick for the first 5 dpi, the KG-injected mouse started to show signs of recovery and I wanted to check if this behavioral change was corresponding to a change in viral yield. As

shown in Figure 35C, the amount of viral DNA recovered from the brain at 3 hpi was significantly lower than the injected amount and varied between the two viruses, indicating the presence of a systematic error caused by the injection and/or DNA isolation procedure

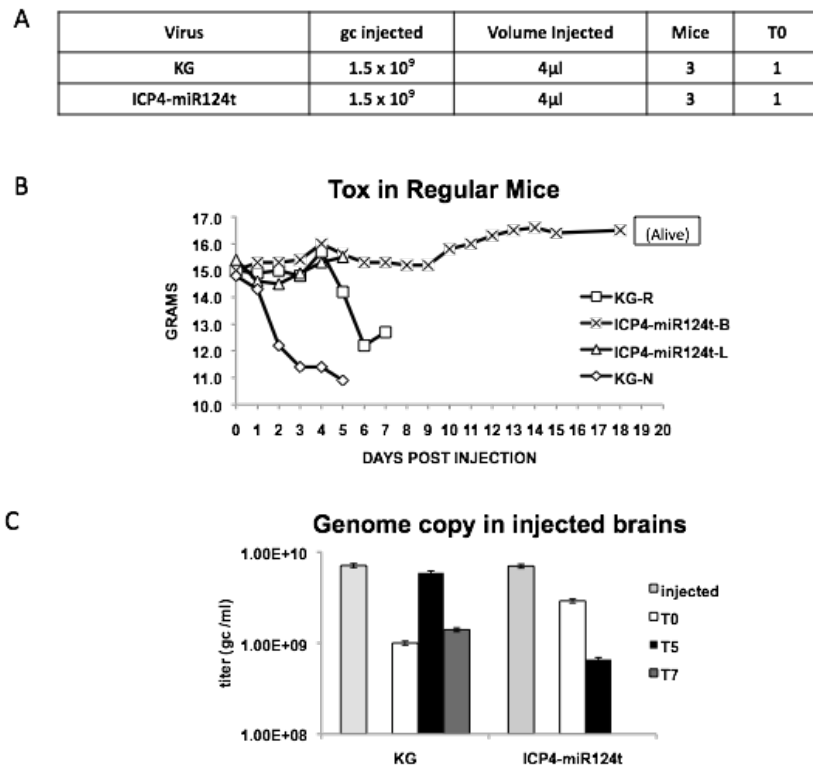


Figure 35: In vivo toxicity testing of ICP4-miR124t for vector safety in immunocompetent mice.

(A): Experiment schematic. Either KG or ICP4-miR124t was administered by intracranial stereotactic injection into the right temporal lobe (cortex) of 3 weeks old female BALB/c mice for a total of three mice per virus. A single 4 μ l dose of each virus (4.8×10^9 gc /animal) was injected in each mouse. **(B): survival results:** animals were monitored for general health (weight, activity, clinical signs) every other day up to 28 days after injection. KG-N was sacrificed at day 5 after injection because of extreme weight loss and other signs of viral-related pathology. ICP4-miR124t –L injected mouse was also sacrificed at the same timepoint. KG-R injected mouse was sacrificed at day 7 after injection, while ICP4-miR124t-B, its injected counterpart, was left alive and monitored to these days (19 dpi) for general health. This mouse is still healthy. **(C): qPCR on injected animal brains.** Total DNA was collected from the brain of each sacrificed animal and qPCR was performed using specific primers for the HSV glycoprotein D (gD) gene to determine the number of viral genome copies compared to the input. The mean value \pm standard deviations from three determinations are illustrated. Results show that the amount of KG virus in the mouse brain 3 hpi was significantly lower than the amount injected, and varied between the two viruses, indicating the presence of a systematic error caused by the injection procedure and/or the DNA extraction procedure. Results also show that the amount of KG virus in the mouse at day five post injection was 5.9 times higher than the amount of KG present in the brain at 3 hpi (T0), while the amount of ICP4-miR124t virus present in the mouse brain at day 5 post injection was 3.3 times lower than the amount present at T0, indicating that only KG but not ICP4-miR124t was able to replicate up to 5 days after injection. At day 7 post injection the amount of KG present in the brain had diminished compared to day 5, a sign that, after having caused severe sickness in the mice in the first 5 days, also the KG control virus eventually had stopped replicating.

From this result it was clear that the amount of viral genome copies at 3 hpi was a better reference for comparison with the amounts of DNA isolated at later timepoints than the injected

amount. The 3 hpi timepoint was thus considered as time-zero (T0) to which all the other qPCR results of this experiment were compared. Figure 35C shows also that the amount of KG virus present in the mouse brain at day 5 post injection was 5.9 times higher than the amount of KG present in the brain at T0, while the amount of ICP4-miR124t virus at day 5 post injection was 3.3 times lower than the amount at T0, indicating that only KG but not ICP4-miR124t was able to replicate up to 5 days after injection. However, at day 7 post injection the amount of KG present in the brain had diminished compared to day 5, an indication that, after having caused signs of disease in the mice in the first 5 days, the KG control virus had stopped replicating, most likely blocked by the host antiviral immune response. This result was consistent with the weight and clinical signs of the KG-injected mouse sacrificed on day 7; after losing 20% of its weight and showing discomfort and impaired behavior up to day 5 post injection, on day 7 this mouse had gained weight and was behaving more normally.

These results proved that at high virus doses, ICP4miR124t was safe in immunocompetent mice where it was never able to replicate and cause disease. Instead the KG control virus, lacking miR124 responsive elements, was clearly more toxic, causing disease in the injected mice for the first 5 days post infection before being blocked by the host immune system.

3.5.2 Toxicity testing for virus safety in immunodeficient mice

The second in vivo experiment was performed in an immunodeficient mouse model to try to emphasize the toxic effect of the KG control virus. Using the same procedure described above, KG or ICP4-miR124t viruses were administered by intracranial stereotactic injection into the right temporal lobe of 3 weeks old female nu/nu BALB/c mice for a total of four mice per virus (Figure 36A). One single dose of 1.5×10^9 gc of each virus was tested by injecting each mouse with 4 μ l of viral prep.

At day 5 after injection, three out of four animals treated with KG control virus had died, while all the mice treated with ICP4-miR124t were still alive and healthy (Figure 36B). At this point, total DNA was collected from the brain of the last very sick KG-treated animal and of one sacrificed ICP4-miR124t-treated animal and qPCR for HSV genomes was performed as above to determine the number of viral genome copies compared to the injected input. The remaining ICP4-miR124t treated animals remained symptom-free until sacrifice on days 14, 21 and 33 after injection and the same procedure was followed to quantify viral genomes in the brains of these sacrificed animals.

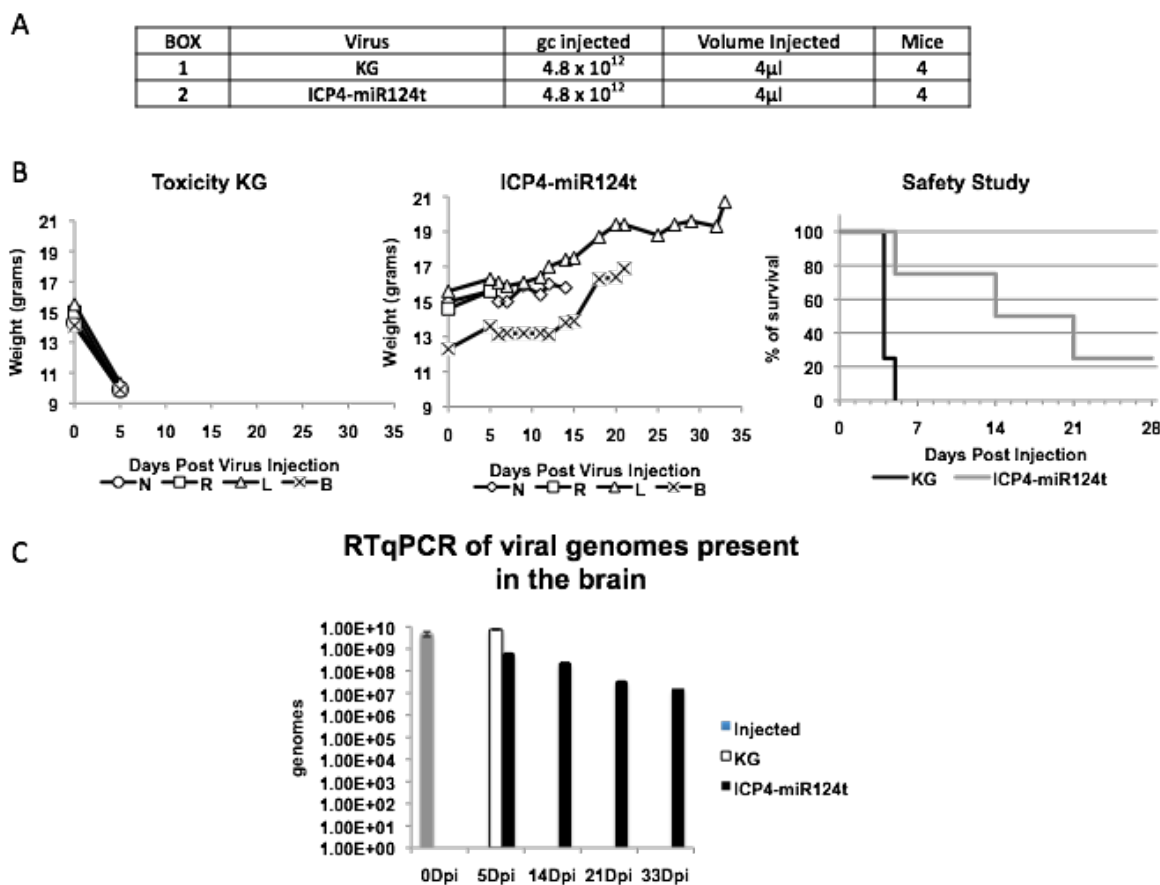


Figure 36: in vivo toxicity testing of the ICP4-miR124t oHSV-1 for vector safety in immunodeficient mice.

36A: Experiment schematic. Either KG or ICP4-miR124t was administered by intracranial stereotactic injection into the right temporal lobe (cortex) of 3 weeks old female nu/nu nude BALB/c mice for a total of four mice per virus. A single 4 μ l dose of each virus (1.5×10^9 gc /animal) was injected in each mouse. **36B: survival results.** At day 5 after injection, three of the four animals treated with KG control virus had died, and the last one very sick was promptly sacrificed. Instead, all the mice treated with ICP4-miR124t were still alive and healthy. One ICP4-miR124t treated animal was then sacrificed, while the remaining ICP4-miR124t animals were sacrificed at days 14, 21 and 33 for qPCR analysis to determine the number of viral genome copies present in the brain of each animal compared to one deceased KG injected animal and to the input virus injected at T0. **36C: qPCR on injected animals brains.** Total DNA was collected from the brain of each sacrificed animal and qPCR was performed using specific primers for the HSV glycoprotein D (gD) gene to determine the number of viral genome copies compared to input. The mean value \pm standard deviations from three determinations are illustrated. qPCR data show that the amount of KG virus at day 5 post injection was 1.5 times higher than the amount injected (day 0), while the amount of ICP4-miR124t virus at day 5 post injection was 7.6 times lower than the injected amount, further decreasing to a 3,000-fold difference at 33 day post injection.

The results in Figure 36C show that the amount of KG virus at day 5 post injection was 1.5 times higher than the amount injected (day 0), most likely a underestimate given that the amount of virus injected was used as T0 rather than the amount of virus recovered from animal brains at 3 hours post injection as in the first *in vivo* experiment. In contrast, the amount of

ICP4-miR124t virus at day 5 was 7.6 times lower than the injected amount, further decreasing to a 3,000-fold difference at 33 dpi. These results demonstrated that at high virus doses, ICP4miR124t remained safe in immunocompromised mice while KG lacking miR124 response elements was lethal in these animals.

In conclusion these data demonstrate that the presence of miR124-responsive elements in the viral backbone make the oHSV-1 safer and less toxic in both immunocompetent and nude mice.

4 DISCUSSION

GBM is the most common form of glioma and no cure exists. The current standard treatment that includes surgical resection of the tumor mass followed by radiotherapy and chemotherapy on average increases the patient's lifespan by only a few months, indicating an urgent need for new treatments of this deadly disease²⁻⁴.

OVs are attenuated lytic viruses specifically designed to infect and kill only tumor cells without affecting the surrounding normal tissue⁷. OVs derived from Herpes Simplex Virus type-1 (oHSVs), made tumor-selective through the deletion of one or more genes that are dispensable for HSV-1 growth in cancer cells, but that are required for efficient replication in normal cells, have been employed as promising alternatives to standard ineffective GBM treatment⁷. However, while results from clinical trials have demonstrated that these oHSV are safe for patients, they are too attenuated to efficiently eradicate GBM^{2-4,17}. To overcome this problem, I developed a new kind of oHSV named ICP4-miR124t that differs from previously described oHSVs in that it is not deleted for any genes but derives its tumor selectivity from the different pattern of miRNA expression between tumor and normal brain^{5,33,62-65}. Indeed by bringing the activity of its essential ICP4 gene under the control of miR124, a miRNA expressed only in normal neurons and microglia but completely absent in tumor cells^{66,67}, I demonstrated that this novel ICP4-miR124t oHSV was able to replicate as strongly as its non-controlled counterpart in tumor cells that don't express miR124, while its replication was essentially shut down in cells that produce miR124. MiR124 was chosen because its expression correlates directly with terminal differentiation and inhibition of cellular proliferation and is incompatible with maintenance of the tumor phenotype and the viability of glioma cells where miR124 is not naturally expressed^{41,42}. As a consequence, glioma cells cannot up-regulate miR124 without losing their tumorigenicity(<http://www.microrna.org/microrna/getExprData.do?matureName=hsa-miR-124&organism=9606>)^{43,62,68}.

Since the start of my study, reports have begun to appear in the literature describing similar approaches to selectively allow lytic replication of different viruses in tumor cells⁶⁹⁻⁷³. Target sequences for tumor-specific miRNA let-7, p53-responsive antiviral-RNAi or liver-specific miR122 have been employed to engineer oncolytic adenovirus for hepatocellular carcinoma therapy⁷⁰⁻⁷³. Target sequences for tumor-specific let-7 miRNA have also been engineered in a

vaccinia virus backbone created to specifically replicate in a panel of several tumor cell lines representative of a wide range of human cancers⁷⁴. Target sequences for brain-specific miR125 have been used to generate a oncolytic vesicular stomatitis virus (oVSV) that replicates efficiently in tumor cells but is less neurotoxic than its wild-type counterpart. Target sequences for muscle-specific miR133 and miR206 have been engineered into an oncolytic picornavirus genome in an attempt to reduce its toxicity⁷⁵. Target sequences for the brain specific miR7 have been used to engineer a measles oncolytic virus for the therapy of GBM⁷⁶. Also an amplicon HSV-1 has been successfully targeted to respond to tumor-specific miRNA expression by inserting prostate-specific miR143 and miR145 target sequences in the 3'UTR of the HSV-1 essential ICP4 gene, confirming my observations that this gene is a suitable target for miRNA-controlled replication of oHSV-1⁵². Consistent with all this literature data, my work illustrates that it is possible to engineer HSV to bring its replication under the control of miR124. What I showed in this study is that indeed my miR124-regulated ICP4-miR124t oHSV replicates in and kills tumor cells as effectively as non-regulated virus without being toxic for normal brain, suggesting that it can be used as a tool for the treatment of GBM.

The first step to create a miR124-controlled oHSV consisted of engineering and testing a miR124 responsive element able to regulate ICP4 protein expression when inserted into the 3'UTR of the ICP4 gene. A tandem of four miR124 target sequences (4xT124), each separated from the next by three different 7-8 nucleotides long spacers, was created according to a design already demonstrated by others to maximize the miRNA effect on the target gene⁴⁹⁻⁵². When inserted in the 3'UTR of a luciferase reporter gene, this miR124 responsive element proved to be extremely effective in responding to the specific presence of miR124 in more than one cell line (see Figure 23).

The second step consisted of engineering the HSV-1 genome to insert the 4xT124 element in the 3'UTR of the ICP4 gene. To create the final ICP4-miR124t oHSV I took advantage of a BAC construct containing a more stable joint-deleted version of the HSV-1 genome already containing the gB:NT mutation recently shown to improve HSV-1 initial infection by accelerating viral entry⁵⁷. As part of a BAC, the HSV-1 genome can replicate in bacteria rendering all manipulations of the virus much faster and easier than in the past, allowing the design and engineering of multiple modifications of the same backbone with relative ease compared to the past⁵⁶. In addition, the absence of the joint, by freezing the viral genome in one of its isoforms and by maintaining only one copy of each of the diploid HSV-1 genes (see section 3.1 and Figure 5), stabilized the vector against undesired recombination events and facilitated accurate engineering of the viral vector without affecting the ability of the virus to kill tumor cells

compared to non-deleted virus (see Figure 22). The insertion of both the T2A-eGFP sequence in frame with gC and the 4xT124 responsive element in the 3'UTR of ICP4 were done in two fairly quick steps using Red/ET based recombination techniques yielding very clean recombination products that were easy to check for accuracy by PCR and FUGE analysis to exclude unwanted changes that would have gone undetected in the past (see Figures 9-10, 15-17). A functional ICP4-miR124t-BAC oHSV virus was then obtained from the BAC-DNA through transfection into U2OS cells that produced actively replicating and spreading green fluorescent virus (see Figure 25). ICP4-miR124t-BAC DNA was then finally transfected into U2OS-Cre to free the oHSV-1of BAC sequences known to negatively affect viral growth. Also this last modification was very easy to check for accuracy by PCR (see Figure 18). Therefore in this first part of the study I demonstrated that the modification of the HSV-1 genome by Red/ET mediated recombination in bacteria is a very convenient way to modify and improve the virus for clinical purposes compared to the slow and tedious classical in-cell recombination strategies.

The third step of the work consisted of testing the response of ICP4-miR124t to miR124 expression. Several different *in vitro* approaches were used. Initially I performed a transient transfection on U2OS cells with either pri-miR124 or another pri-miRNA one day before infection with either ICP4-miR124t or its non-regulated counterpart KG. The results showed that ICP4-miR124t replication was reduced by the transient expression of miR124 but not of another miRNA, while KG viral growth was not affected by the presence of miR124 (see Figure 26). However, this experiment had two limitations. First, like all small RNAs, miR124 is unstable *in vitro* and was quickly degraded after transfection. Second, transient transfection is not 100% efficient and not all the cells expressed miR124. In the cells that did express the miRNA, the amount varied, reducing the overall effect on ICP4-miR124t replication. To obtain stronger evidence of the inhibitory effect of miR124 on ICP4-miR124t replication and to overcome the limitations of a pri-miRNA transient transfection, I generated stable U2OS cell lines for doxycycline-inducible controlled expression of miR124. In two different clones, induced expression of miR124 48 h before infection greatly reduced ICP4-miR124t viral growth compared to the growth of KG, its non-miRNA-regulated viral counterpart. In both clones this inhibitory effect was not observed in the absence of Dox pre-treatment and was dependent on the amount of miR124 expressed relative to the amount of virus used for the infection (Figures 30). Specifically, induced TetO-miR124-10 cells expressing the higher level of miR124 (Figure 28) were able to block ICP4-miR124t viral replication after infection at both low and high MOI, while induction of the TetO-miR124-84 clone producing less miR124 blocked replication only at the lower MOI. These results pointed out that in order to efficiently block ICP4-miR124t

replication, it was necessary for a cell to express a certain amount of miR124 capable of handling the amount of virus present, confirming results already published by others that the higher the expression of a given miRNA, the higher the fold suppression of its target mRNA⁵¹.

Having confirmed that ICP4-miR124t viral growth could effectively be regulated by exogenous miR124 expression, I next designed experiments to understand the behavior of ICP4-miR124t in response to endogenous levels of miR124. Initially I tested ICP4-miR124t replication in SHSY5Y cells that endogenously express elevated levels of miR124, but I found that these cells were unable to block viral replication. Determination of the amount of miR124 in these cells showed that it was lower than that in either of the induced miR124-expression clones (Figure 31). Therefore I concluded that the miR124 level in SHSY5Y was probably below the threshold necessary for a measurable effect on ICP4-miR124t replication. An explanation of this result could be that it is known from the literature that miRNA expression has to exceed a certain level to efficiently suppress its target mRNA⁵¹ and the amount of miR124 expressed in SHSY5Y cells was below this threshold. Another possible explanation could be that not all miR124 present in SHSY5Y is active. Recently presented data (http://www.abstracts2view.com/asgct/view.php?nu=ASGT12L1_99) have elegantly demonstrated that not all the miRNAs expressed in a cell are active. Therefore the detection of an miRNA in a certain cell type by RT-qPCR does not guarantee that this miRNA is active when checked for its ability to regulate the expression of its target gene. In the case of SHSY5Y, this kind of explanation wouldn't be surprising considering that miR124 is a key player in neuronal differentiation by controlling the cell's ability to progress through the cycle via direct regulation of CDK6^{41,42}. Tumor cells like SHSY5Y replicate actively in vitro and thus cannot have high levels of activity of an miRNA like miR124 that induces terminal differentiation. Expression of endogenous miR124 was also evaluated in two other cell lines, 50B11 and PC12, after induction of neuronal differentiation according to published protocols^{47,48}. However, RT-qPCR analysis (Figure 31) showed that these procedures did not induce miR124 levels that were higher or even as high as in SHSY5Y. Consistent with this result, ICP4-miR124t viral growth was not blocked in either of these two cell lines with or without differentiation treatment, reaffirming that miR124 levels below those observed in Dox-induced miR124-expression clones could not significantly reduce ICP4-miR124t viral replication in cultured cells.

Although SHSY5Y cells express elevated levels of miR124 when compared to many other cell lines, these levels are much lower than those in adult brain (<http://www.microrna.org/microrna/getExprData.do?matureName=hsa-miR-124&organism=9606>), suggesting that *in vitro* experiments like the ones described above could

not properly predict the behavior of ICP4-miR124t in the brain. Therefore the ICP4-miR124t viral response to endogenous levels of miR124 in the brain had to be assessed *in vivo*, a preferred read-out also because the diversity of brain cells cannot be faithfully recapitulated in cell culture. The miR124-hairpin sequence is very well conserved throughout evolution and human and murine hairpins perfectly overlap³⁴, making mice a suitable animal model to test the behavior of ICP4-miR124t in response to the levels of miR124 existing in the brain.

ICP4-miR124t was tested in both an immunodeficient and an immunocompetent mouse model. In the first experiment, healthy immunocompetent mice were inoculated in the brain with the highest possible dose of either ICP4-miR124t or its non-miR-regulated counterpart KG. Brains were collected at different timepoints after injection to quantify through qPCR the amount of viral DNA present over time. One ICP4-miR124t mouse was left alive and to date has shown no adverse effects of the viral inoculation. The decrease in the amount of ICP4-miR124t viral DNA over time (~5 times reduced at 5 days after injection (dpi) clearly demonstrated the inability of the virus to effectively replicate in healthy brain *in vivo* (Figure 35C). This was in contrast with the results obtained from the KG control virus where the viral DNA amount increased ~6 times in the first 5 dpi. Interestingly, however, the amount of KG DNA then decreased in the next 2 days to the level immediately after inoculation (T0), indicating that the virus had stopped replicating, most likely blocked by the murine immune system. Consistent with these results, while both ICP4-miR124t treated animals looked healthy throughout without any weight loss or manifestation of disease (Figure 35B), KG treated animals looked extremely sick for the first 5 days after injection before the remaining animal showed signs of recovery. This experiment demonstrated that ICP4-miR124t oHSV was very safe and non-toxic when injected into healthy brain, where the endogenous levels of expressed miR124 were clearly sufficient to block its replication even after injection of a very high dose. In contrast, KG control virus caused severe toxicity for the first 5 dpi because of its lack of miR124 responsive elements.

In the second experiment, healthy immunodeficient mice were inoculated in the brain with the highest possible dose of either ICP4-miR124t or its non-miR-regulated counterpart KG. At 5 dpi three out of four KG injected mice had died, while all the ICP4-miR124t treated animals were alive and healthy, a first demonstration that miR124-mediated control of viral replication was effective in eliminating toxicity associated with HSV-1 growth in normal brain (Figure 36B). These observations were in line with the qPCR data obtained from the brains of the animals that survived viral injection, showing an opposite behavior between KG control virus, whose genome copies increased compared to the amount of injected virus, and ICP4-miR124t, whose genome

copies gradually decreased over time after injection (Figure 36C). These results demonstrated how much safer ICP4-miR124t oHSV-1 was compared to its unregulated counterpart KG in an immunodeficient mouse model where the absence of a functional immune system made KG extremely toxic.

This very positive result confirms data from the literature that have shown that non-neuronal cells, specifically glia and neuronal precursor cells (NPCs) that do not express the neuronal-specific miR124^{33,35-37}, are not favorable to HSV replication in vivo. Non-neuronal cells have been investigated for susceptibility to HSV-1 infection and all of them can be infected by HSV-1 given that HSV-1 receptors (nectin-1, HVEM, 3-OS HS) are expressed in virtually all cells⁷⁷⁻⁷⁹. However data from the literature have shown that following in-vivo infection of mouse brains with high doses of HSV-1, the cells which predominantly express HSV-1 proteins are neurons, while in non-neuronal cells HSV-1 proteins are almost undetectable⁷⁷. The reason why in-vivo HSV-1 viral infection seems to involve mainly neurons is not known and needs to be further investigated, but this observation may well explain the absence of toxicity detected for ICP4-miR124t following injection in mouse brains. Nonetheless, to further reduce the possibility of brain toxicity caused by potential oHSV-1 infection of non-neuronal cells, it is possible in the future to further modify ICP4-miR124t oHSV to have multiple miRNA target sequences regulating the expression of ICP4 and/or ICP27 HSV-1-essential genes, each one responding to a specific non-neuronal miRNA (e.g., miR219 or miR338 for oligodendrocytes, miR23 or miR29 for astrocytes, miR7 for NPCs)³³. For example, target sequences for one or more of these other miRNAs can be added to the miR124 responsive element in ICP4 to expand the regulation of viral replication to additional cell types. A similar design with a tandem of target sequences for multiple miRNAs has already been described and validated in the literature⁸⁰. Alternatively, a tandem of identical target sequences for a different miRNA can be inserted in the 3'UTR of ICP27 to regulate the expression of this other essential HSV IE gene, a design already successfully tested in our laboratory (unpublished data). A different strategy to reduce oHSV toxicity to the normal brain while increasing viral specificity to the tumor would be retargeting ICP4-miR124t to be able to enter cells by recognizing a receptor specifically expressed only on tumor cells, another design successfully developed in our laboratory using the human epidermal growth factor receptor (EGFR) widely expressed on GBM cells (H. Uchida et al, submitted for publication). This strategy can be combined with miRNA-mediated regulation of HSV replication.

Despite the fact that ICP4-miR124t was absolutely non-toxic after injection in the animals a major safety concern is the possibility that the oHSV could lose or mutate part or the entire 4xT124 responsive element in ICP4 and revert to an unregulated replication-competent virus,

an occurrence already described in the literature with a similar miRNA-regulated flavivirus⁸¹. The odds for this to happen in ICP4-miR124t oHSV1 were considered small because the 4xT124 responsive element was designed to be so close to the ICP4 stop codon that a recombination event in that area would have most likely affected the ICP4 coding sequence, creating a replication-defective virus. However, internal recombination events within the 4xT124 element cannot be excluded and these could cause the loss of half or more of the four identical miR124 target sequences, potentially leaving the ICP4 gene with too few target sequences to be effectively regulated by miR124. To minimize this possibility, the 4xT124 responsive element in ICP4-miR124t could be modified to move the respective copies of the target sequence farther apart and/or by mixing in target sequences for other miRNAs. These modifications can potentially improve the ICP4-miR124t design given that both kinds have already been shown to be very effective in reducing the occurrence of recombination events in other viral systems⁸⁰.

In the final step of this study, ICP4-miR124t virus was tested *in vitro* for efficacy in killing GBM cells through lytic replication to ensure that the presence of the 4xT124 responsive element in the ICP4 3'UTR didn't impair the ability of the virus to replicate in tumor cells compared to its non-regulated counterpart KG. The primary human GBM-derived cells (GICs) used for this purpose, GBM30 and Gli68, are both representative of the mesenchymal molecular subtype of GBM (E.A. Chiocca, personal communication), the most common of the four GBM kinds according to the Verhaak classification⁶. Compared to established GBM cell lines like U87, SNB19 or U251 routinely used in the past, GICs represent a much better model of GBM for both *in vitro* and *in vivo* studies because they grow in culture in suspension as multipotent spheroid aggregates, and when injected into immunocompromised animals, they form highly invasive brain tumors closely resembling human GBM. On the contrary, most of the established GBM cell lines grow as monolayers in culture and don't form invasive tumors *in vivo*. This is an important distinction, since key issues with current GBM therapy include the inability to cleanly resect the tumor mass and to reach migrating cells by focused radiation. ICP4-miR124t efficacy data on GICs cells in culture were very encouraging. Specifically, the virus was able to infect and replicate as efficiently as its non-regulated viral counterpart KG in both Gli68 and GBM30 cells, ultimately killing all cells (Figure 32). This result is very important because the goal of my study was to develop a new oHSV that was safer than wild-type HSV-1 virus when injected in the brain, but not impaired for tumor cell killing, unlike current oHSVs, which are safe but whose replication efficacy in tumor cells is reduced compared to wild type virus because of the removal of virulence genes like ICP34.5^{2,4}. To confirm that vigorous ICP4-miR124t viral replication in GICs was possible only because of the absence of miR124, a lentivirus was used

to express miR124 in both Gli68 and GBM30 before super-infection with ICP4-miR124t. The results of these experiments showed that ICP4-miR124t viral replication was greatly impaired in both GICs by prior infection with lenti-miR124, but not by prior infection with a lentivirus expressing an unrelated miRNA (Figure 33)

Together, my results have shown that introduction of the 4xT124 responsive element into the ICP4 3'UTR is a very effective strategy to impede viral replication in normal brain cells without decreasing the ability of the virus to efficiently replicate in and kill GBM tumor cells compared to non-miRNA-regulated virus. However, replication efficiency is not the only determinant of the therapeutic efficacy of oncolytic viruses and the design of ICP4-miR124t oHSV can be further modified to address other impediments to successful therapy. One of the biggest limitations in the use of oHSV for the treatment of GBM is viral spread away from the site of injection to reach all tumor cells, given that one problematic characteristic of GBM cells is their ability to migrate away from the tumor core and infiltrate the surrounding normal tissue. Data from clinical trials have indeed highlighted that oHSV can only reach the tumor cells that are closest to the site of injection, mainly because of the thick tumor extracellular matrix (ECM) that physically traps the virus and impedes its spread. To address this problem, the oHSV could be de-targeted to eliminate the elements of HSV glycoproteins B and C that bind to heparan and chondroitin sulfates, abundant components of the ECM contributing to oHSV entrapment in the ECM^{82,83}. Moreover, the virus could be armed with genes expressing metalloproteinases capable of degrading the ECM⁸⁴. The HSV-1 genome is large and contains multiple regions that are not essential for efficient viral growth and that can thus be substituted with transgenes to be expressed at the site of infection⁸⁵⁻⁸⁷. Finally, the oHSV could be armed with transgenes for molecules that are able to activate the host immune system against infected tumor cells^{88,89}.

In summary, the results of this study indicate that it is possible to produce a safe oHSV that is effective against GBM by regulating one or more of its essential genes to be only expressed in tumor cells while maintaining the full complement of viral genes without attenuating deletions.

BIBLIOGRAPHY

1. Ohgaki H, Kleihues P. Genetic pathways to primary and secondary glioblastoma. *Am J Pathol* 2007;170(5):1445-53.
2. Grandi P, Peruzzi P, Reinhart B, Cohen JB, Chiocca EA, Glorioso JC. Design and application of oncolytic HSV vectors for glioblastoma therapy. *Expert Rev Neurother* 2009;9(4):505-17.
3. Chiocca EA, Aghi M, Fulci G. Viral therapy for glioblastoma. *Cancer J* 2003;9(3):167-79.
4. Haseley A, Alvarez-Breckenridge C, Chaudhury AR, Kaur B. Advances in oncolytic virus therapy for glioma. *Recent Pat CNS Drug Discov* 2009;4(1):1-13.
5. Skalsky RL, Cullen BR. Reduced expression of brain-enriched microRNAs in glioblastomas permits targeted regulation of a cell death gene. *PLoS One*;6(9):e24248.
6. Verhaak RG, Hoadley KA, Purdom E, Wang V, Qi Y, Wilkerson MD, Miller CR, Ding L, Golub T, Mesirov JP and others. Integrated genomic analysis identifies clinically relevant subtypes of glioblastoma characterized by abnormalities in PDGFRA, IDH1, EGFR, and NF1. *Cancer Cell*;17(1):98-110.
7. Chiocca EA. Oncolytic viruses. *Nat Rev Cancer* 2002;2(12):938-50.
8. Post DE, Fulci G, Chiocca EA, Van Meir EG. Replicative oncolytic herpes simplex viruses in combination cancer therapies. *Curr Gene Ther* 2004;4(1):41-51.
9. Spear PG. Herpes simplex virus: receptors and ligands for cell entry. *Cell Microbiol* 2004;6(5):401-10.
10. Akhtar J, Shukla D. Viral entry mechanisms: cellular and viral mediators of herpes simplex virus entry. *FEBS J* 2009;276(24):7228-36.
11. Roizman B, Taddeo B. The strategy of herpes simplex virus replication and takeover of the host cell. 2007.
12. Knopf CW. Molecular mechanisms of replication of herpes simplex virus 1. *Acta Virol* 2000;44(5):289-307.
13. Placek BJ, Berger SL. Chromatin dynamics during herpes simplex virus-1 lytic infection. *Biochim Biophys Acta*;1799(3-4):223-7.

14. Nicoll MP, Proenca JT, Efstathiou S. The molecular basis of herpes simplex virus latency. *FEMS Microbiol Rev*;36(3):684-705.
15. Roizman B. The function of herpes simplex virus genes: a primer for genetic engineering of novel vectors. *Proc Natl Acad Sci U S A* 1996;93(21):11307-12.
16. Jenkins FJ, Roizman B. Herpes simplex virus 1 recombinants with noninverting genomes frozen in different isomeric arrangements are capable of independent replication. *J Virol* 1986;59(2):494-9.
17. Kelly KJ, Wong J, Fong Y. Herpes simplex virus NV1020 as a novel and promising therapy for hepatic malignancy. *Expert Opin Investig Drugs* 2008;17(7):1105-13.
18. Harrow S, Papanastassiou V, Harland J, Mabbs R, Petty R, Fraser M, Hadley D, Patterson J, Brown SM, Rampling R. HSV1716 injection into the brain adjacent to tumour following surgical resection of high-grade glioma: safety data and long-term survival. *Gene Ther* 2004;11(22):1648-58.
19. Papanastassiou V, Rampling R, Fraser M, Petty R, Hadley D, Nicoll J, Harland J, Mabbs R, Brown M. The potential for efficacy of the modified (ICP 34.5(-)) herpes simplex virus HSV1716 following intratumoural injection into human malignant glioma: a proof of principle study. *Gene Ther* 2002;9(6):398-406.
20. Rampling R, Cruickshank G, Papanastassiou V, Nicoll J, Hadley D, Brennan D, Petty R, MacLean A, Harland J, McKie E and others. Toxicity evaluation of replication-competent herpes simplex virus (ICP 34.5 null mutant 1716) in patients with recurrent malignant glioma. *Gene Ther* 2000;7(10):859-66.
21. Markert JM, Medlock MD, Rabkin SD, Gillespie GY, Todo T, Hunter WD, Palmer CA, Feigenbaum F, Tornatore C, Tufaro F and others. Conditionally replicating herpes simplex virus mutant, G207 for the treatment of malignant glioma: results of a phase I trial. *Gene Ther* 2000;7(10):867-74.
22. Huszthy PC, Goplen D, Thorsen F, Immervoll H, Wang J, Gutermann A, Miletic H, Bjerkvig R. Oncolytic herpes simplex virus type-1 therapy in a highly infiltrative animal model of human glioblastoma. *Clin Cancer Res* 2008;14(5):1571-80.
23. Markert JM, Liechty PG, Wang W, Gaston S, Braz E, Karrasch M, Nabors LB, Markiewicz M, Lakeman AD, Palmer CA and others. Phase Ib trial of mutant herpes simplex virus G207 inoculated pre-and post-tumor resection for recurrent GBM. *Mol Ther* 2009;17(1):199-207.
24. Hu JC, Coffin RS, Davis CJ, Graham NJ, Groves N, Guest PJ, Harrington KJ, James ND, Love CA, McNeish I and others. A phase I study of OncoVEXGM-CSF, a second-generation oncolytic herpes simplex virus expressing granulocyte macrophage colony-stimulating factor. *Clin Cancer Res* 2006;12(22):6737-47.
25. Zhang X, Zhao L, Hang Z, Guo H, Zhang M. Evaluation of HSV-1 and adenovirus vector-mediated infection, replication and cytotoxicity in lymphoma cell lines. *Oncol Rep*;26(3):637-44.

26. Geevarghese SK, Geller DA, de Haan HA, Horer M, Knoll AE, Mescheder A, Nemunaitis J, Reid TR, Sze DY, Tanabe KK and others. Phase I/II study of oncolytic herpes simplex virus NV1020 in patients with extensively pretreated refractory colorectal cancer metastatic to the liver. *Hum Gene Ther*;21(9):1119-28.
27. Krol J, Loedige I, Filipowicz W. The widespread regulation of microRNA biogenesis, function and decay. *Nat Rev Genet*;11(9):597-610.
28. Kim VN, Han J, Siomi MC. Biogenesis of small RNAs in animals. *Nat Rev Mol Cell Biol* 2009;10(2):126-39.
29. Friedman RC, Farh KK, Burge CB, Bartel DP. Most mammalian mRNAs are conserved targets of microRNAs. *Genome Res* 2009;19(1):92-105.
30. Fabian MR, Sonenberg N, Filipowicz W. Regulation of mRNA translation and stability by microRNAs. *Annu Rev Biochem*;79:351-79.
31. Chekulaeva M, Filipowicz W. Mechanisms of miRNA-mediated post-transcriptional regulation in animal cells. *Curr Opin Cell Biol* 2009;21(3):452-60.
32. Lagos-Quintana M, Rauhut R, Yalcin A, Meyer J, Lendeckel W, Tuschl T. Identification of tissue-specific microRNAs from mouse. *Curr Biol* 2002;12(9):735-9.
33. Meza-Sosa KF, Valle-Garcia D, Pedraza-Alva G, Perez-Martinez L. Role of microRNAs in central nervous system development and pathology. *J Neurosci Res*;90(1):1-12.
34. Cao X, Pfaff SL, Gage FH. A functional study of miR-124 in the developing neural tube. *Genes Dev* 2007;21(5):531-6.
35. Gao FB. Context-dependent functions of specific microRNAs in neuronal development. *Neural Dev*;5:25.
36. Li X, Jin P. Roles of small regulatory RNAs in determining neuronal identity. *Nat Rev Neurosci*;11(5):329-38.
37. Smirnova L, Grafe A, Seiler A, Schumacher S, Nitsch R, Wulczyn FG. Regulation of miRNA expression during neural cell specification. *Eur J Neurosci* 2005;21(6):1469-77.
38. Lim LP, Lau NC, Garrett-Engle P, Grimson A, Schelter JM, Castle J, Bartel DP, Linsley PS, Johnson JM. Microarray analysis shows that some microRNAs downregulate large numbers of target mRNAs. *Nature* 2005;433(7027):769-73.
39. Fiore R, Siegel G, Schrott G. MicroRNA function in neuronal development, plasticity and disease. *Biochim Biophys Acta* 2008;1779(8):471-8.
40. Papagiannakopoulos T, Kosik KS. MicroRNA-124: micromanager of neurogenesis. *Cell Stem Cell* 2009;4(5):375-6.
41. Cheng LC, Pastrana E, Tavazoie M, Doetsch F. miR-124 regulates adult neurogenesis in the subventricular zone stem cell niche. *Nat Neurosci* 2009;12(4):399-408.

42. Silber J, Lim DA, Petritsch C, Persson AI, Maunakea AK, Yu M, Vandenberg SR, Ginzinger DG, James CD, Costello JF and others. miR-124 and miR-137 inhibit proliferation of glioblastoma multiforme cells and induce differentiation of brain tumor stem cells. *BMC Med* 2008;6:14.
43. Papagiannakopoulos T, Kosik KS. MicroRNAs: regulators of oncogenesis and stemness. *BMC Med* 2008;6:15.
44. Krichevsky AM, Sonntag KC, Isacson O, Kosik KS. Specific microRNAs modulate embryonic stem cell-derived neurogenesis. *Stem Cells* 2006;24(4):857-64.
45. Yoo AS, Staahl BT, Chen L, Crabtree GR. MicroRNA-mediated switching of chromatin-remodelling complexes in neural development. *Nature* 2009;460(7255):642-6.
46. Sato F, Tsuchiya S, Meltzer SJ, Shimizu K. MicroRNAs and epigenetics. *FEBS J*;278(10):1598-609.
47. Chen W, Mi R, Haughey N, Oz M, Hoke A. Immortalization and characterization of a nociceptive dorsal root ganglion sensory neuronal line. *J Peripher Nerv Syst* 2007;12(2):121-30.
48. Prins JM, Park S, Lurie DI. Decreased expression of the voltage-dependent anion channel in differentiated PC-12 and SH-SY5Y cells following low-level Pb exposure. *Toxicol Sci*;113(1):169-76.
49. Doench JG, Petersen CP, Sharp PA. siRNAs can function as miRNAs. *Genes Dev* 2003;17(4):438-42.
50. Amendola M, Passerini L, Pucci F, Gentner B, Bacchetta R, Naldini L. Regulated and multiple miRNA and siRNA delivery into primary cells by a lentiviral platform. *Mol Ther* 2009;17(6):1039-52.
51. Brown BD, Venneri MA, Zingale A, Sergi Sergi L, Naldini L. Endogenous microRNA regulation suppresses transgene expression in hematopoietic lineages and enables stable gene transfer. *Nat Med* 2006;12(5):585-91.
52. Lee CY, Rennie PS, Jia WW. MicroRNA regulation of oncolytic herpes simplex virus-1 for selective killing of prostate cancer cells. *Clin Cancer Res* 2009;15(16):5126-35.
53. Giersch WW, Zimmerman DL, Ward SL, Vanheyningen TK, Romine JD, Leib DA. Construction and characterization of bacterial artificial chromosomes containing HSV-1 strains 17 and KOS. *J Virol Methods* 2006;135(2):197-206.
54. Sternberg N, Hamilton D. Bacteriophage P1 site-specific recombination. I. Recombination between loxP sites. *J Mol Biol* 1981;150(4):467-86.
55. Stricklett PK, Nelson RD, Kohan DE. The Cre/loxP system and gene targeting in the kidney. *Am J Physiol* 1999;276(5 Pt 2):F651-7.

56. Tischer BK, von Einem J, Kaufer B, Osterrieder N. Two-step red-mediated recombination for versatile high-efficiency markerless DNA manipulation in *Escherichia coli*. *Biotechniques* 2006;40(2):191-7.
57. Uchida H, Chan J, Goins WF, Grandi P, Kumagai I, Cohen JB, Glorioso JC. A double mutation in glycoprotein gB compensates for ineffective gD-dependent initiation of herpes simplex virus type 1 infection. *J Virol*;84(23):12200-9.
58. Doronina VA, Wu C, de Felipe P, Sachs MS, Ryan MD, Brown JD. Site-specific release of nascent chains from ribosomes at a sense codon. *Mol Cell Biol* 2008;28(13):4227-39.
59. Kaji K, Norrby K, Paca A, Mileikovsky M, Mohseni P, Woltjen K. Virus-free induction of pluripotency and subsequent excision of reprogramming factors. *Nature* 2009;458(7239):771-5.
60. Poffenberger KL, Tabares E, Roizman B. Characterization of a viable, noninverting herpes simplex virus 1 genome derived by insertion and deletion of sequences at the junction of components L and S. *Proc Natl Acad Sci U S A* 1983;80(9):2690-4.
61. Zhu Z, Zheng T, Lee CG, Homer RJ, Elias JA. Tetracycline-controlled transcriptional regulation systems: advances and application in transgenic animal modeling. *Semin Cell Dev Biol* 2002;13(2):121-8.
62. Godlewski J, Newton HB, Chiocca EA, Lawler SE. MicroRNAs and glioblastoma; the stem cell connection. *Cell Death Differ*;17(2):221-8.
63. Lawler S, Chiocca EA. Emerging functions of microRNAs in glioblastoma. *J Neurooncol* 2009;92(3):297-306.
64. Fowler A, Thomson D, Giles K, Maleki S, Mreich E, Wheeler H, Leedman P, Biggs M, Cook R, Little N and others. miR-124a is frequently down-regulated in glioblastoma and is involved in migration and invasion. *Eur J Cancer*;47(6):953-63.
65. Lang MF, Yang S, Zhao C, Sun G, Murai K, Wu X, Wang J, Gao H, Brown CE, Liu X and others. Genome-Wide Profiling Identified a Set of miRNAs that Are Differentially Expressed in Glioblastoma Stem Cells and Normal Neural Stem Cells. *PLoS One*;7(4):e36248.
66. Ponomarev ED, Veremeyko T, Barteneva N, Krichevsky AM, Weiner HL. MicroRNA-124 promotes microglia quiescence and suppresses EAE by deactivating macrophages via the C/EBP-alpha-PU.1 pathway. *Nat Med*;17(1):64-70.
67. Soreq H, Wolf Y. NeurimmiRs: microRNAs in the neuroimmune interface. *Trends Mol Med*;17(10):548-55.
68. Xia H, Cheung WK, Ng SS, Jiang X, Jiang S, Sze J, Leung GK, Lu G, Chan DT, Bian XW and others. Loss of brain-enriched miR-124 microRNA enhances stem-like traits and invasiveness of glioma cells. *J Biol Chem*;287(13):9962-71.
69. Kelly EJ, Russell SJ. MicroRNAs and the regulation of vector tropism. *Mol Ther* 2009;17(3):409-16.

70. Gurlevik E, Woller N, Schache P, Malek NP, Wirth TC, Zender L, Manns MP, Kubicka S, Kuhnel F. p53-dependent antiviral RNA-interference facilitates tumor-selective viral replication. *Nucleic Acids Res* 2009;37(12):e84.
71. Cawood R, Chen HH, Carroll F, Bazan-Peregrino M, van Rooijen N, Seymour LW. Use of tissue-specific microRNA to control pathology of wild-type adenovirus without attenuation of its ability to kill cancer cells. *PLoS Pathog* 2009;5(5):e1000440.
72. Leja J, Nilsson B, Yu D, Gustafson E, Akerstrom G, Oberg K, Giandomenico V, Essand M. Double-detargeted oncolytic adenovirus shows replication arrest in liver cells and retains neuroendocrine cell killing ability. *PLoS One*;5(1):e8916.
73. Jin H, Lv S, Yang J, Wang X, Hu H, Su C, Zhou C, Li J, Huang Y, Li L and others. Use of microRNA Let-7 to control the replication specificity of oncolytic adenovirus in hepatocellular carcinoma cells. *PLoS One*;6(7):e21307.
74. Hikichi M, Kidokoro M, Haraguchi T, Iba H, Shida H, Tahara H, Nakamura T. MicroRNA regulation of glycoprotein B5R in oncolytic vaccinia virus reduces viral pathogenicity without impairing its antitumor efficacy. *Mol Ther*;19(6):1107-15.
75. Kelly EJ, Hadac EM, Greiner S, Russell SJ. Engineering microRNA responsiveness to decrease virus pathogenicity. *Nat Med* 2008;14(11):1278-83.
76. Leber MF, Bossow S, Leonard VH, Zaoui K, Grossardt C, Frenzke M, Miest T, Sawall S, Cattaneo R, von Kalle C and others. MicroRNA-sensitive oncolytic measles viruses for cancer-specific vector tropism. *Mol Ther*;19(6):1097-106.
77. Shukla D, Scanlan PM, Tiwari V, Sheth V, Clement C, Guzman-Hartman G, Dermody TS, Valyi-Nagy T. Expression of nectin-1 in normal and herpes simplex virus type 1-infected murine brain. *Appl Immunohistochem Mol Morphol* 2006;14(3):341-7.
78. Aravalli RN, Hu S, Rowen TN, Gekker G, Lokengsgard JR. Differential apoptotic signaling in primary glial cells infected with herpes simplex virus 1. *J Neurovirol* 2006;12(6):501-10.
79. Bello-Morales R, Fedetz M, Alcina A, Tabares E, Lopez-Guerrero JA. High susceptibility of a human oligodendroglial cell line to herpes simplex type 1 infection. *J Neurovirol* 2005;11(2):190-8.
80. Heiss BL, Maximova OA, Thach DC, Speicher JM, Pletnev AG. MicroRNA targeting of neurotropic flavivirus: effective control of virus escape and reversion to neurovirulent phenotype. *J Virol*;86(10):5647-59.
81. Heiss BL, Maximova OA, Pletnev AG. Insertion of microRNA targets into the flavivirus genome alters its highly neurovirulent phenotype. *J Virol*;85(4):1464-72.
82. Laquerre S, Anderson DB, Argnani R, Glorioso JC. Herpes simplex virus type 1 glycoprotein B requires a cysteine residue at position 633 for folding, processing, and incorporation into mature infectious virus particles. *J Virol* 1998;72(6):4940-9.

83. Bishop JR, Schuksz M, Esko JD. Heparan sulphate proteoglycans fine-tune mammalian physiology. *Nature* 2007;446(7139):1030-7.
84. Hong CS, Fellows W, Niranjan A, Alber S, Watkins S, Cohen JB, Glorioso JC, Grandi P. Ectopic matrix metalloproteinase-9 expression in human brain tumor cells enhances oncolytic HSV vector infection. *Gene Ther*;17(10):1200-5.
85. Benencia F, Courreges MC, Conejo-Garcia JR, Mohamed-Hadley A, Zhang L, Buckanovich RJ, Carroll R, Fraser N, Coukos G. HSV oncolytic therapy upregulates interferon-inducible chemokines and recruits immune effector cells in ovarian cancer. *Mol Ther* 2005;12(5):789-802.
86. Moriuchi S, Oligino T, Krisky D, Marconi P, Fink D, Cohen J, Glorioso JC. Enhanced tumor cell killing in the presence of ganciclovir by herpes simplex virus type 1 vector-directed coexpression of human tumor necrosis factor-alpha and herpes simplex virus thymidine kinase. *Cancer Res* 1998;58(24):5731-7.
87. Krisky DM, Marconi PC, Oligino TJ, Rouse RJ, Fink DJ, Cohen JB, Watkins SC, Glorioso JC. Development of herpes simplex virus replication-defective multigene vectors for combination gene therapy applications. *Gene Ther* 1998;5(11):1517-30.
88. Benencia F, Courreges MC, Conejo-Garcia JR, Mohammed-Hadley A, Coukos G. Direct vaccination with tumor cells killed with ICP4-deficient HSVd120 elicits effective antitumor immunity. *Cancer Biol Ther* 2006;5(7):867-74.
89. Farrell CJ, Zaupa C, Barnard Z, Maley J, Martuza RL, Rabkin SD, Curry WT, Jr. Combination immunotherapy for tumors via sequential intratumoral injections of oncolytic herpes simplex virus 1 and immature dendritic cells. *Clin Cancer Res* 2008;14(23):7711-6.